

FRET-BASED CONFORMATIONAL SENSOR FOR THE m1 MUSCARINIC
CHOLINERGIC RECEPTOR

APPROVED BY SUPERVISORY COMMITTEE

Elliott M. Ross, PhD

Johann Deisenhofer, Ph.D.

Donald Hilgemann, Ph.D.

Rama Ranganathan, M.D., Ph.D.

DEDICATION

Looking back, I am very grateful for all I have received throughout these years. It has certainly shaped me as a person and a scientist.

First, I want to thank my mentor Elliott Ross for his encouragement, advice and invaluable training. He has taught me in a fatherly way how to do experiments, write, present, and think logically and critically. The depth and thoroughness of his approach to research are something I would like to maintain in my own career. Thank you members of my dissertation committee, Drs. Johann Deisenhofer, Donald Hilgemann and Rama Ranganathan, for guidance and support. I also would like to thank all the members of the Ross lab, especially Jimmy Woodson and Elisha White for their enormous help. Thank Lei Shi, who helped me during his rotation in the lab. I also have to thank Dali Liu, a former postdoc, whose previous work saved me much time. I want to thank David Sauer who gave me enormous help in writing my thesis.

Finally, I would like to thank my family and friends for their love and encouragement. Thank God.

FRET-BASED CONFORMATIONAL SENSOR FOR THE m1 MUSCARINIC
CHOLINERGIC RECEPTOR

by

SEUNGWOO CHANG

DISSERTATION

Presented to the Faculty of the Graduate School of Biomedical Sciences

The University of Texas Southwestern Medical Center at Dallas

In Partial Fulfillment of the Requirements

For the Degree of

DOCTOR OF PHILOSOPHY

The University of Texas Southwestern Medical Center at Dallas

Dallas, Texas

Nov, 2011

Copyright

by

SEUNGWOO CHANG, 2011

All Rights Reserved

FRET-BASED CONFORMATIONAL SENSOR FOR THE m1
MUSCARINIC CHOLINERGIC RECEPTOR

SEUNGWOO CHANG

The University of Texas Southwestern Medical Center at Dallas, 2011

ELLIOTT M. ROSS, Ph.D.

Signaling behaviors of G-protein-mediated signaling are the outcome of a regulated cycle of GTP binding and hydrolysis. Binding of GTP, which activates G proteins, is promoted by an agonist-activated receptor; and hydrolysis of bound GTP, which deactivates G proteins, is accelerated by a GTPase-activating protein (GAP). These two processes need to be coordinately regulated to achieve fast turning on and off of signaling with robust signal output.

I developed an optical conformational sensor for the m1 muscarinic cholinergic receptor (M1), a prototypical G protein-coupled receptor (GPCR), to study how receptor activity is regulated by the coordinated action of agonist, G protein and GAP. To create the sensor, I adopted an underlying design originally developed by the Lohse group. The sensor exploits intramolecular fluorescence

resonance energy transfer, FRET, to monitor activation-associated conformational changes in intracellular loop 3 of the receptor. In the sensor, a CFP FRET donor and a labeling site for FIAsh (fluorescein-based biarsenical dye) FRET acceptor are engineered into the M1 receptor at the C terminus and loop 3, respectively. The development proceeded through several distinct optimization steps that probably reflect general considerations for developing such sensors for class A GPCRs. After optimizing the labeling conditions to approach stoichiometric derivatization by FIAsh, I found that the fluorescence response of the sensor depended on: (1) the location of the FIAsh labeling site in loop 3; (2) the length of the C-terminal region, which apparently acts as a lever arm, prior to placement of the CFP; and (3) the choice among circularly permuted CFP moieties. Finally, based on a homology-modeled structure of the M1 receptor, placement of the FIAsh site and the length of its flexible linkers were re-optimized to prevent interference with binding of the sensor to $G\alpha_q$.

The sensor retained essentially wild-type agonist binding and signaling activity of the M1 receptor in living cells and cell membranes. Fluorescence responses of the sensor to muscarinic agonists paralleled their cellular efficacies. The sensor in living cells faithfully reported agonist-driven conformational change of the M1 receptor. Therefore, the FRET-based sensor proves to be a useful tool to investigate the mechanisms by which conformational dynamics of the M1 receptor is regulated by agonist in living cells and membranes. Effects of $G\alpha_q$ on the conformation of the M1 receptor could not be determined because stable interaction between the M1 receptor and $G\alpha_q$ could not be detected in cells or

cell membranes either by fluorescence change or by agonist binding affinity; this is also true for wild-type receptor.

Although the sensor reconstituted in phospholipid vesicles retained wild-type agonist binding and signaling function, fluorescence response to agonist was not detected in the vesicles. I demonstrated that solubilization of the sensor denatured a substantial fraction of the sensor, resulting in low fractional ligand binding activity of *in vitro* labeled sensor and thus artifactually low fluorescence response to agonist.

TABLE OF CONTENTS

Chapter 1. Regulation of G-protein-mediated signaling	1
GPCR and G-protein-mediated signaling	1
Structure of GPCR	2
Agonist-activated G protein cycle	5
Two-state model of receptor activation	7
Agonist binding of GPCR	10
Effect of GAP on the regulation of receptor activity	13
Motivation of the thesis research	14
Chapter 2. Development of a FRET-based conformational sensor for the m1 acetylcholine receptor (m1 AChR) in mammalian cells	16
Introduction	16
Conformational sensor	16
Sensors based on environment sensitive fluorescent dye ..	16
Sensors based on intramolecular fluorescence resonance energy transfer (FRET)	17
Principles of FRET and relevance to the development of a FRET-based sensor	19
Experimental Procedures	24
Results	31
Initial design and optimization of labeling site for FIAsh in ICL3 .	31
Oligo-proline spacer to extend the C-terminal placement of the CFP FRET donor	34
Circularly permuted CFP FRET donor increases the agonist- driven FRET change	38

Optimization of a fusion site for a circularly permuted cerulean (cp173cer); first-generation sensor	38
The first-generation sensor loses signaling function in cells	40
Creation of a second-generation sensor; re-optimization of the insertion site for the TC	43
Creation of a second-generation sensor; effect of the length of linkers	48
Change in intramolecular FRET is responsible for the agonist-driven	50
Second-generation sensor retains wild-type signaling function	52
Second-generation sensor displays nearly wild-type ligand binding features in membranes	55
Agonist-driven Δ FRET parallels agonist binding	58
Agonist-driven FRET changes parallel cellular efficacies of agonists	61
The sensor reports agonist-driven conformational changes of the M1 receptor in living cells	63
Discussion	67
Creation of a FRET-based conformational sensor for the m1 acetylcholine receptor	67
Optimizing geometry of a FRET donor and an acceptor within a protein; distance between a donor and an acceptor	67

Optimizing geometry of a FRET donor and an acceptor within a protein; orientation	69
Retaining GEF activity in a FRET-based sensor; structure-guided design	69
Estimating the distance change between ICL3 and C terminus upon activation	71
Studying conformational dynamics of the M1 receptor in living cells	73
Probing interactive effects of $G\alpha_q$ on the conformation of the M1 receptor in cell membrane preparations	74
Guanine nucleotides do not change the FRET of the sensor in cellular membrane preparations	76
Optimizing binding assay conditions for agonist in membrane preparations	76
Increasing the amount of $G\alpha_q$ in membrane preparations ..	78
Chapter 3. Reconstitution of the FRET-based M1 receptor conformational sensor in phospholipid vesicles	80
Introduction	80
Experimental Procedures	82
Results	91
Reconstituted biosensor retains wild-type agonist binding; formation of stable agonist-M1- $G\alpha_q$ complex	91
Reconstituted biosensor retains GEF activity	94

Agonist-driven FRET change of M1S-2-FLAsH is not detected in reconstituted phospholipid vesicles	95
Solubilization of the M1S-2-FIAsH in cell membranes obliterates agonist-driven FRET changes	95
Fractional binding activity of M1S-2-FIAsH in solution and reconstituted vesicles is low	100
Discussion	103
Reconstituting fluorescence responses of the sensor in lipid vesicles	103
Increasing fractional binding activity of <i>in vitro</i> labeled sensor	104
Reconstitution	105
Enhancing the stability of the sensor in micelles	105
Potential applications of the sensor	106
Measuring fractional agonist-activated receptor engaged in active signaling complex	106
Studying the mechanisms of biphasic agonist binding	108
Bibliography	110

LIST OF FIGURES

Figure 1.	M1-G α_q -PLC- β signaling module	3
Figure 2.	Agonist-activated GTPase cycle	6
Figure 3.	G protein monocyte for the M1-G α_q -PLC- β signaling module	8
Figure 4.	Two-state receptor model	9
Figure 5.	Simple receptor model for agonist binding	11
Figure 6.	Relationship between FRET efficiency and distance between two interacting fluorescence dipoles	21
Figure 7.	Diagram of a FRET-based conformational sensor for GPCR	32
Figure 8.	Expression and fluorescence emission of a M1 biosensor	33
Figure 9.	Optimized placement of a TC in ICL3 of the M1 receptor	35
Figure 10.	Optimization of a fusion site for CFP at C terminus of the receptor	37
Figure 11.	Effect of circular permutation of cerulean on CCh-driven FRET change	39
Figure 12.	Agonist-stimulated Ca ²⁺ transients are inhibited in cells that express the first-generation biosensor	42
Figure 13.	Homology-modeled structures of the M1 receptor	44
Figure 14.	Re-optimized placement of the TC reduced the inhibition of signaling by FIAsh	46
Figure 15.	Effect of linkers surrounding the TC insertion site	49
Figure 16.	Intramolecular FRET of the sensor is responsible for the FRET and agonist-driven FRET changes	51

Figure 17.	Inhibition of agonist-stimulated Ca^{2+} transient by FIAsh is substantially alleviated in cells expressing the second-generation sensor (M1S-2-FIAsh)	53
Figure 18.	Agonist and antagonist binding to M1S-2-FIAsh in HeLa cell membranes	56
Figure 19.	CCh-driven FRET change parallels agonist binding to the M1S-2-FIAsh	59
Figure 20.	FRET responses of M1S-2-FIAsh to partial agonists	62
Figure 21.	ACh-driven FRET changes of M1S-2-FIAsh in live HeLa cells	64
Figure 22.	ACh-driven FRET changes of the M1S-2-FIAsh in cells; dose-response relationship	66
Figure 23.	Fluorescent properties of purified M1S-2 with and without FIAsh labeling	84
Figure 24.	Agonist binding to M1S-2-FIAsh reconstituted in phospholipid vesicles	92
Figure 25.	Carbachol-stimulated binding of $\text{GTP}\gamma\text{S}$ to M1- $\text{G}\alpha_q$ and M1S-2-FIAsh- $\text{G}\alpha_q$ vesicles	95
Figure 26.	<i>In vitro</i> labeled sensor reconstituted in lipid vesicles loses agonist-driven FRET change	97
Figure 27.	Effect of solubilization on the basal FRET of the sensor	99
Figure 28.	Fractional ligand binding activity of the M1S-2 reconstituted in lipid vesicles is low	101

LIST OF TABLES

Table 1.	Signaling activity of the sensor in cells	54
Table 2.	Summary of CCh binding to wild-type M1 receptor and second-generation sensor (M1S-2-FIAsh) in HeLa cell membranes	57
Table 3.	EC ₅₀ for CCh-driven FRET change of M1S-2-FLASH in HeLa cell membranes	60
Table 4.	Summary of CCh binding to wild-type M1 receptor and second-generation sensor (M1S-2-FIAsh) in reconstituted phospholipid vesicles	93

LIST OF ABBREVIATIONS

Atr	atropine
CCh	carbachol
cDNA	complementary deoxyribonucleic acid
CHS	cholesteryl hemisuccinate
DAG	diacylglycerol
DTT	dithiothreitol
EDTA	ethylenediaminetetraacetic acid
FIAsH	fluorescein arsenical hairpin binder
FRET	fluorescence resonance energy transfer
GAP	GTPase-activating protein
GDP	guanosine diphosphate
Gpp(NH)p	guanylyl-imidodiphosphate
GTP	guanosine triphosphate
GTP γ S	guanosine 5'-3-O-(thio)triphosphate
Hepes	4-(2-hydroxyethyl)-1-piperazineethanesulfonic acid
ICL3	intracellular loop 3 of the M1 receptor
IP ₃ R	IP ₃ receptor
kD	kilodalton
M1	muscarinic acetylcholine receptor 1
M1-Del	simplified M1 receptor
2-ME	2-mercaptoethanol
mFRET	microscopic FRET
M1S-1	M1 receptor prototype for the first-generation sensor
M1S-2	M1 receptor prototype for the second-generation sensor

M1S-1-FIAsh	FIAsh-labeled M1S-1
M1S-2-FIAsh	FIAsh-labeled M1S-2
Ni-NTA	nickel-nitrilotriacetic acid
PE	phosphatidylethanolamine
PIP ₂	phosphatidylinositol 4, 5-bisphosphate
PS	phosphatidylserine
QNB	1-quinuclidinyl benzilate
sFRET	spectroscopic FRET
TC	tetracysteine motif, CCPGCC

CHAPTER 1

Regulation of G-protein-mediated signaling

GPCR and G-protein-mediated signaling

G protein-coupled receptors (GPCRs) are ligand-activated cell-surface proteins that sense extracellular activating-ligands such as hormones, neurotransmitters, odorants, and light. GPCRs transmit extracellular signals into intracellular space by activating heterotrimeric G proteins on the inner leaflet of the plasma membrane (Pierce et al., 2002). These heterotrimeric G proteins are plasma-membrane-associated guanine nucleotide binding proteins; dissociable trimers of $G\alpha$, $G\beta$ and $G\gamma$ subunits whose $G\alpha$ subunit is responsible for binding of guanine nucleotides (Gilman, 1987). Upon activation, trimeric G protein complexes dissociate into $G\alpha$ and $G\beta\gamma$, which acts as a unit. Both $G\alpha$ and $G\beta\gamma$ directly modulate activities of various effector proteins, connecting extracellular signaling to cellular response. Once extracellular signaling molecules are removed, $G\alpha$ subunit becomes deactivated and reforms an inactive $G\alpha\beta\gamma$ trimer.

There are > 1,000 GPCRs encoded in mammalian genomes. In contrast to the huge diversity of receptors, only 16, 5 and 12 genes for $G\alpha$, $G\beta$ and $G\gamma$ subunits are known in mammalian genomes. Although both $G\alpha$ and $G\beta\gamma$ act as signaling molecules, G proteins are generally identified by their α subunits. The intracellular signaling pathway activated by a GPCR is determined by the $G\alpha$ subunit activated by that particular receptor (Gudermann et al., 1996). Based on

similarities in sequence, $G\alpha$ subunits are classified into 4 subfamilies, which coincides with their effector proteins: (1) G_s subfamily, best known as activators of adenylyl cyclases, (2) G_i subfamily, inhibitors of adenylyl cyclases and, (3) G_q subfamily, activators of phospholipase $C\beta$ (PLC- β) and (4) G_{12} subfamily, activators of the Rho guanine nucleotide exchange factors (GEF).

In this dissertation, the m1 muscarinic acetylcholine receptor (M1) served as a model system. The M1 receptor primarily activates $G\alpha_q$, which is the most potent stimulator of PLC- β . $G\alpha_q$ -stimulated PLC- β hydrolyzes phosphatidylinositol-bisphosphate in the inner leaflet of a plasma membrane, generating inositol 1,4,5-trisphosphate (IP₃) and diacylglycerol (DAG) (Figure 1) (Nathanson, 1987; Schimerlik, 1989). IP₃, a Ca²⁺ mobilizing second messenger, binds and opens the IP₃ receptor, Ca²⁺ channel located in the endoplasmic reticulum, generating cytosolic Ca²⁺ transients. DAG activates protein kinase C on the cell membrane. Even though other GPCRs engage different subfamilies of $G\alpha$ and activate distinct effector proteins, they all follow the common scheme of receptor → G protein → effector.

Structure of GPCR

GPCRs have seven transmembrane helices connected by 3 intracellular loops (ICL) and 3 extracellular loops (ECL), with N- and C-termini outside and inside of the cell, respectively (Cherezov et al., 2007; Palczewski et al., 2000; Rosenbaum et al., 2007). The extracellular half of the helical bundle forms a ligand binding site, which is accessible from the extracellular space. The

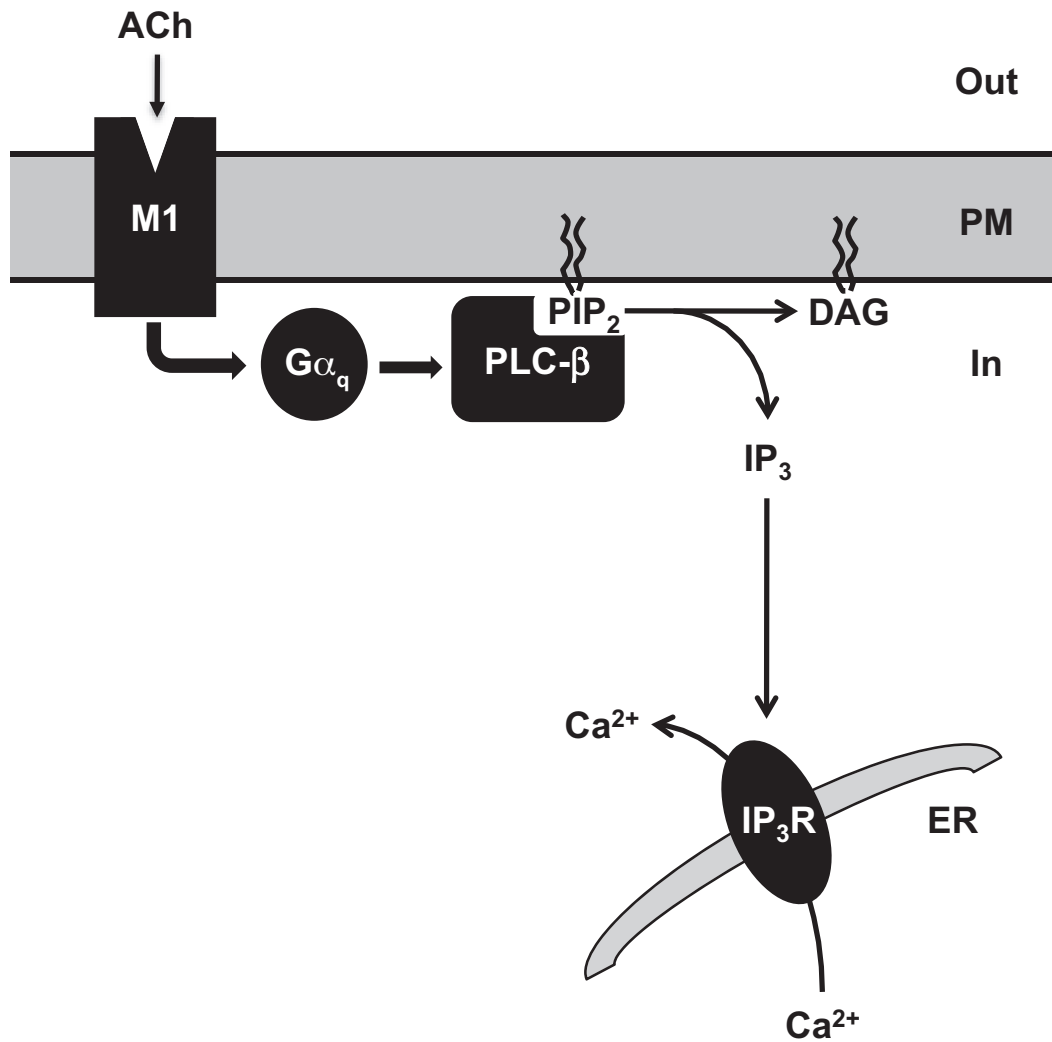


Figure 1. M1-G α_q -PLC- β signaling module

Acetylcholine (ACh) binding to the m1AChR (M1) receptor activates G α_q . Activated G α_q binds and activates phospholipase C- β (PLC- β). G α_q -activated PLC- β hydrolyzes phosphatidylinositol 4,5-bisphosphate (PIP₂) in the inner leaflet of the plasma membrane, generating two intracellular metabolites, inositol 1,4,5-trisphosphate (IP₃) and diacylglycerol (DAG). IP₃ diffuses across the cytosol and binds to and opens IP₃R, a Ca²⁺ channel located on the endoplasmic reticulum (ER). Opening of the IP₃R mobilizes Ca²⁺ stored in ER to cytosol and generates Ca²⁺ transient. DAG activates protein kinase C. PM, plasma membrane.

cytoplasmic surface of the helical bundle provides structural elements required for activation of the G protein. Binding of agonist drives structural changes around agonist binding site and these local changes propagate to the cytoplasmic surface of the receptor by rotational movement of transmembrane helices, called "rigid body movement" (Farrens et al., 1996). The most prominent structural changes occur at the cytoplasmic ends of transmembrane helices 5 and 6 which are connected by the third intracellular loop (ICL3), resulting in the exposure of residues involved in the activation of G protein (Rasmussen et al., 2011; Scheerer et al., 2008).

Many GPCRs, including the M1 receptor, form homo- or hetero-dimers, which are in fast equilibrium with monomeric receptor (Angers et al., 2002; Goin et al., 2006; Hern et al., 2010). However, it is poorly understood which receptor form, monomer or dimer, is responsible for specific regulatory behaviors of the receptor, such as G protein activation and internalization, etc. Furthermore, the physiological relevance of dimerization is largely elusive, with a few exceptions. For some receptors, dimerization is required for maturation and proper localization to plasma membrane (White et al., 1998). Receptor hetero-dimerization is also involved in signaling crosstalk for some receptors (Jordan et al., 1999; Mellado et al., 2001). However, spatial organization of monomers within a dimer and the role of monomeric and dimeric receptors in the activation of G protein are not clearly understood. Recently, for rhodopsin, β_2 AR, and μ -opioid receptor, it was shown that monomeric receptors reconstituted in nano-disc retained GEF activity (Kuszak et al., 2009; Whorton et al., 2007; Whorton et al., 2008), suggesting that receptor monomer might be a minimal functional unit.

However, at least for β_2 AR reconstituted in nano-disc, activation of G protein was inefficient (one receptor activated ~ 0.5 G protein in the presence of ~ 50 fold molar excess of G protein) and the activity was not compared with that of a homogeneous population of dimeric receptor under similar conditions. Therefore, although monomer is the minimal functional unit, it is not clear whether the monomer is the minimal physiological unit or is physiologically less active than an oligomer.

Agonist-activated G protein cycle

G proteins convey signals from hormone-bound receptors to various effector proteins as they pass through regulated cycles of GTP binding and hydrolysis (Figure 2). The GDP-bound state of the G protein (G-GDP) is inactive and activated to GTP-bound state (G^* -GTP) by the GEF (Guanine Nucleotide Exchange Factor) activity of agonist-activated receptors. The agonist-activated receptor promotes the guanine nucleotide exchange reaction by accelerating both dissociation of bound GDP and association of GTP (Turcotte et al., 2008). Deactivation of G^* -GTP is caused by hydrolysis of bound GTP to GDP by the intrinsic GTPase activity of the $G\alpha$ subunit. The GTPase activity is markedly potentiated by GTPase-activating proteins (GAPs), which bind to G^* -GTP and enhances GTPase activity of the $G\alpha$ subunit (Berstein et al., 1992; Ross et al., 2000). GAPs include some effectors (e.g. PLC- β and p115RhoGEF) and RGS proteins (Regulators of G protein Signaling). In the M1- $G\alpha_q$ -PLC- β signaling module, PLC- β , the effector, also acts as a GAP for its own stimulator, $G\alpha_q$.

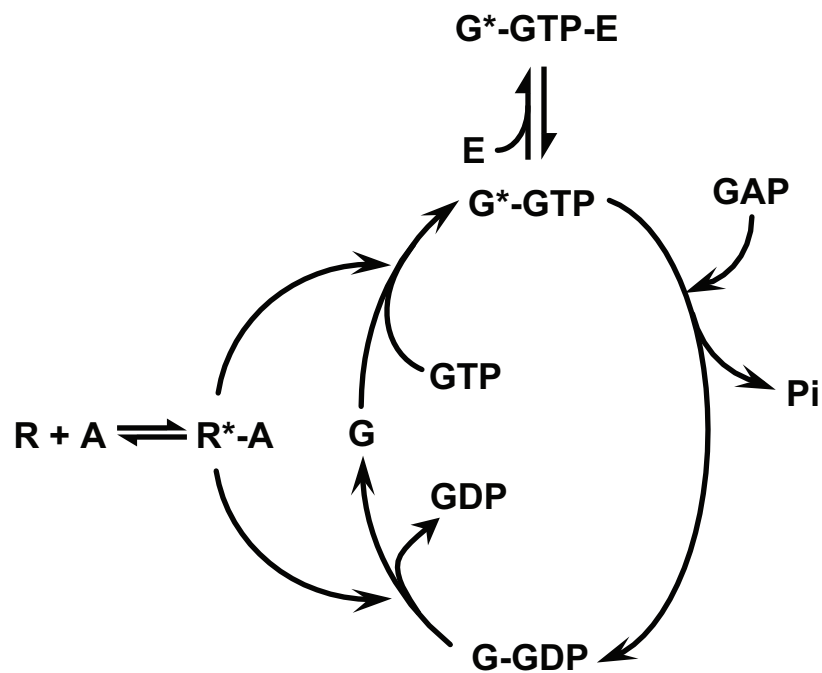


Figure 2. Agonist-activated GTPase cycle

Equilibrium binding of agonist to receptor activates the receptor. Agonist-bound receptor (R*-A) activates G protein by promoting nucleotide exchange reaction on G protein. R*-A accelerates the reaction by increasing the dissociation rate of GDP and association rate of GTP. GTP-bound activated G protein (G*-GTP) binds to an effector protein and regulates its activity. Activated G protein (G*-GTP) gets inactivated to GDP-bound form (G-GDP) upon hydrolysis of bound GTP by intrinsic GTPase activity. Slow intrinsic GTPase activity is boosted by GTPase-activating proteins (GAPs). R, receptor; A, agonist; G, G α subunit; E, effector; GAP, GTPase-activating protein; Pi, inorganic phosphate; *, activated state.

Signal output (activation of effector) is proportional to the amount of G^{*}-GTP. A simple G protein monocyclus model defines signal output and turning on and off kinetics of signal with two rate constants: (1) k_{on} , receptor-promoted binding of GTP and (2) k_{off} , GAP-accelerated hydrolysis of bound GTP (Figure 3). At steady-state, fractional G α^* -GTP is simply defined by $k_{on}/(k_{on} + k_{off})$, a balance of receptor-promoted generation of G α^* -GTP (k_{on}) and GAP-accelerated hydrolysis of bound GTP to GDP (k_{off}) (Figure 3). Upon perturbation (e.g. addition of agonist or removal of agonist), a certain steady-state reaches another steady-state with apparent rate constant $k_{on} + k_{off}$. Both activation (k_{on}) and deactivation (k_{off}) are regulated processes and their coordinated regulation determines the rates of activation and deactivation and signal amplitude (Ross, 2008; Turcotte et al., 2008).

Two-state model of receptor activation

The activation of a GPCR is regulated by agonist binding. Agonist-regulation of receptor activation has been described by two-state model, in which binding of agonist alters the equilibrium between inactive and active states of the receptor (Leff, 1995). In this model, a receptor can exist in one of two states, either relatively inactive (R) or highly active (R^{*}), with the intrinsic conformational equilibrium described by the isomerization constant J (J, equilibrium isomerization constant, R^{*}/R) (Figure 4). J is related to basal activity of a receptor, which is an intrinsic property of receptors and increased by constitutively activating mutations (Parnot et al., 2002). In the two-state model, potency of a ligand is determined by both the binding affinity of the ligand (K_L), J

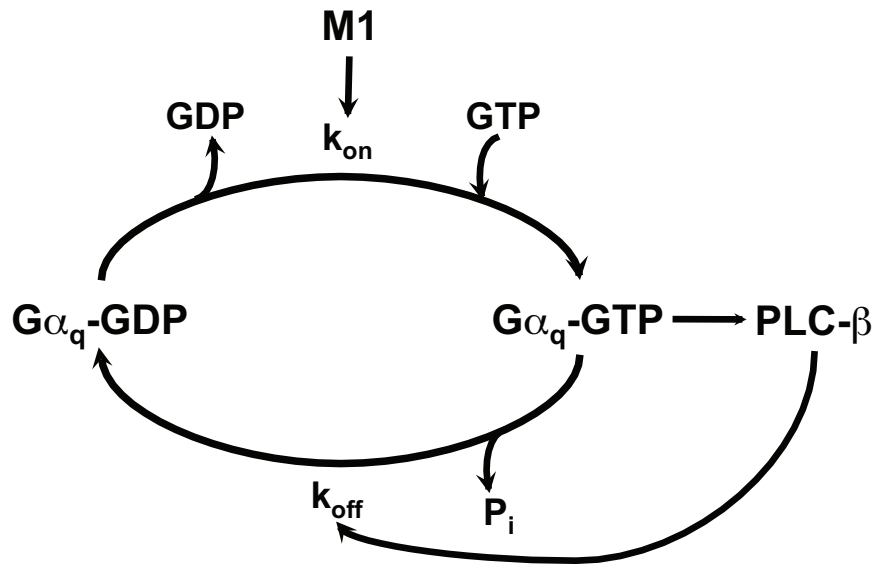


Figure 3. G protein monocyclus for the M1-G α_q -PLC- β signaling module

G α_q transits a regulated cycle of GTP binding and hydrolysis. k_{on} is a reaction rate constant for M1-promoted guanine nucleotide exchange reaction on G α_q . (G α_q -GDP to G α_q -GTP). k_{off} is a rate constant for GAP-potentiated hydrolysis of GTP to GDP. In M1-G α_q -PLC- β signaling module, the effector, PLC- β , acts as a GAP for its own activator G α_q . Fractional G α_q -GTP is determined by the balance between k_{on} and k_{off} . At steady-state, the fractional concentration of G α_q -GTP is $k_{on}/(k_{on} + k_{off})$. Upon perturbation, one steady-state reaches another steady-state with rate of $k_{on} + k_{off}$.

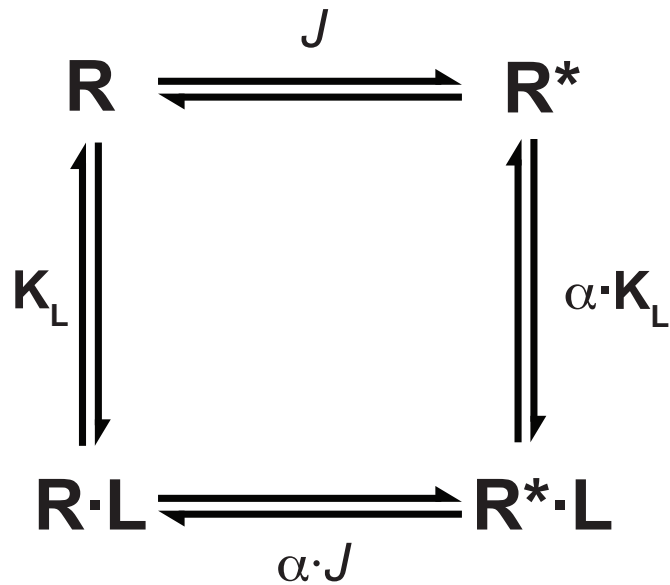


Figure 4. Two-state receptor model

Receptor can exist in one of two states, either inactive (R) or active (R*), with the intrinsic conformational equilibrium described by the isomerization constant J ($[\text{R}^*]/[\text{R}]$). Ligand (L) can bind to inactive state with association constant K_L ($[\text{R} \cdot \text{L}]/[\text{R}] \cdot [\text{L}]$) and to active state with association constant $\alpha \cdot K_L$. Agonist binds to active state more tightly ($\alpha > 1$), antagonist binds to active or inactive states with equal affinity ($\alpha = 1$), and inverse agonist binds to inactive state more tightly ($\alpha < 1$).

and α , and relative efficacy of a ligand is determined by its preferential binding to either inactive or active state receptor (α , preferential binding constant). There are three classes of ligands based on their effect on the conformational equilibrium of the receptor: (1) a ligand with $\alpha > 1$, classified as an agonist, which can elicit receptor activity higher than basal activity, (2) a ligand with $\alpha = 1$, classified as an antagonist (or neutral antagonist), which can inhibit the binding of an agonist but can not elicit receptor activity, and (3) a ligand with $\alpha < 1$, classified as an inverse agonist, which can inhibit the binding of an agonist and can suppress basal activity. In the two-state model, partial agonism can be viewed as a graded preferential binding and ligands with higher α are more efficacious.

Agonist binding of GPCR

Agonist binding of GPCR is biphasic (Maguire et al., 1976) with a fraction of binding sites displaying higher binding affinity (Figure 5A). In the presence of guanine nucleotides (GTP or GDP), the binding becomes monophasic with the single binding affinity indistinguishable from the low binding affinity seen in the absence of guanine nucleotides (Hoffman et al., 1980; Rodbell et al., 1971). Removal of G protein makes agonist binding monophasic with only low binding affinity for agonist (Sternweis et al., 1979). For example, agonist binding of the M1 receptor is biphasic, where $G\alpha_q$ enhances binding affinity more than 100 fold ($\beta > 100$)(Figure 5A). High-affinity binding disappears in the presence of $GTP\gamma S$ or when $G\alpha_q$ is removed. Based on these observations and others, interactive

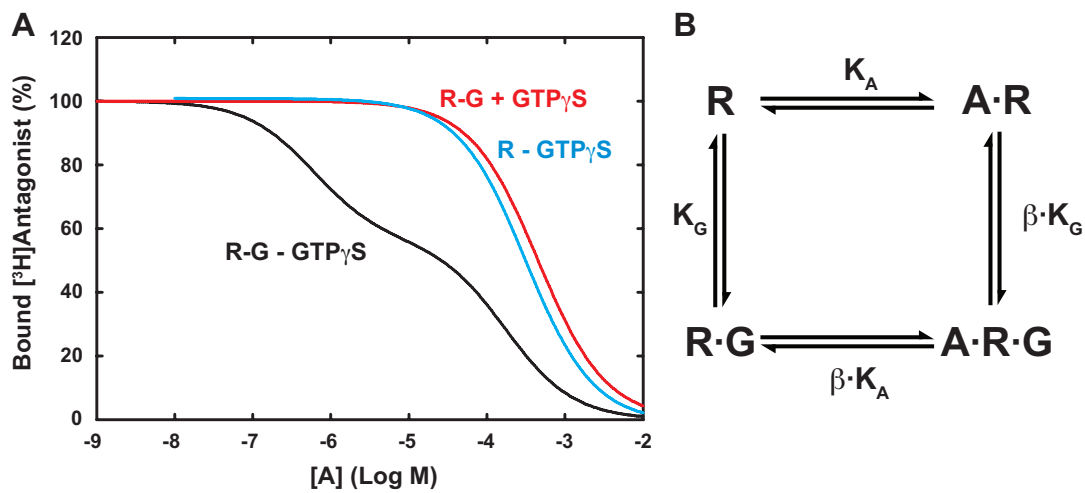


Figure 5. Simple receptor model for agonist binding

A. Curves represent typical agonist binding patterns determined by competition with radiolabeled antagonist (³H]Antagonist). In the absence of GTP_γS, (black curve, R-G - GTP_γS), agonist binding is biphasic with high and low affinity binding. In the presence of GTP_γS (red curve, R-G + GTP_γS), agonist binding becomes monophasic with only low affinity binding. This binding curve is indistinguishable from agonist binding curve in the absence of G_α (cyan, R - GTP_γS). Curves are from real measurements using the M1 receptor and G_{αq} reconstituted in phospholipid vesicles like those shown in Figure 24.

B. Simple receptor model for agonist binding. Receptor (R) can bind agonist (A) and G protein (G) at non-overlapping sites with association constants K_A and K_G. G-protein-bound receptor (R·G) binds agonist more tightly (β > 1) than receptor (R). R, receptor; A, agonist; G, G protein; K_A, equilibrium association constant for A·R complex; K_G, equilibrium association constant for R·G complex; β, cooperative factor.

effects of G protein and guanine nucleotides on the agonist binding are formulated in a simple receptor model (Figure 5B) Agonist-bound receptor, A-R, forms A-R-G complex, where $G\alpha$ enhances binding affinity for agonist. When a guanine nucleotide binds to the G protein, it drives dissociation of the G protein from agonist-bound receptor, resulting in an A-R complex, which binds agonist with low affinity (De Lean et al., 1980). The negatively cooperative interaction between agonist-bound receptor and guanine nucleotides is at the center of this model and believed to be part of the mechanism by which agonist-bound receptor promotes nucleotide exchange reaction on $G\alpha$ subunits.

However, the simple receptor model does not explain biphasic agonist binding behavior. According to the model, G protein merely shifts the agonist binding to the left without changing the slope of binding. Therefore, although this model explains G protein-dependent creation of high affinity agonist binding, it does not explain why binding of G protein to receptor converts only a fraction of the binding sites to high affinity binding site. This discrepancy suggests that the receptor population consists of behaviorally heterogeneous receptor species (Damian et al., 2006; Damian et al., 2008; Hlavackova et al., 2005) but how the biphasic agonist binding behavior is related to agonist-regulation of receptor activity is poorly understood.

Receptor dimerization (Angers et al., 2002; Hebert et al., 1996) has been widely suspected as an underlying mechanism of biphasic agonist binding. Sunahara *et al.* recently reported that “monomerized” receptors form a high affinity binding site in the presence of G protein and retain full GEF activity (Kuszak et al., 2009; Whorton et al., 2007; Whorton et al., 2008). Further, they

claimed that single-affinity binding could be created by adding excess amount of $G\alpha$ subunit. This result, if correct, indicates receptor dimerization is not required for G-protein-dependent high affinity agonist binding and GEF function. However, it does not explain why agonist binding of receptors in membrane preparations and reconstituted phospholipid vesicles is biphasic and how the biphasic agonist binding is related to the regulation of GEF activity in native context.

Effect of GAP on the regulation of receptor activity

Although agonist activation of the receptor is the principle regulatory step in the activation of G protein, efficiency of G protein activation by agonist-activated receptor may be further regulated by GAPs. This possibility has been suggested by the observations where GAPs accelerate deactivation of signal without significantly inhibiting signal output. For example, Chen *et al.* demonstrated that in mouse lacking RGS9-1, the principle photoreceptor GAP, currents generated by photoreceptor cells decay slowly but the amplitude of the currents did not change (Chen et al., 2000). Similar effects of GAPs on termination and amplitude of G-protein-mediated signaling were reported for other receptors and GAPs (Doupnik et al., 1997; Zhang et al., 2002). In some cases, effectors (e.g. PLC- β) are themselves GAPs and how such effectors can be activated at the same time as they deactivate their own activator $G\alpha$ is puzzling (Berstein et al., 1992; Kozasa et al., 1998; Turcotte et al., 2008). For example, in the M1- $G\alpha_q$ -PLC- β 1 module, PLC- β 1 is a GAP as well as effector. The PLC- β 1 GAP increases the GTP hydrolysis rate (k_{off}) by > 1,000 fold (Biddlecome et al., 1996; Mukhopadhyay et al., 1999). According to the simple

GTPase monocyte shown in Figure 3, faster termination of the signaling in the PLC- β 1 could be intuitively explained because increased k_{off} increases apparent termination rate constant, $k_{\text{on}} + k_{\text{off}}$. However, it is not clear how the signaling module produces robust signal output in the presence of GAP activity because $> 1,000$ fold increase of k_{off} will drive the fraction of active $G\alpha_q$, $k_{\text{on}}/(k_{\text{on}} + k_{\text{off}})$, close to zero. A plausible explanation is that k_{on} might be somehow increased in the presence of a GAP to catch up with increased hydrolysis of GTP. In this case, conceptually, there seem to be two possible ways to increase k_{on} . First, the PLC- β 1 GAP could enhance intrinsic GEF activity of agonist-activated receptor. Second, sensitivity of $G\alpha_q$ to receptor could be increased in the presence of the PLC- β 1 GAP. However, these possibilities are fairly speculative and need to be experimentally tested.

Motivation of the thesis research

As described above, the M1- $G\alpha_q$ -PLC- β signaling module exemplifies problems found in G-protein-mediated signaling. From my perspective, there are two questions that remain unsolved regarding the biochemical mechanisms by which receptor activates G protein. First, what is the molecular mechanism of biphasic agonist binding and how is it related to the regulation of receptor activation? The biphasic agonist binding suggests that receptor population consists of behaviorally heterogeneous receptor species. However, their molecular identities, regulatory behaviors and roles in G protein activation are poorly understood. Second, PLC- β , acting as a GAP, might promote the G protein

activation by activated receptor. This can be achieved by directly potentiating catalytic activity of the receptor or increasing the sensitivity of $G\alpha_q$ to the agonist-activated receptor.

I believed these two problems could be addressed by investigating the effects of $G\alpha_q$ and PLC- β , either alone or combined, on the agonist-driven conformation changes of the M1 receptor. This idea prompted me to develop a conformational sensor for the M1 receptor. In Chapter 2, I will focus on how I developed the sensor and its optical and functional characterization in mammalian cells. In chapter 3, I will discuss the optical and biochemical characterization of the sensor in reconstituted phospholipid vesicles.

Chapter 2

Development of a FRET-based conformational sensor for the m1 acetylcholine receptor (m1 AChR) in mammalian cells

Introduction

Regulatory behaviors of GPCRs are the outcome of structural changes within receptor, which in turn, are driven by transient interactions with agonists and G proteins. Biophysical studies such as X-ray crystallography and molecular dynamics have revealed many aspects of the structural mechanisms by which agonist-driven local structural changes in a ligand binding site lead to the structural changes on the cytoplasmic surface, which enable the activation of G protein (Cherezov et al., 2007; Farrens et al., 1996; Palczewski et al., 2000; Rasmussen et al., 2011; Rosenbaum et al., 2007; Rosenbaum et al., 2011). By nature the structural changes of GPCRs are dynamic. Fluorescence-based conformational sensors have played important roles in understanding the effects of ligands and interacting proteins such as G proteins on the conformational dynamics of GPCRs.

Conformational sensors

Sensors based on environment sensitive fluorescent dye

First type of fluorescence-based sensors use environment-sensitive fluorescent dyes attached to the receptor to monitor the conformational changes

of the receptor. Conformational changes of a receptor alter the molecular environment around the dye, leading to the changes in fluorescence emission intensity and λ_{max} of the dye. Kobilka's group applied this method to investigate the effect of various types of ligands on the conformation of the β_2 -adrenergic receptor ($\beta_2\text{AR}$) (Gether et al., 1997; Gether et al., 1995; Swaminath et al., 2004). However, two problems limited the usefulness of the sensor. First, the agonist-driven fluorescence changes were too slow to result from activation-associated isomerization of the receptor (several seconds to several hundred seconds). Second, the regulatory behaviors of the sensor were not adequately characterized.

Sensors based on intramolecular fluorescence resonance energy transfer (FRET)

A second and more successful approach to fluorescence-based conformational sensors exploits intramolecular FRET. The first such FRET sensor used a covalently attached bimane FRET donor and tryptophan FRET quencher to monitor conformational change in $\beta_2\text{AR}$ (Mansoor et al., 1999; Yao et al., 2006). In the sensor, the bimane FRET donor was covalently attached at cytoplasmic end of transmembrane helix 6 of a modified $\beta_2\text{AR}$ where the tryptophan FRET quencher was genetically introduced at cytoplasmic end of transmembrane helix 5. The sensor was specifically designed to investigate the effect of various ligands on the salt bridge between the conserved DRY motif and a glutamate on the cytoplasmic ends of transmembrane helices 3 and 6, respectively. However, fluorescent and regulatory behaviors of the FRET-based

sensor were incoherently characterized in micelles and phospholipid bilayer respectively. Moreover, the sensor's ability to activate G protein was impaired and isomerization kinetics has not been reported. Because this approach requires purified receptors, application are limited to GPCRs whose purification is well established and the β_2 AR sensor has been the only example of this approach.

In another type of FRET-based sensors developed by Lohse' group, agonist-driven conformational changes of a receptor are also detected by exploiting intramolecular FRET (Hoffmann et al., 2005b; Vilardaga et al., 2003). In these FRET-based sensors, a FRET donor and acceptor are genetically engineered into a receptor at C terminus and ICL3 (intracellular loop 3) (Hoffmann et al., 2005b; Vilardaga et al., 2003). Agonist-driven conformational changes in ICL3 of a GPCR lead to changes in the distance between the FRET donor and acceptor. Because FRET efficiency is a function of distance between two interacting fluorescence dipoles, conformational changes of the receptor lead to changes in FRET efficiency. Because the sensor uses intramolecular FRET with fixed acceptor:donor stoichiometry, the ratio of acceptor emission to donor emission can be used to represent relative FRET efficiency (ratiometric FRET), which eliminates the laborious tasks of fluorescence spillover corrections. Initially many of such sensors were created using a CFP-YFP FRET pair and agonist-driven percent FRET change was <10%. In some cases, signaling activities were severely impaired in the sensors, presumably because the bulky YFP inserted in ICL3 inhibited the interaction with G protein. For example, the α_{2A} -adrenergic receptor and the M1 receptor sensors based on a CFP-YFP FRET pair did not

signal though displaying ~5% agonist-driven FRET changes (Hoffmann et al., 2005a; Jensen et al., 2009; Vilardaga et al., 2003). In an alternative approach, the YFP FRET acceptor in ICL3 of α_{2A} -adrenergic receptor was replaced with FIAsh, a fluorescein-based biarsenical dye, and both fluorescence response and signaling activity were improved (Adams et al., 2002; Griffin et al., 1998; Hoffmann et al., 2005a). In FIAsh-based sensors, FIAsh is conjugated to a receptor via reaction with a CCPGCC tetracysteine motif (TC), which is genetically engineered in ICL3 (Hoffmann et al., 2005b). The most salient feature of the sensor is compatibility with cellular measurements, such as fluorescence microscopy and various cellular functional assays. As opposed to the slow fluorescence changes of the β_2 AR sensors with environment-sensitive dyes, ligand-driven fluorescence changes of the FRET-based sensors in living cells were fast (< 1 second), which seemed reasonable for a signaling protein. However, this type of FRET sensors has never been reconstituted in phospholipid vesicles for quantitative studies, which are not feasible in cell-based experiments.

Principles of FRET and relevance to the development of a FRET-based sensor

Because this chapter is dedicated to the development of a FRET-based conformational sensor for the M1 receptor, I am going to introduce some of the important principles of FRET as related to the design and optimization processes for the sensor.

FRET is a function of distance between two interacting fluorescence dipoles. The distance dependency of FRET efficiency (E) is described in the Förster equation (Lakowicz, 2006):

$$E = 1/(1 + (R/R_0)^6)$$

E: FRET efficiency

R: distance between two fluorescence dipoles

R₀: Förster radius, R at which energy transfer efficiency (E) is 50%.

FRET efficiency (E) is inversely proportional to the 6th power of the distance between two fluorescence dipoles (Figure 6). Because of this distance dependency, a change in distance leads to a change in FRET efficiency only within a limited distance range (~0.5 x R₀ to ~1.5 x R₀), ~ Förster radius of a given FRET pair. Förster radii of widely used FRET pairs are usually ~50 Å. This distance matches the size of most cellular proteins, which makes FRET ideal for monitoring structural changes in proteins. In FRET-based conformational sensors, stimulus-driven conformational changes in a protein are associated with the changes in the FRET efficiency. Importantly, the sensitivity of FRET efficiency to distance change is the greatest when the distance between two interacting fluorescence dipoles (R) is equal to the Förster radius (R₀) (Figure 6). Therefore, in cases where distance changes are smaller than R₀, maximum FRET change will be achieved by optimizing donor-acceptor distance in a way that the distance is symmetrically away from Förster radius before and after stimulus. If stimulus-

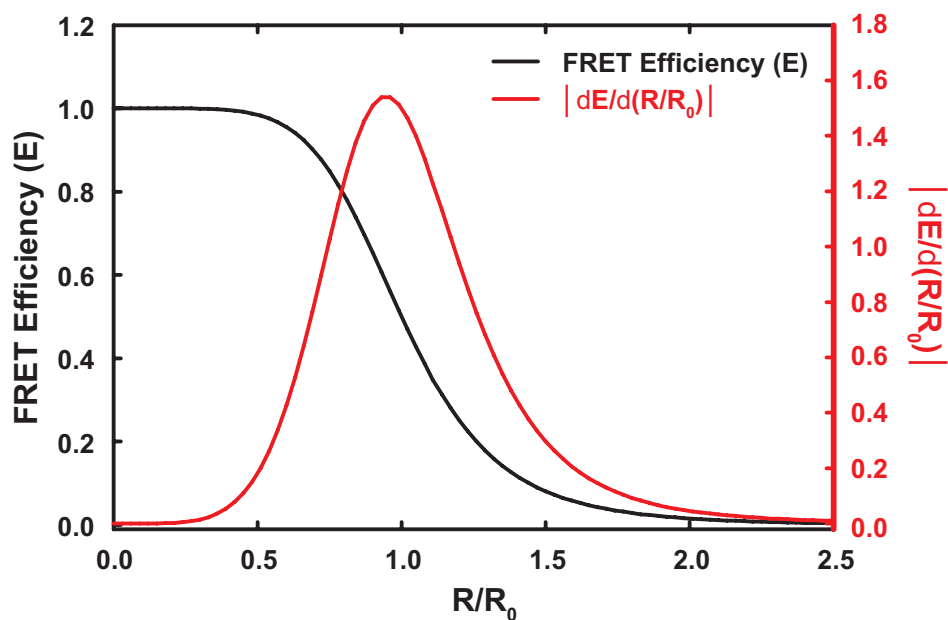


Figure 6. Relationship between FRET efficiency and distance between two interacting fluorescence dipoles

FRET efficiency (E , black plot, left vertical axis) and absolute value of first derivative of FRET efficiency ($|dE/d(R/R_0)|$), red plot, right vertical axis) are shown as functions of R/R_0 . $|dE/d(R/R_0)|$ shows sensitivity of the change in E in response to a change in distance, which is greatest at $R/R_0 = 1$. $E = 1/(1 + (R/R_0)^6)$. R , distance between two fluorescence dipoles; R_0 , Förster radius for a given FRET pair.

driven distance changes are bigger than R_0 , maximum FRET change will be accomplished by optimizing donor-acceptor distance around $0.5x R_0$ or $1.5x R_0$ depending upon the direction of the distance change.

FRET is also a function of the orientation factor (κ^2) of two interacting fluorescence dipoles;

$$R_0^6 = 9\Phi_0(\ln 10)k^2J/128\pi^5n^4N_A$$

Φ_0 : quantum yield of the donor

J : spectral overlap integral

k^2 : dipole orientation factor

n : refractive index of the medium

N_A : Avogadro's number

For two freely rotating fluorescence dipoles, the orientation factor averages to $2/3$. However, when the rotation of either one of two fluorescence dipoles is limited, FRET efficiency can be changed by varying the orientation between the two dipoles. Therefore, when rotational freedom of FRET donor and acceptor in a FRET-based sensor is limited, relative orientation could be optimized to improve the fluorescence response of the sensor. In cases where fluorescent proteins (FPs) are used as FRET donor and/or acceptor, relative orientation between donor and acceptor can be varied by introducing circular permutation to the FPs. However, it should be noted that circular permutation in an FP changes both orientation and distance between FRET donor and acceptor because the

fluorophore in an FP is much smaller than the size of an FP and probably quantum yield changes as well. Because FRET efficiency (E) is a complex function of distance (R) and orientation (k^2) between the two fluorescence dipoles, it would be ideal to optimize distance against varying orientations for the best results.

Experimental Procedures

Nomenclature

FRET ratio (FR) is the ratio of emission intensity at 530 nm to emission intensity at 475 nm upon excitation at 433 nm (for spectroscopy) and 430 nm (for microscopy). sFRET ratio is spectroscopic FRET ratio measured using fluorometer and mFRET ratio is microscopic FRET ratio measured using fluorescence microscope. Pro_n is an oligomer of n Pro residues. As only one type of HeLa tet-on cell line was used for the entire research, it will be simply referred to as HeLa cells. FP is a fluorescent protein. cpNcer is a circularly permuted cerulean CFP with new N and C termini after Nth and before (N+1)th residue of wild-type cerulean CFP, respectively.

Materials

[³H]-Quinuclidinyl benzilate ([³H]QNB)(50 Ci/mmol) was from Amersham Pharmacia Biotech; GTP γ S was from Boehringer Mannheim; carbachol, McN-A-343, oxotremorine, pilocarpine, pirenzepine and atropine were from Sigma; oxotremorine M was from Research Biochemicals International; arecoline was from Fluka; HeLa tet-on cells were from Clontech; and 293T cells were from Dr. Lily Jiang (UT Southwestern Medical Center at Dallas). Black wall 96 well optical bottom plates were from Nunc.

Sensor construction and expression

cDNA constructs for sensors were based on the human m1 AChR (the M1 receptor) modified to have; (1) a signal sequence and FLAG epitope preceding the wild-type N-terminus (MKTIIALSYIFCLVFADYKDDDDALIST); (2) no N-glycosylation sites (S4A and N12L); (3) six C-terminal His residues; and (4) a large deletion in the third cytoplasmic loop (described in the text). The cDNAs were transferred into the pcDNA3.1 vector (Invitrogen) for expression in mammalian cells.

To create sensors that report agonist-driven conformational changes according to changes in intramolecular FRET, a CFP or a circularly permuted cerulean CFP (cpNcer) was appended to the C terminus of the M1 receptor and an optimized CCPGCC tetracysteine motif (TC) plus SG at C-terminal end of the TC motif (Adams et al., 2002) was inserted into a shortened intracellular loop 3 (ICL3), as suggested by the work of Hoffmann (Hoffmann et al., 2005b). To create circularly permuted cerulean CFPs, the native N and C termini of cerulean were connected through a GGSGG sequence and new N and C termini were created at residues 49/50, 157/158, 173/174 and 229/230 using overlap extension PCR. The monomerizing A206K mutation was introduced into all the fluorescent proteins used in this research (Zacharias et al., 2002).

HeLa cells (100 mm dishes, 2×10^6 cells) were transfected with 15 μ g of DNA for 30–36 h using the Fugene 6 transfection reagent (Roche) as described in the instructions. Cells were grown in DMEM supplemented with 10% FCS.

FIAsh labeling and preparation of crude membrane fractions

Labeling conditions for FIAsh were optimized in many cell lines to secure stoichiometric labeling of the TC motif and the labeling was most efficient in HeLa cells. The HeLa cells do not express muscarinic acetylcholine receptors (confirmed by [³H]QNB binding) Therefore, unless mentioned, all the experiments presented here were performed using HeLa cells. HeLa cells that express sensor prototypes were labeled with FIAsh (Molecular Probes) 30 – 36 hours after transfection as described by Gaietta *et al.* except that the pH of the HBSS buffer was 6.4, which substantially increased labeling efficiency (Gaietta *et al.*, 2002). Cells were then harvested in a cold lysis buffer (20 mM NaHepes, pH 7.4, 2 µg/ml Leupeptin, 1 µg/ml Aprotinin and 0.1 mM PMSF) and lysed by passing through a 25 Ga needle 10-15 times. Nuclei were removed by centrifugation at 1 k x g for 5 min and membranes were pelleted by centrifugation at 100 k x g for 1 h. The pellet was washed twice with H₂O/M₂N₁₀₀ buffer (20mM NaHepes, pH 7.4, 2 mM MgCl₂, and 100 mM NaCl), and resuspended in an appropriate volume of H₂O/M₂N₁₀₀ buffer (~10 nM [³H]QNB binding sites). Protein content of the membrane preparations was measured according to the Bradford assay (Bradford, 1976). Labeled membranes were stored at –80 °C.

Measuring FRET using membrane preparations and ratiometric FRET

Fluorescence emission was measured at 30 °C with a Fluorolog®-3 spectrophotometer (JY-Horiba). Suspensions of labeled membranes were diluted in H₂O/M₂N₁₀₀ buffer (1–2 nM [³H]QNB binding sites) and incubated at 30 °C for

1-5 min before the fluorescence measurements. Each sample was excited at 433 nm (excitation maximum for CFP and cerulean CFP) and emission was scanned from 465 to 560 nm. Bandpass for both excitation and emission was 5 nm and integration time was 100 or 300 ms. Background fluorescence was determined using the same protein concentration of membranes from labeled cells that expressed wild-type M1 receptor. Fluorescence spectra were smoothed with a 7-point Savitzky-Golay algorithm (Savitzky et al., 1964). With a background-corrected spectrum, a FRET ratio (FR), ratio of acceptor emission at 530 nm (FA) to donor emission at 475 nm (FD) was calculated (Figure 8B). Percent change in FRET ratio upon ligand binding was calculated as $100 \times (FR_S - FR_B) / FR_B$, where FR_B , basal FRET ratio, is the FRET ratio in the absence of ligand and FR_S , stimulated FRET ratio, is the FRET ratio in the presence of ligand. FR_B and FR_S were measured in triplicate. Average values and standard deviations derived from triplicate measurements were used to calculate the percent change of FRET and errors. Errors were calculated by propagating standard deviations at each step of operation.

Measurement of intracellular Ca^{2+} concentration

Transfected HeLa cells were trypsinized 24 h after transfection and dispensed into 96-well plates (black well transparent bottom plates, Nunc) at 3×10^4 cells/well. After an additional 18 h incubation, cells were incubated in HBSS (pH 7.4) containing 4 μ M Fluo-3-AM (Molecular Probes) for 30 min at room temperature and further incubated in HBSS for 45 min at 37 °C to complete the hydrolysis of the Fluo-3 AM ester. Unloaded fluorescent dye was removed by

washing cells twice with HBSS. If cells were labeled with FIAsh, labeling was done before loading with Fluo3-AM. Time traces of Fluo-3 fluorescence ($\lambda_{ex} = 485$ nm and $\lambda_{em} = 538$ nm) were measured with a Fluoroskan Ascent Microplate fluorometer. Fluorescence emission was acquired every 3 seconds and integration time was 50 ms. Baseline fluorescence was measured for 90 s before addition of carbachol (CCh). Cytosolic Ca^{2+} concentration was calculated as $[Ca^{2+}] = K_d \times (F - F_{min}) / (F_{max} - F)$ where K_d is the dissociation constant for Ca^{2+} binding to Fluo-3 (380 nM), F is the Fluo-3 fluorescence in the experiment, F_{min} is fluorescence after addition of 1 μ M ionomycin plus 1 mM EDTA, and F_{max} is fluorescence after the further addition of 25 mM Ca^{2+} .

Homology modeling of the M1 receptor

Homology-modeled structures of the M1 receptor were generated in SWISS-MODEL using the crystal structures of rhodopsin in its inactive state (pdb 1F88) and active state (pdb 3CAP) as templates. Homology-modeled active state structure of M1 receptor was aligned with opsin- G_t C-terminal fragment complex structure (pdb 3DQB) to estimate the distances between the TC motif insertion sites and G_t C-terminal fragment (Scheerer et al., 2008). Transmembrane helices shown in Figure 9 were predicted using 'The HMMTOP Server.'

[3 H]QNB binding assay

Binding assays on wild-type M1 receptor and M1 sensors in HeLa cell membrane preparations were performed using (-)-[3 H]QNB as a radioligand. Equilibrium binding affinity of (-)-[3 H]QNB to the M1 receptor in HeLa cell

membranes was determined by direct binding assays. In competition binding assays, membrane preparations were incubated with 0.5 or 2 nM (-)-[³H]QNB in H₂O/M₂N₁₀₀ buffer containing varying concentration of carbachol or pirenzepine at 30 °C for 1 hour (Berstein et al., 1992).

Data Analysis

Ligand binding, CCh-stimulated Ca²⁺ transient, and agonist-driven ΔFRET were analyzed using SigmaPlot (SPSS Software Inc.).

Microscopy

HeLa cells were trypsinized 24 h after transfection with an expression plasmid encoding a receptor prototype for second-generation sensor and dispensed into 35 mm glass bottom dishes (TetMak). After an additional 12-18 h incubation, cells were labeled with FIAsh as described above and used for imaging. Time-lapse fluorescence imaging was performed using an Axiovert 200M (Zeiss) controlled by Slidebook 3.0 software. For ratiometric FRET measurement, cells were excited at 430 nm (25) and emissions at 470 nm (30) and 535 nm (30) were sequentially acquired. Numbers in parentheses are the bandpass of the filters. One cycle of acquisition took ~1.2 sec. Ligands were manually added at desired time points and the addition was completed within a second. To minimize ligand mixing time, 2X and 3X ligand solutions were added. Baseline fluorescence was measured for ~23 seconds before agonist was added. After an agonist was added, agonist-driven fluorescence changes were measured for the following ~30 seconds during which agonist-driven FRET

change reached a plateau. Finally, agonist binding was blocked by the addition of 1 mM atropine (Atr) and agonist-driven fluorescence changes were reversed. Fluorescence images were analyzed with Image J software. Background-corrected images were used for the analysis. The intensities of cp173cer and FIAsH emissions were plotted against time and fitted with a single exponential equation to obtain the baseline. To determine the baseline, data points resulting from agonist activation were omitted. To create the time traces of cp173cer and FIAsH emission, baseline-corrected fluorescence was normalized to 1. Time traces of FRET ratio, FIAsH/cp173cer, were created using normalized time traces of cp173cer and FIAsH emission. The maximum change in FRET ratio in response to a given concentration of agonist was calculated by averaging 5-10 points on the plateaus of agonist-driven FRET changes.

Results

Initial design and optimization of labeling site for FIAsh in ICL3

The sensor is intended to detect activation-associated movement of intracellular loop 3 (ICL3) of the receptor by intramolecular FRET from CFP FRET donor at C-terminal end to FIAsh FRET acceptor in ICL3 (Figure 7). Therefore, in order to create a successful FRET sensor, it was critical to optimize the placement of the TC motif, the labeling site for FIAsh FRET acceptor, and the CFP FRET donor. The starting construct for optimization was the human m1 AChR (M1) simplified by removal of much of the large ICL3 and N-terminal N-glycosylation sites (refer to Experimental Procedures). While this construct is probably deficient in desensitization (Haga et al., 1996; Lameh et al., 1992; Maeda et al., 1990), it retained full signaling activity in reconstituted systems (D. Liu, unpublished). The receptor variant will be referred to as M1-Del. Subsequent constructs were based on this prototype. To facilitate the optimization processes, a membrane-based fluorescence assay was devised. In the assay, HeLa cells were transfected with expression plasmids for receptor variants with a TC motif and labeled with FIAsh (Figure 8A). Crude cellular membrane fractions were prepared from the labeled cells and used to measure changes in FRET in response to carbachol (CCh), a muscarinic full agonist (Figure 8B)(for details, refer to Experimental Procedures).

The TC motif insertion site in ICL3 was first optimized by scanning for sites near helices 5 and 6 with the CFP FRET donor fused to the receptor at the native C-terminus (Figure 9). A SG linker was added at the C-terminal end of the

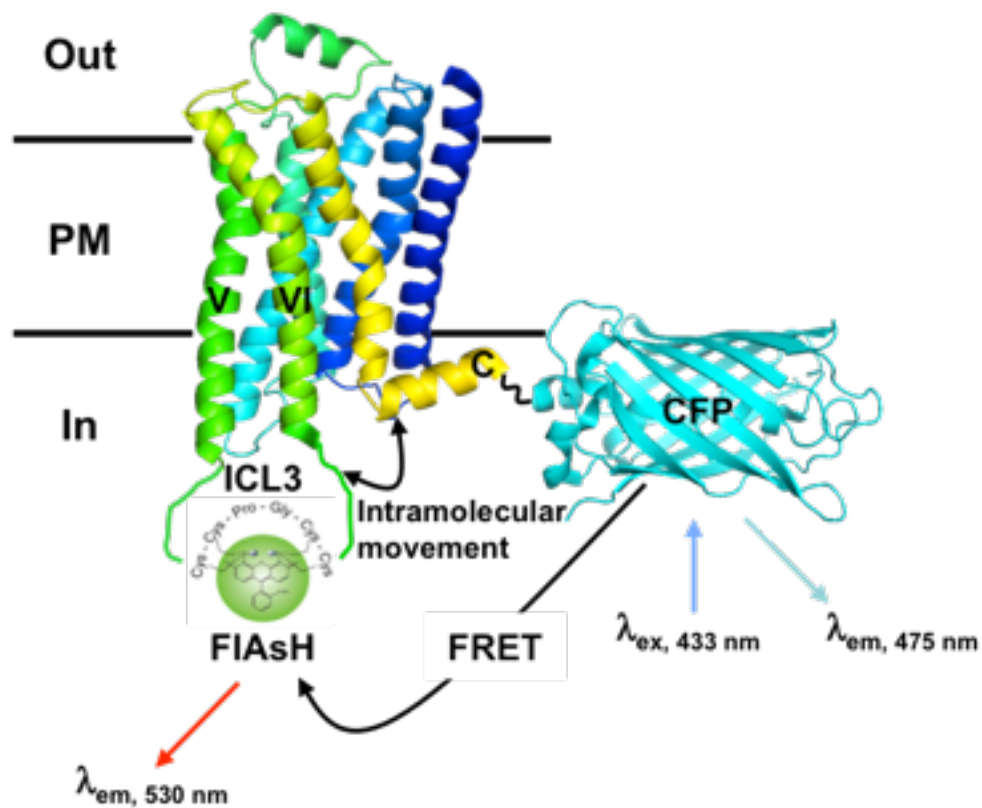


Figure 7. Diagram of a FRET-based conformational sensor for GPCR

To create a biosensor, a CFP FRET donor is added to the C terminus of the receptor and a CCPGCC TC motif for reaction with the FRET acceptor FIAsh is introduced into the shortened intracellular loop 3 (ICL3). CFP is excited at 433 nm and CFP and FIAsh emission are acquired at 475 nm and 530 nm, respectively. The diagram uses crystal structures of bovine rhodopsin (pdb 1F88) and CFP (pdb 2WSN). Out, extracellular space; In, intracellular space; PM, plasma membrane; V and VI, transmembrane helices 5 and 6.

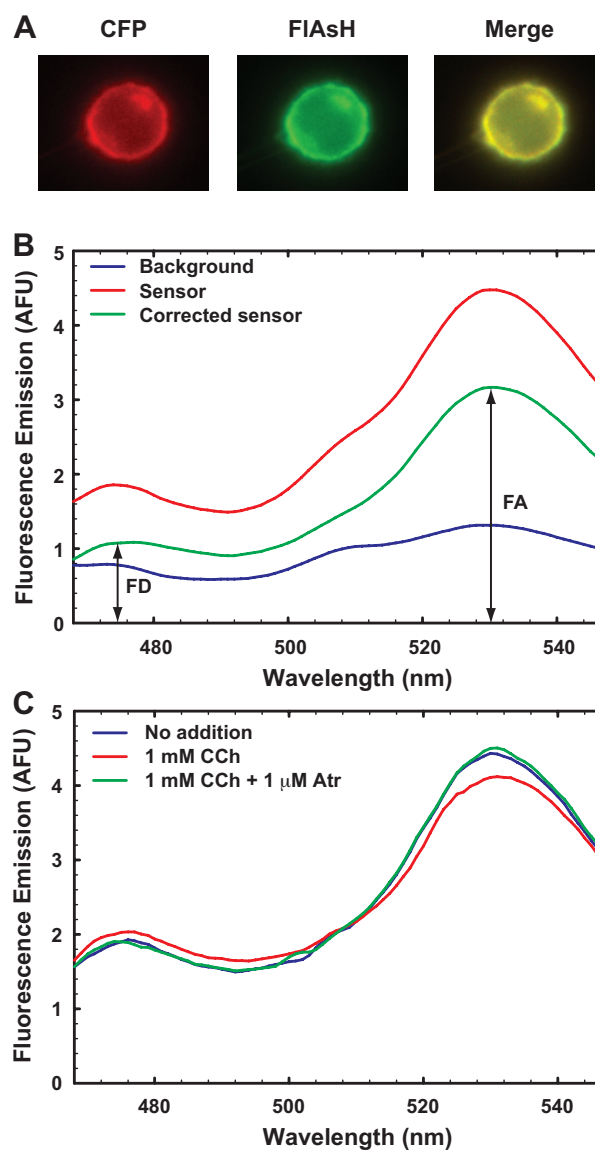


Figure 8. Expression and fluorescence emission of a M1 biosensor

A. An early sensor prototype was expressed in HeLa cells and labeled with FIAsH. CFP, direct excitation of CFP showing expression and localization of the sensor. FIAsH, direct excitation of FIAsH at 510 nm. Merge, merged image of CFP and FIAsH. B. Fluorescence emission spectra of HeLa cell membranes used for the calculation of the FRET ratio. Sensor, spectrum of membranes with FIAsH-labeled M1S-1. Background, membranes from cells that express wild-type receptor and labeled with FIAsH to quantitate nonspecific labeling. Corrected sensor, “sensor” minus “background”. C. Background-corrected spectra of membranes measured without addition (buffer), with 1 mM CCh or with both 1 mM CCh and 1 μ M Atr. Each spectrum was obtained with a separate sample because of irreversible bleaching of the fluorophores. The spectra were smoothed as described in Experimental Procedures.

TC motif for all of the initial constructs. Because the presumed cytoplasmic extension of helix 6 probably experiences substantial rotational movement upon activation (Dunham et al., 1999; Farrens et al., 1996; Ghanouni et al., 2001), I scanned residues K342 to K359 near helix 6 for C-terminal end of the TC motif, and tested sparsely spaced positions near helix 5 for the N-terminal end (Figure 9). Placing the TC motif between A223 and K359 produced a sensor that displayed a ~10% decrease in FRET in response to 1 mM CCh, and that decrease was blocked by atropine, a muscarinic antagonist (Figures 8C and 9). During this process, I noticed that basal FRET ratio and the fractional change in FRET promoted by agonist varied somewhat from day to day and this variation was primarily related to the quality of membrane preparations and the expression level of a construct, which in turn was determined by transfection efficiency. Data sets were therefore compared using a common construct in each experiment.

Oligo-proline spacer to extend the C-terminal placement of the CFP FRET donor

To increase the effect of agonist on the FRET signal, I next varied the position of the CFP FRET donor in the C-terminal end of the M1 receptor. I noted that the CCh-driven FRET change in the first group of constructs varied significantly even among the TC motif insertion site variants that displayed similar basal FRET ratios (0 to 10%). This suggested that the primary determinant of agonist-driven FRET change is a conformational change in ICL3 rather than a movement of the C-terminal CFP moiety. I therefore used only the best TC motif placement to optimize the CFP fusion site to bring the distance between CFP and

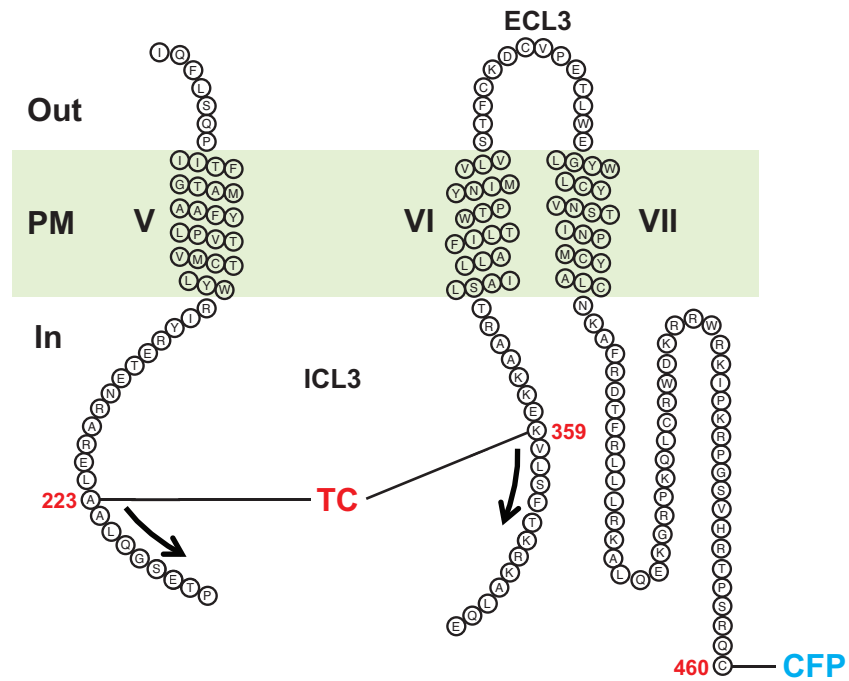


Figure 9. Optimized placement of a TC in ICL3 of the M1 receptor

Initial sensor constructs contained a shortened ICL3 (at least residues 232-341 removed). Placement of the TC, CCPGCCSG, was varied over the regions indicated with arrows in the diagram, and the TC linked A223 and K359 in the M1S-1 construct.

FIAsH as close as possible to the Förster radius R_0 , where the change in FRET with change in distance is maximal. In the initial set of constructs with CFP at progressively deleted C terminus, constructs with CFP at most deleted C termini (S451, K447 and R443 in Figures 10A and B) displayed higher basal FRET ratios than the starting construct (C460), but decreased CCh-driven FRET changes. These changes suggested that the two fluorophores were getting closer to each other with greater deletion. In this case, if the distance is shorter than Förster radius of the CFP-FIAsH FRET pair, basal FRET will increase but CCh-driven FRET change will decrease. Consistently, in all of the available crystal structures of GPCRs, the C-termini form helical structures stretching away from ICL3 (Figure 7)(Cherezov et al., 2007; Chien et al., 2010; Palczewski et al., 2000; Shimamura et al., 2011; Warne et al., 2011; Wu et al., 2010; Xu et al., 2011), where the FIAsH is attached. Therefore, it might be possible that extension of the distance would increase the FRET response.

To test whether extending the distance between the fluorophores would improve the FRET response, I inserted relatively inflexible oligo-proline (Pro_n) spacers (Stryer et al., 1967) between native C terminus (C460) and the CFP (Figure 10A). The basal FRET ratio dropped with more Pro residues (Pro_6 to Pro_{12}), suggesting that the Pro_n spacers extend the distance between the fluorophores. Importantly, the extensions increased the CCh-driven FRET change to a maximum at about 6 Pro residues (Figure 10C) ($P < 0.05$, $n=3$).

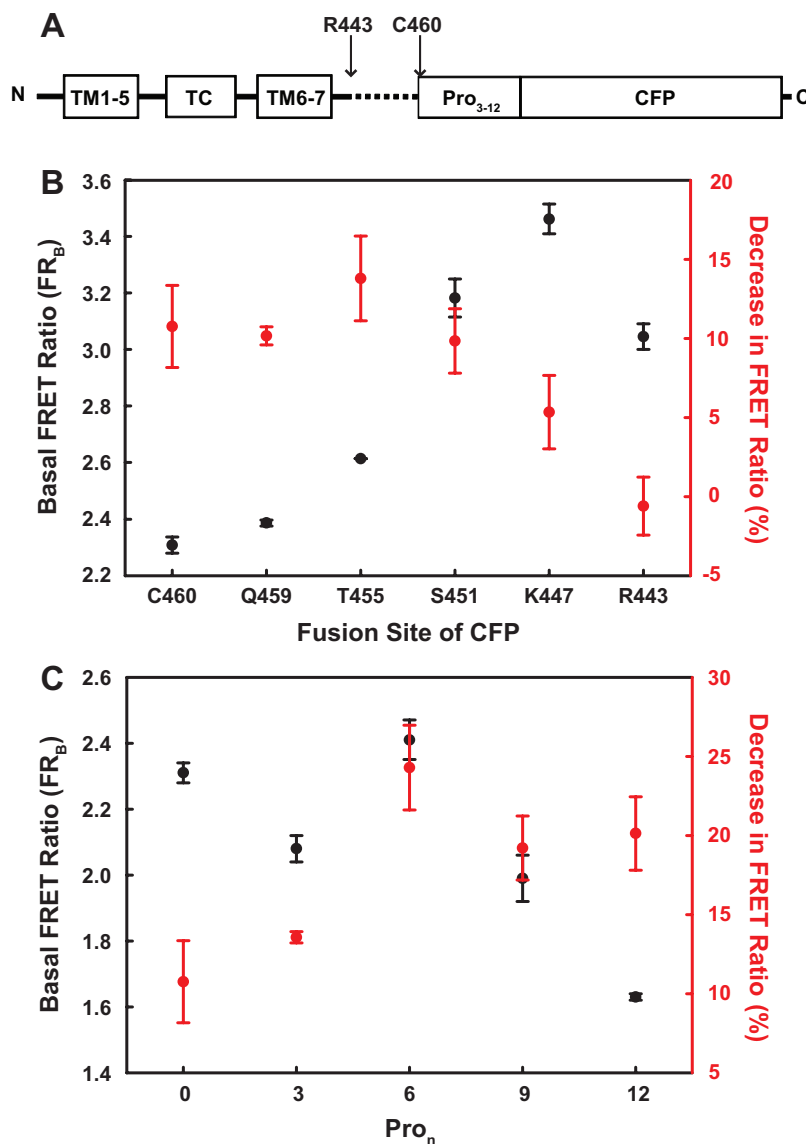


Figure 10. Optimization of a fusion site for CFP at C terminus of the receptor

A. The position of the CFP donor was varied by truncation of wild-type C-terminal residues before the attachment site or by introduction of oligo-proline sequences (Pro_n) after C460, as shown in panel A. Membrane preparations prepared from FIAsh-labeled HeLa cells expressing these variants were used to measure basal FRET ratio (FR_B) and CCh-stimulated FRET ratio (FR_S). Decrease in FRET ratio (%) in response to 1 mM CCh was calculated as described in Experimental Procedures. B. Sensors with CFP after truncated C-terminal domains. C. Sensors with CFP after oligo-proline sequences. Data are averages and standard deviations from triplicate measurements. Similar results were reproduced in a separate experiment. Pro_n , oligo-proline spacers with n Pro residues.

Circularly permuted CFP FRET donor increases the agonist-driven FRET change

Because FRET is also a function of the relative orientation between two fluorophores, I examined whether varying orientation between the CFP FRET donor and FIAsh FRET acceptor could increase CCh-driven FRET change. To vary the orientation, I replaced the CFP FRET donor with circularly permuted cerulean (a variant of CFP) (Rizzo et al., 2004). I started using cerulean because of improved optical properties (e.g. brightness). In a circularly permuted cerulean, native N and C termini were connected with a short flexible linker and new N and C termini were created at indicated residues shown in the structure of cerulean (Figure 11A). I created 4 different circularly permuted ceruleans designed to rotate the FP fluorophore as much as possible. Among 4 circularly permuted ceruleans, one with new N and C termini created at a.a. 173 of cerulean (cp173cer) substantially increased the CCh-driven FRET change (Figure 11B) ($P < 0.05$, $n=3$).

Optimization of a fusion site for a circularly permuted cerulean (cp173cer); first-generation sensor

As the size of actual fluorophore (shown in cyan, Figure 11A) of cerulean is much smaller than that of the entire protein, circular permutation of cerulean also substantially changes the distance factor. Therefore, C-terminal placement of cp173cer needed to be re-optimized regardless of initially optimized site for CFP (with Pro₆ spacer). I examined the effect of C-terminal placement of cp173cer with deletion and oligo-proline spacers on the CCh-driven FRET

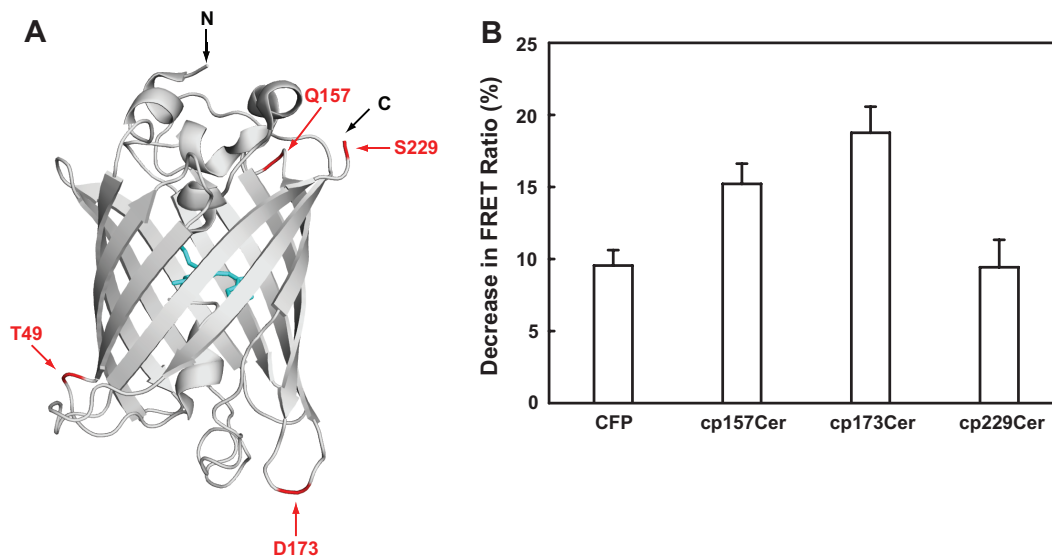


Figure 11. Effect of circular permutation of cerulean on CCh-driven FRET change

A. To create circular permutations of cerulean CFP, native N and C termini were connected through GSSSG linker and new N and C termini were created next to the residues indicated with red arrows in the structure of cerulean (pdb 2Q57). B. Decreases in FRET ratio in the presence of 1 mM CCh. Data are averages and standard deviations from triplicate measurements. Similar results were reproduced in a separate experiment using other membrane preparations. cp49cer did not fluoresce.

change. Placement of cp173cer was varied from G450, a 10 amino acid deletion, to an extended C terminus with up to Pro₁₂. Initially, because sensors are expressed several fold better in 293T cells than in HeLa cells, I examined the effect of C-terminal placement of cp173cer in 293T cells. The placement of cp173cer at V452 with 8 amino acids deleted from the C terminus stood out among the constructs tested. Based on the result in 293T cells, I chose a construct with cp173cer at V452 as the first-generation sensor. It should be noted that there was a SG linker at the C-terminal end of the TC motif. However, in HeLa cells, combined effect of C-terminal placement and cp173cer was no better than the effect of cp173cer or Pro₆ alone. I do not clearly understand the reason but sub-optimal labeling conditions in 293T cells might be one reason. FRET ratio for a construct was lower in 293T cells and thus, fractional CCh-driven FRET changes (%) in 293T cells were ~60% of the changes in HeLa cells. For the first-generation sensor (M1S-1-FIAsh) in HeLa cell membrane preparations, maximal CCh-driven decrease in FRET ratio was ~20% and the change was blocked by atropine, indicating that the CCh-driven decrease in FRET ratio resulted from CCh-driven conformational changes in the receptor. Characterizations of the first-generation sensor were all performed using HeLa cells.

The first-generation sensor loses signaling function in cells

Although the first-generation sensor faithfully reported agonist-driven conformational changes of the M1 receptor in membrane preparations, its signaling function in cells was severely impaired. To assess the signaling activity of the sensor, I examined CCh-stimulated Ca²⁺ transients after expression of

either the wild-type M1 receptor or the sensor in HeLa cells. In cells that expressed the wild-type M1 receptor, CCh elicited typical cytosolic Ca^{2+} transients and this activity was not inhibited by labeling the cells with FIAsh (Figures 12A and B and Table 1). However, the ability of M1S-1 to elicit Ca^{2+} transient was only ~10% that of wild-type M1 receptor as indicated by ~8 fold increase in EC_{50} (from ~80 nM to ~600 nM)(Figure 12B and Table 1). The signaling activity was further inhibited to ~1% by the labeling of M1S-1 with FIAsh as indicated by additional ~8 fold increase in EC_{50} (from ~600 nM to 5 μM) and the maximal $\Delta[\text{Ca}^{2+}]_{\text{cyto}}$ reduced by 50% (Figure 12B and Table 1). Because the expression level of the M1S-1 was ~2 fold higher than that of wild-type M1 receptor, signaling activity of M1S-2-FIAsh was less than 1% of that of wild-type M1 receptor.

Signaling activity of M1S-1 was similar to that of M1S-1 without the cp173cer moiety and the simplified M1 receptor (M1-Del), which has no C-terminal deletion (Table 1), indicating that the placement of cp173cer at the deleted C terminus and C-terminal deletion itself were not responsible for the reduced signaling activity. Therefore, it was clear that the placement of the TC motif in ICL3 and formation of the TC-FIAsh complex compromised the signaling function in the first-generation sensor.

FIAsh is known to generate reactive oxygen species (ROS) upon illumination and compromise the function of nearby proteins (Marek et al., 2002). However, addition of ROS scavengers and reduced illumination time did not prevent the reduction of the CCh-stimulated Ca^{2+} transient by the labeling with FIAsh. The TC motif is short and presumably flexible by itself when it is reduced

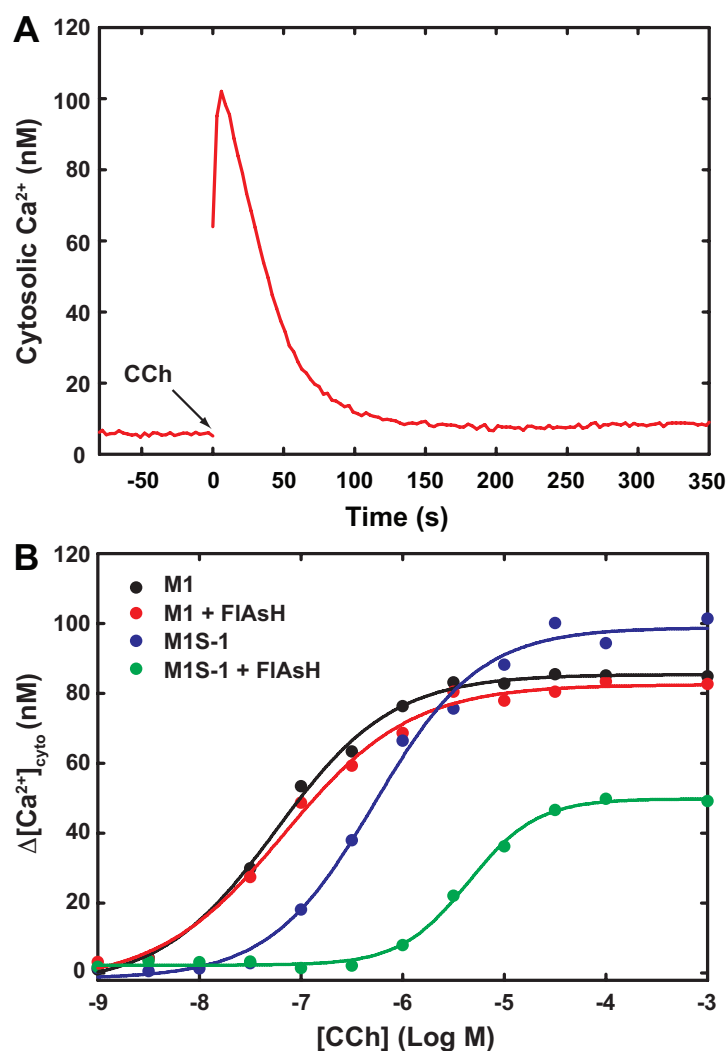


Figure 12. Agonist-stimulated Ca^{2+} transients are inhibited in cells that express the first-generation biosensor

Cells that transiently expressed either the wild-type M1 receptor or M1S-1 were used for the Ca^{2+} assays. A. Time course of the CCh-stimulated cytosolic Ca^{2+} transient in HeLa cells that expressed the wild-type M1 receptor. At $t = 0$ s, 1 mM CCh was added to stimulate the receptor. $\Delta[\text{Ca}^{2+}]_{\text{cyto}}$ is the difference between the peak and the baseline cytosolic Ca^{2+} concentration. B. Cells that expressed either wild-type M1 receptor or M1S-1 were labeled with FIAsh (+FIAsh) or mock-labeled before the Ca^{2+} assays. $\Delta[\text{Ca}^{2+}]_{\text{cyto}}$ is plotted against the logarithm of the carbachol concentration and fitted with a sigmoidal dose-response curve with varying slope ($\Delta[\text{Ca}^{2+}]_{\text{cyto}} = \text{min} + (\text{max} - \text{min}) / (1 + 10^{((\text{Log EC}_{50} - L) \cdot \text{Hillslope}))}$). L, log [CCh]; min and max, minimal and maximal $\Delta[\text{Ca}^{2+}]_{\text{cyto}}$. For the wild-type M1 receptor, data for 3 and 10 nM CCh were omitted because of slowly rising small Ca^{2+} peaks. EC_{50} values are summarized in Table 1.

but when labeled with FIAsH it becomes relatively inflexible because its four Cys residues chelate two arsenates in the rigid planar structure of FIAsH. In the sensor, TC motif was placed near residues involved in the activation of G protein and thus it seemed possible that the TC motif and TC-FIAsH complex might have altered the local structures required for the activation of $G\alpha_q$.

Creation of a second-generation sensor; re-optimization of the insertion site for the TC

To test the idea that the TC motif changed structures important for the activation of $G\alpha_q$ and that FIAsH labeling made it worse, I modeled this region of the M1 receptor and constructed new sensors that were altered in this region. In order to homology-model the structure of the M1 receptor, I chose the crystal structures of rhodopsin, because rhodopsin was the only GPCR whose interaction with $G\alpha$ had been seen in a crystal structure (Scheerer et al., 2008). First, I generated a homology-modeled structure of the M1 receptor using the SWISS-MODEL server (Arnold et al., 2006) with the structure of bovine rhodopsin in the inactive state (Palczewski et al., 2000) as a template (Figure 13A). According to the homology-modeled structure, in the first-generation sensor (M1S-1-FIAsH), the N- and C-terminal ends of the TC motif (A223 and K359) were both in the middle of cytoplasmic extensions of transmembrane helices 5 and 6 (Figure 13A). Considering the dimension of the cytoplasmic extensions and a TC motif, the motif was presumed to connect cytoplasmic helical extensions 5 and 6 with limited flexibility. The distance between two backbone carbons of A223 and K359 was $\sim 20\text{\AA}$ and the length of a fully

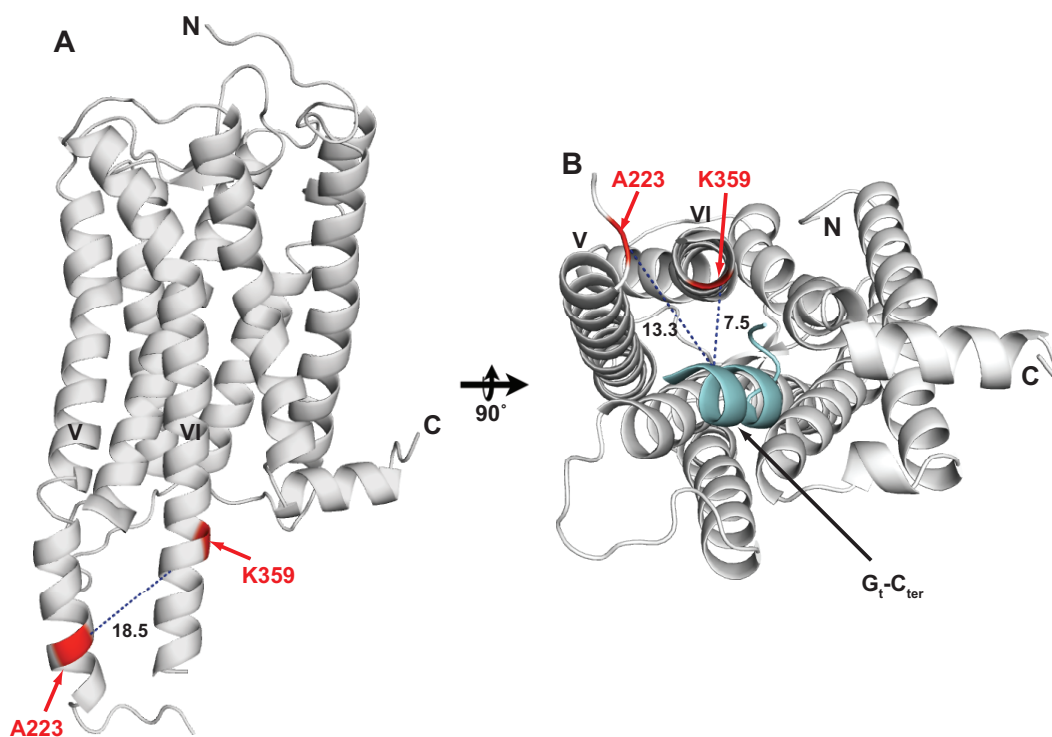


Figure 13. Homology-modeled structures of the M1 receptor

A. Homology-modeled structures of the M1 receptor were created in SWISS-MODEL using a crystal structure of bovine rhodopsin in inactive state (pdb 1F88) as a template. Indicated residues (A223 and K359) are N and C terminal insertion sites of the TC in the first generation sensor. B. View of cytosolic face of a homology-modeled structure of the M1-G_t-C_{ter} (G_t-C_{ter}, C-terminal fragment of G_t) complex. To create the complex structure, first, active state structure of the M1 receptor was homology-modeled using the crystal structure of opsin in active state (pdb 3CAP) as a template (white). Then, the homology-modeled receptor structure was aligned with the structure of opsin-G_t-C_{ter} complex (pdb 3DQB) using PyMol. Finally, the structure of opsin in the alignment was removed. G_t-C_{ter} (cyan) is indicated with an arrow.

stretched TC motif (including one SG linker) would be little longer than 20Å. Therefore, depending upon where the insertion sites are located in two helical wheels, a TC may be tilted, to varying degrees, toward the central axis of seven helical bundle or away from the axis.

I noticed two potential problems from this structural analysis. First, connection of cytoplasmic ends of helix 5 and 6 by the TC motif might be too tight to allow the full rotational movements of transmembrane helices 5 and 6, which is believed to be a common structural mechanism of GPCR activation (Dunham et al., 1999; Farrens et al., 1996). Second, if a TC motif is pointing toward the central axis of the helical bundle, formation of FIAsh-TC complex can sterically interrupt the interaction of the receptor with $G\alpha$ as the distance between the TC motif insertion sites and C terminus of $G\alpha$ subunit would be only ~10 Å, which could be covered by the TC-FIAsh complex (Figure 13B) (Scheerer et al., 2008).

According to these structural speculations, it seemed possible to restore the receptor function (or interaction with $G\alpha$) through a two-step optimization processes. First, restriction of the rotational movements of helices 5 and 6 by the TC motif needs to be relieved. Second, the TC motif needs to be pointing away from the central axis of helical bundle. To test this idea, I first examined whether relocation of the TC motif could improve signaling function of the sensor. I speculated that the TC could be moved to the opposite side of the helices by changing either the N- or C-terminal insertion site of the TC motif along the helical extensions 5 and 6. Therefore, I scanned residues from E221 to P231 for a N-terminal end of the TC motif (Figure 14A). I did not change the C-terminal end of the TC motif (K359) because during initial placement, I noticed this site

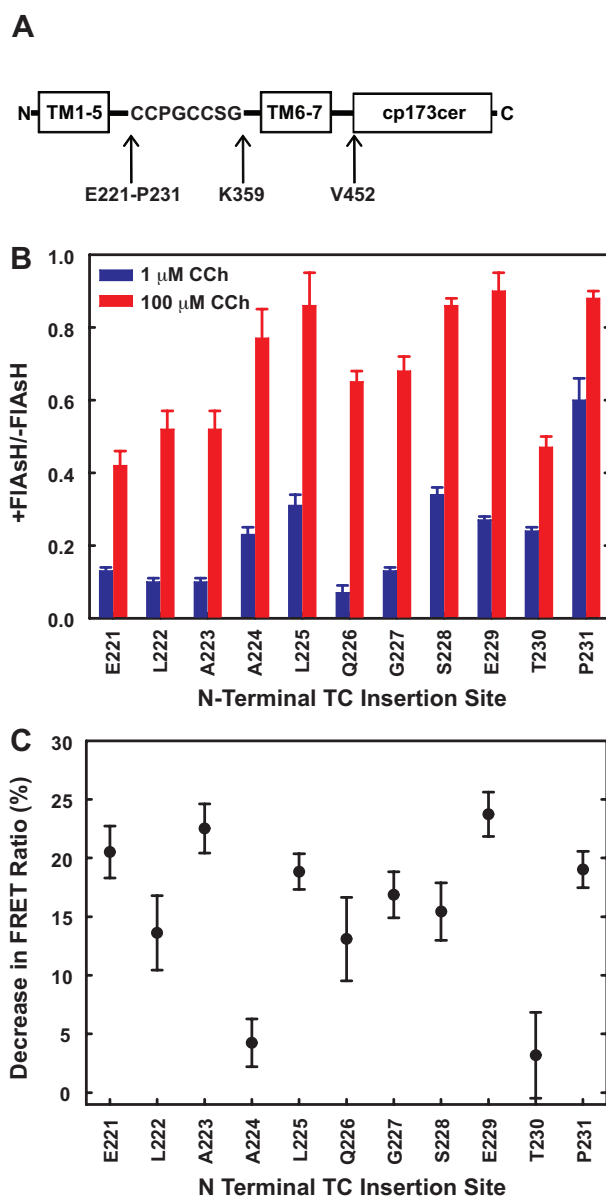


Figure 14. Re-optimized placement of the TC reduced the inhibition of signaling by FIAsH

First-generation sensors were created with the TC at various sites in ICL3 as shown in panel A, with all TC sequences terminating before K359. B. Cells that express each construct were either labeled with FIAsH or mock-labeled (no FIAsH) and tested for cytosolic Ca^{2+} transients in response to either 1 μM or 100 μM CCh as shown in Figure 12A. The graph shows the ratio of the peak Ca^{2+} responses in labeled and mock-labeled cells for each CCh concentration. The residue that precedes the TC motif in each construct is shown on the X axis. Data are averages and ranges from duplicate measurements. C. Membranes from cells that express the same constructs were assayed for change in FRET in response to 1 mM CCh. Data are averages and standard deviations from triplicate measurements.

was critical for the CCh-driven FRET change. First, each construct was tested for the CCh-stimulated Ca^{2+} transient in HeLa cells. To expedite the process, I used only two concentrations of CCh, 1 μM (subsaturating) and 100 μM (saturating). These two concentrations were chosen because (1) the 100 fold difference covers the dynamic range of pharmacological responses and (2) the concentration range would cover the EC_{50} of labeled M1S-1 ($\sim 10 \mu\text{M}$) and thus any change (both positive and negative) in receptor function should be detected with these two concentrations. In many of the constructs, FIAsh suppression of the CCh-stimulated Ca^{2+} transient was significantly alleviated (Figure 14B). For example, in L225, S228, E229, and P231, there was only about 10% inhibition at 100 μM CCh. However, at low concentration of CCh, inhibition was still larger than 50% (except P231). Interestingly, FIAsh inhibition of CCh-stimulated Ca^{2+} transient seemed to oscillate every 3 or 4 residues, which might reflect that N terminal insertion sites were indeed in a helical structure. The oscillatory pattern was more conspicuous at 1 μM .

In parallel, all the constructs were tested for CCh-driven FRET changes. Many of the constructs retained CCh-driven FRET changes comparable to the first-generation sensor ($\sim 20\%$) (Figures 14A and C). Among these, I chose only 3 constructs (S228, E229, and P231) for further modifications because (1) they displayed improved signaling function as well as relatively high CCh-driven FRET change ($>15\%$) and (2) the four consecutive residues (including T230) would completely cover one helical turn.

Creation of a second-generation sensor; effect of the length of linkers

The TC motif was also suspected to inhibit full signaling function of the receptor by restraining efficient rotational movement of transmembrane helices 5 and 6. To examine this possibility, I tested two flexible linkers, SG or SGGGS, between M1 and the TC motif at positions A223, S228, E229, P231 for the N-terminal end and K359 for the C-terminal end. (Figure 15A) The linkers were inserted at both N- and C-terminal ends of a TC motif in a symmetric manner. The effect of FIAsh labeling on the signaling function of these linker variants was tested with the simplified Ca^{2+} assay described in Figure 14B. For all the variants, both the SG and SGGGS linkers further alleviated the inhibition of CCh-driven Ca^{2+} transient by FIAsh labeling (Figure 15B). Notably, for the P231 construct with SGGGS linker, FIAsh labeling did not inhibit the CCh-driven Ca^{2+} transient.

In parallel, all the constructions were tested for CCh-driven FRET changes. Overall, the effect of linkers on CCh-driven FRET change varied depending upon insertion sites. Unfortunately, the SGGGS linker, which eliminated FIAsh inhibition of CCh-stimulated Ca^{2+} transient for the P231 construct, also reduced CCh-driven FRET change to only ~10%, making it less useful as a sensor (Figure 15C). Finally, I chose the P231 construct with the SG linker for the second-generation sensor because inhibition of the signaling function by the labeling with FIAsh was relatively small (~20%) at low concentration of CCh while its CCh-driven FRET change was relatively high (>15%).

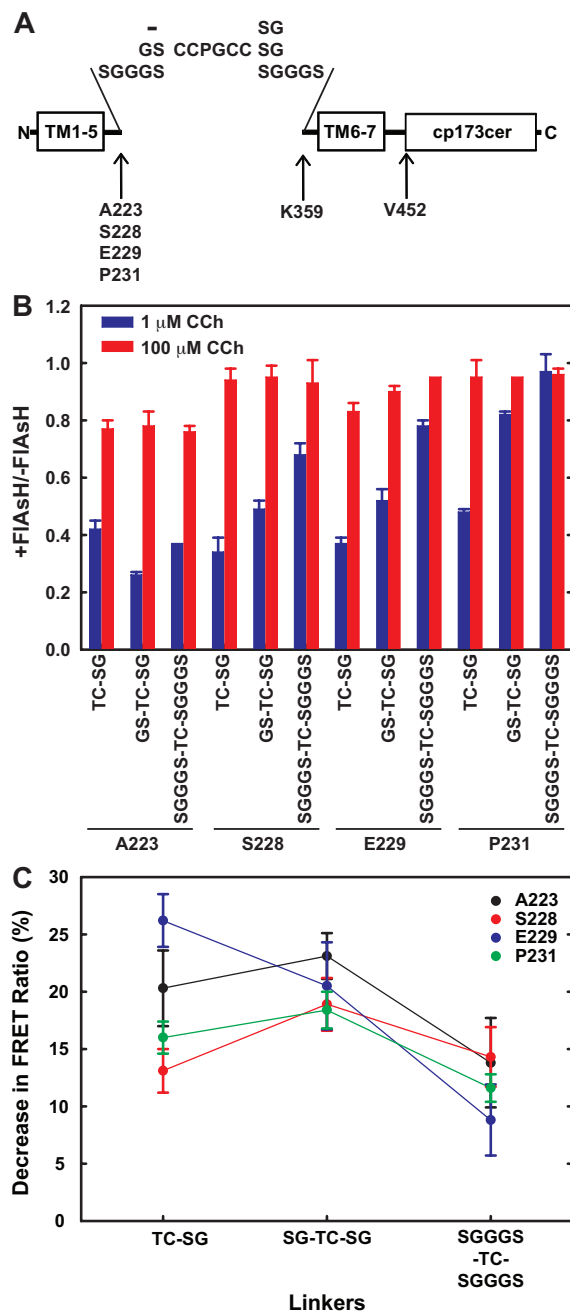


Figure 15. Effect of linkers surrounding the TC insertion site

Sensors similar to those shown in Figure 14 were created with linkers. TCs and linkers were inserted between the residues shown in panel B and K359. B. Cytosolic Ca^{2+} transients were measured in cells that express each construct, with or without FIAsH labeling, in response to 1 μM and 100 μM CCh. Data are averages and ranges from duplicate assays. C. CCh-driven FRET changes in membranes are shown for the same constructs. Data are averages and standard deviations derived from triplicate measurements. Similar results were reproduced in a separate experiment.

Change in intramolecular FRET is responsible for the agonist-driven FRET change

The sensor was designed to use intramolecular FRET from the cp173cer FRET donor at the C terminus to the FIAsh FRET acceptor in ICL3. In cells, however, FIAsh labeling was not highly selective for the TC motif under the conditions that enabled stoichiometric labeling (Figure 8B), which has also been observed by others (Stroffekova et al., 2001). Therefore, it might be possible that non-selectively labeled FIAsh contributed to the FRET and thus agonist-driven FRET changes.

To test this possibility, I first mutated the TC motif in ICL3 and examined its effect on the basal FRET ratio and CCh-induced FRET changes (Figures 16A and B). Mutation of the TC motif (M1S-2/sTC) markedly reduced FIAsh emission around 530 nm, resulting in decrease in sFRET ratio from ~2.4 to ~0.6, which was close to the emission ratio (530 nm/475 nm) of cp173cer by itself, indicating essentially no energy transfer. Moreover, CCh did not change the emission spectrum. Then, introduction of the TC motif next to cp173cer moiety (MS-2/sTC/C-TC) restored high FIAsh emission with sFRET ratio ~3.2 but not CCh-driven FRET changes (Figure 16A and B). These results clearly demonstrated that FIAsh attached to the TC motif in ICL3 is necessary and sufficient for FRET and CCh-driven FRET changes of the sensor.

The M1 receptor is known to form a homodimer (Goin et al., 2006; Hern et al., 2010). Therefore, it might have been possible that the CCh-driven FRET change was at least partly due to the change in intermolecular FRET from the cp173cer donor in one protomer to the FIAsh acceptor in the other protomer in a

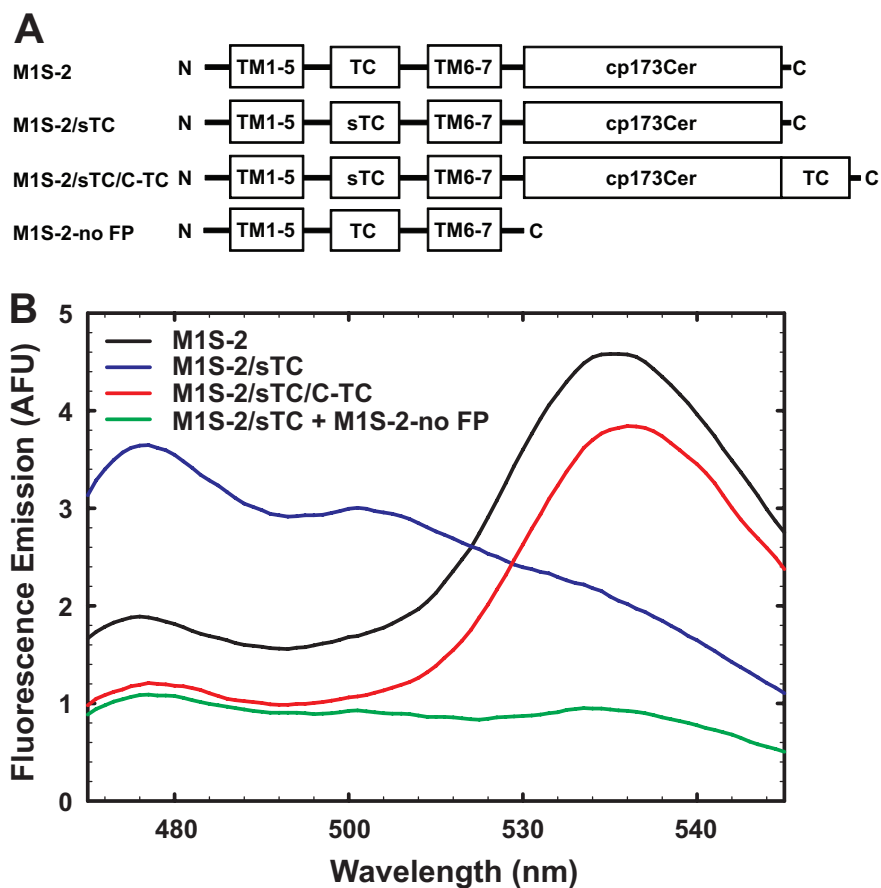


Figure 16. Intramolecular FRET of the sensor is responsible for the FRET and agonist-driven FRET changes

A. Variants of M1S-2 were constructed to contain either a scrambled TC (CGSPCGCGCS)(sTC), a scrambled TC plus an additional C-terminal TC (sTC/C-TC), or no fluorescent protein (no FP). B. Fluorescence spectra of membrane preparations from FIAsh-labeled cells expressing indicated constructs were measured with and without 1 mM CCh. Spectra without CCh are shown. CCh had no effect except for the standard M1S-2 membranes.

receptor dimer. However, when M1S-2/sTC and M1S-2-no FP were co-expressed as a FRET donor and an acceptor respectively, neither of which can emit around FIAsh emission maximum alone, the sFRET ratio was ~0.8, which was only ~20% the FRET ratio of standard sensor (M1S-2) and CCh did not change the emission spectrum (Figures 16A and B). Therefore, the CCh-driven FRET changes reflect agonist-driven structural changes occurring within a M1 receptor protomer.

Second-generation sensor retains wild-type signaling function in cells

Re-optimization of the TC motif placement and addition of a flexible linker markedly reduced the inhibition of agonist-stimulated Ca^{2+} transients by labeling with FIAsh, which was the main problem of the first-generation sensor. However, in the simplified Ca^{2+} assay used for the screening, it was difficult to estimate relative activity of the sensor to that of the wild-type M1 receptor. To evaluate the cellular signaling function, I examined CCh-stimulated Ca^{2+} transients after expression of either the wild-type M1 receptor or M1S-2. In cells that expressed M1S-2, the CCh-stimulated Ca^{2+} was reduced to ~35% of wild-type receptor with EC_{50} increased from ~100 nM to ~300 nM (Figure 17 and Table 1). Labeling these cells with FIAsh further reduced CCh-stimulated Ca^{2+} transient to ~20% of wild-type receptor with EC_{50} increased from ~300 nM to ~600 nM (Figure 17 and Table 1). Considering M1S-2 expressed ~2 fold higher than wild-type M1 receptor, overall signaling function of the sensor was ~10% that of the wild-type receptor. Nevertheless, the signaling function of the second-generation sensor was ~10 times better than that of the first-generation sensor.

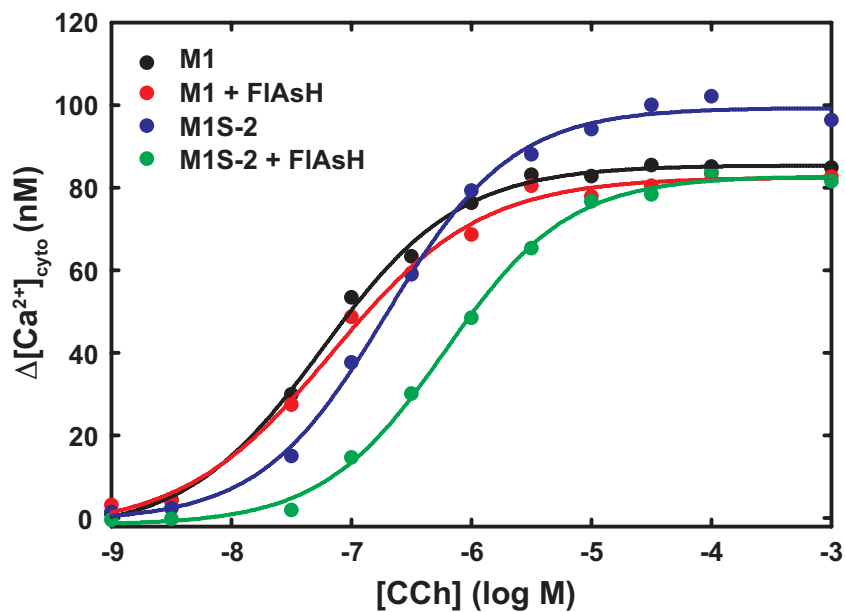


Figure 17. Inhibition of agonist-stimulated Ca^{2+} transient by FIAsh is substantially alleviated in cells expressing the second-generation sensor (M1S-2-FIAsh)

HeLa cells that expressed either the wild-type M1 receptor or the M1S-2 were labeled with FIAsh (+FIAsh) or control-treated before the Ca^{2+} assays. Control treatment was the same as FIAsh labeling except FIAsh was omitted. Data for cells expressing wild-type receptor are the same as those in Figure 12B. EC_{50} values are summarized in Table 1.

Receptor	Treatment	CCh-stimulated Ca ²⁺ transient, EC ₅₀ (nM)	Relative maximum $\Delta[\text{Ca}^{2+}]_{\text{cyto}}$
M1	No	90 ± 23 (n = 6)	1
M1	+ FIAsh	90 ± 20 (n = 4)	
M1S-1	No	620 ± 190 (n = 4)	~1.3
M1S-1	+ FIAsh	5100 ± 950 (n = 2)	~0.6
M1S-1 (no FP)	No	630 ± 210 (n = 2)	
M1S-1 (no FP)	+ FIAsh	ND	
M1S-2	No	300 ± 70 (n = 8)	~1.2
M1S-2	+ FIAsh	630 ± 40 (n = 8)	~1
M1-Del	No	280 ± 110 (n = 2)	
M1-Del	+ FIAsh	ND	

Table 1. Signaling activity of the sensor in cells

EC₅₀ of CCh-stimulated $\Delta[\text{Ca}^{2+}]_{\text{cyto}}$ in HeLa cells that expressed receptors shown. Cells were mock-labeled (No) or labeled with FIAsh (+ FIAsh) before the Ca²⁺ measurements. M1, wild-type M1 receptor; M1S-1, the first-generation sensor; M1S-1 (no FP), M1S-1 with no cp173cer; M1S-2, the second-generation sensor; M1-Del, simplified M1 receptor described in the text. Data are means ± standard deviation. ND, not determined. Relative maximum $\Delta[\text{Ca}^{2+}]_{\text{cyto}}$ was calculated from 2 sets of measurements where wild-type M1, M1S-1, and M1S-2 were tested under the same conditions. Expression level of M1S-1 and M1S-2 was ~2 fold higher than that of wild-type M1 receptor. Because maximum $\Delta[\text{Ca}^{2+}]_{\text{cyto}}$ for the same construct varied day to day, it was not adequate to derive means and SD.

Labeling with FIAsH inhibited the maximum CCh-stimulated $\Delta[\text{Ca}^{2+}]_{\text{cyto}}$ by ~20% relative to maximum $\Delta[\text{Ca}^{2+}]_{\text{cyto}}$ of the M1S-2 (Figure 17 and Table 1). This might suggest that during the labeling procedure, a fraction of receptor lost ligand binding activity. Unfortunately, this possibility was not examined. If the number of ligand binding sites is reduced during the labeling procedure, the signaling function of the sensor would be better than estimated here.

Second-generation sensor displays wild-type ligand binding features in membranes

Signaling activity of the sensor was ~10% of the wild-type receptor. One possible explanation is that agonist binding activity of the sensor was impaired. To test this possibility, I examined whether the agonist binding behaviors were conserved in the sensor in HeLa cell membrane preparations. CCh binding to wild-type M1 receptor and the sensor was measured by competition with [³H] QNB. In these membranes, the wild-type M1 receptor bound CCh with K_i of ~70 μM and Hill slope of ~1 (Figure 18A and Table 2). Under the same condition, the sensor bound CCh with K_i of ~15 μM and Hill slope of ~1 (Figure 18A and Table 2), indicating that the sensor in the membrane retained essentially wild-type agonist binding. Binding of pirenzepine, a muscarinic antagonist, to the wild-type M1 receptor and the sensor was identical (Figure 18B). Therefore, reduced signaling activity of the sensor was not due to impaired ligand binding.

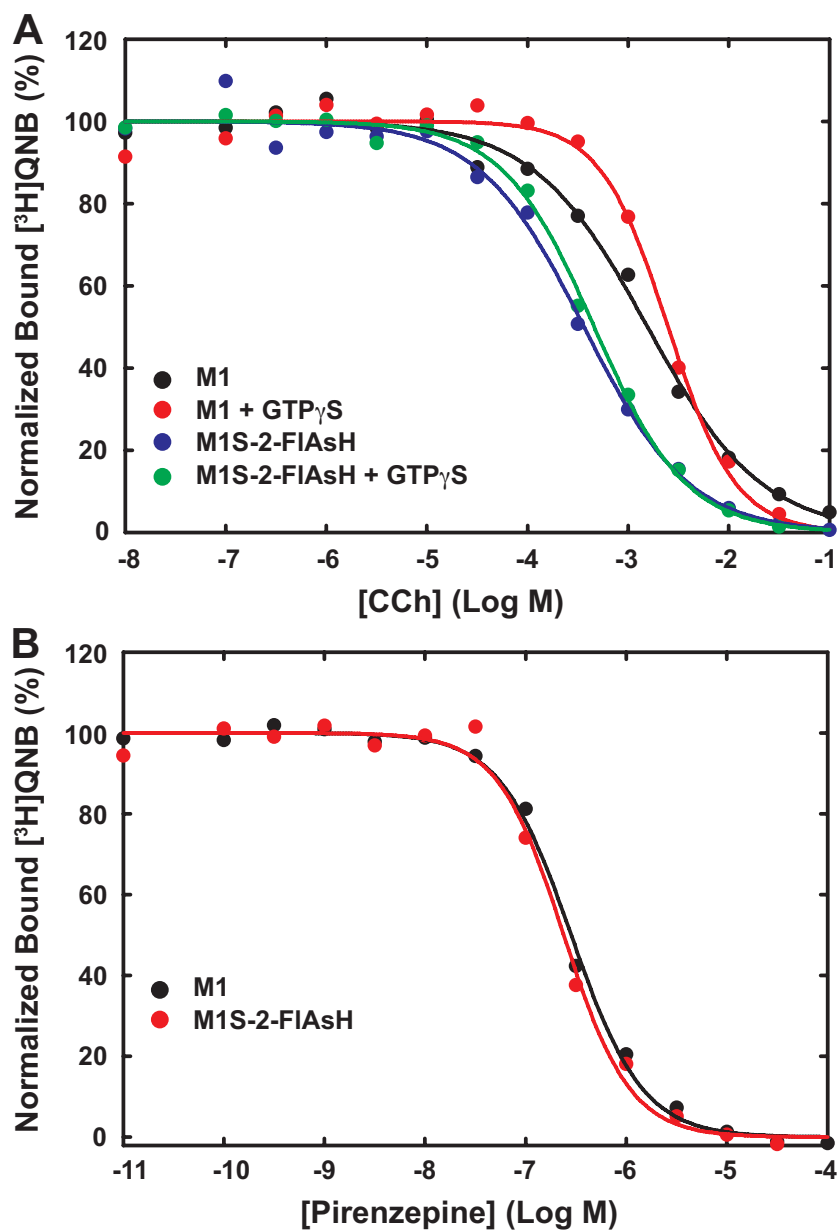


Figure 18. Agonist and antagonist binding to M1S-2-FIAsh in HeLa cell membranes
 Binding of CCh (A) and pirenzepine (B), an antagonist, were measured by competition against 0.5 nM [³H]QNB. When indicated, 50 μM GTP_γS was included in the assay. Data are averages from duplicate measurements and expressed as percent of total binding. Data are fitted with Hill equation. Results are summarized in Table 2.

Receptor	- GTP γ S		+ GTP γ S	
	K _i (μ M)	Slope	K _i (μ M)	Slope
M1	70 \pm 10	0.77 \pm 0.03	90 \pm 20	1.10 \pm 0.20
M1S-2-FIAsh	20 \pm 10	0.77 \pm 0.04	20 \pm 20	0.82 \pm 0.08

Table 2. Summary of CCh binding to wild-type M1 receptor and second-generation sensor (M1S-2-FIAsh) in HeLa cell membranes

Competitive binding assays on the receptors in membrane preparations prepared from HeLa cells expressing indicated receptor were performed using [³H]QNB as a radioligand tracer. Cells expressing M1S-2 were labeled with FIAsh (M1S-2-FIAsh). The concentration of [³H]QNB was 0.5 nM. When indicated, 50 μ M GTP γ S was included in the binding reaction. Data were fitted with Hill equation to obtain Log IC₅₀ and slope. K_i was calculated by correcting IC₅₀ for 0.5 nM [³H]QNB according to $K_i = IC_{50}/(1 + [QNB]/K_{d,QNB})$. K_{d,QNB} was 20 pM. Results shown in table are averages and standard deviations derived from at least 3 independently performed binding assays using separately prepared membrane preparations.

Agonist-driven Δ FRET parallels agonist binding

As the sensor retained wild-type agonist binding behaviors, it was possible to investigate how agonist-driven Δ FRET was related to agonist binding. To examine this relationship, CCh-driven FRET changes (Δ FRET) were measured at varying concentrations of CCh (Figure 19). CCh-driven FRET changes paralleled the binding of CCh to the receptor with identical half maximal concentrations of CCh and identical slopes (Figure 19 and Tables 2 and 3). I next determined whether the interactive effect of $G\alpha_q$ on agonist-driven conformational changes of the M1 receptor could be monitored by fluorescence changes. To examine this, CCh-driven FRET changes were measured in the presence or absence of Gpp(NH)p, a nonhydrolyzable analogue of GTP which uncouples $G\alpha_q$ from agonist-bound receptor. Gpp(NH)p did not change the CCh- Δ FRET relationship (Table 3). However, in membranes, binding between the agonist-bound M1 receptor and $G\alpha_q$ was not detected in the agonist binding assays. Under optimal conditions, binding of $G\alpha_q$ to the M1 receptor increases binding affinity for agonist by more than 100 fold and this enhanced binding disappears when $G\alpha_q$ is uncoupled by guanine nucleotides. As shown in Figure 18A and Table 2, in HeLa membranes, $GTP\gamma S$, a nonhydrolyzable analogue of GTP, did not change the agonist binding of both wild-type M1 receptor and the sensor, indicating that receptors did not form an agonist-receptor-G protein complex. Therefore, the membrane system was not appropriate to examine whether the sensor can detect the binding of $G\alpha_q$. Non-optimal binding conditions

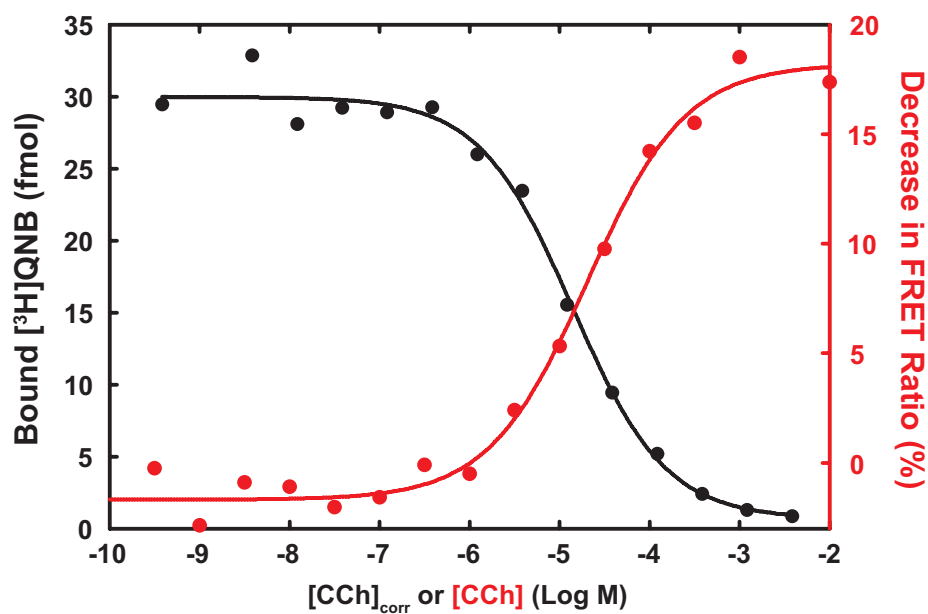


Figure 19. CCh-driven FRET change parallels agonist binding to the M1S-2-FIAsH
 CCh binding (black) and CCh-driven FRET changes (red) were measured in membrane preparations from FIAsH-labeled HeLa cells expressing M1S-2. Data are averages derived from duplicate measurements. Data are fitted with Hill equation to create binding curve and FRET response curve. For easy visual comparison of CCh binding and CCh-driven FRET changes, the concentration of CCh for the agonist binding curve was corrected for 0.5 nM [³H]QNB ([CCh]_{corr}) used in binding assay according to $K_{d,CCh} = IC_{50} / (1 + [QNB] / K_{d,QNB})$. $K_{d,CCh}$, dissociation constant for CCh; IC_{50} , half maximal inhibitory concentration; $K_{d,QNB}$, dissociation constant for QNB, 20 pM. The EC_{50} and slope of FRET response curve are summarized in Table 3. [³H]QNB binding data are those shown in Figure 18A.

Nucleotide	ΔFRET	EC₅₀ (μM)	Slope
No	20 \pm 2	30 \pm 10	0.7 \pm 0.1 (n = 3)
Gpp(NH)p	19 \pm 3	20 \pm 5	0.7 \pm 0.1 (n = 2)

Table 3. EC₅₀ for CCh-driven FRET change of M1S-2-FLASH in HeLa cell membranes

In fluorescence measurements, instead of GTP γ S, Gpp(NH)p was used because FIAsh emission itself was quenched in the presence of GTP γ S.

or substoichiometric amount of endogenous $G\alpha_q$ might be the problems. This issue will be detailed in the Discussion.

Agonist-driven FRET changes parallel cellular efficacies of agonists

The sensor displayed graded FRET responses to full and partial agonists. Agonist-driven FRET change was tested with a panel of muscarinic agonists with differing signaling efficacies: (1) full agonists including acetylcholine, carbachol, and oxotremorine-M and (2) partial agonists including arecoline, pilocarpine, oxotremorine and McN-A-343 (Brauner-Osborne et al., 1996; Hu et al., 1990; Schwarz et al., 1993). As shown in Figure 20, all the partial agonists (except arecoline) displayed lower maximum agonist-driven Δ FRET than full agonists. Most of the pair-wise comparisons between full agonists and partial agonists had statistically meaningful differences ($P < 0.05$). Signaling efficacy of arecoline is known to be close to full agonist (Schwarz et al., 1993) and consistently arecoline-driven Δ FRET was comparable to those of full agonists. Because relative cellular efficacies of the agonists vary depending on the cell types and signaling molecules assayed, it was not feasible to reliably correlate the FRET changes with cellular efficacies but there was a qualitative correlation between the FRET changes and cellular efficacies found in the literature. Therefore, examining relative agonist-driven Δ FRET may be a quick way to evaluate cellular efficacies of novel compounds. Importantly, this result also implies the sensor can detect relatively small conformational changes of the receptor.

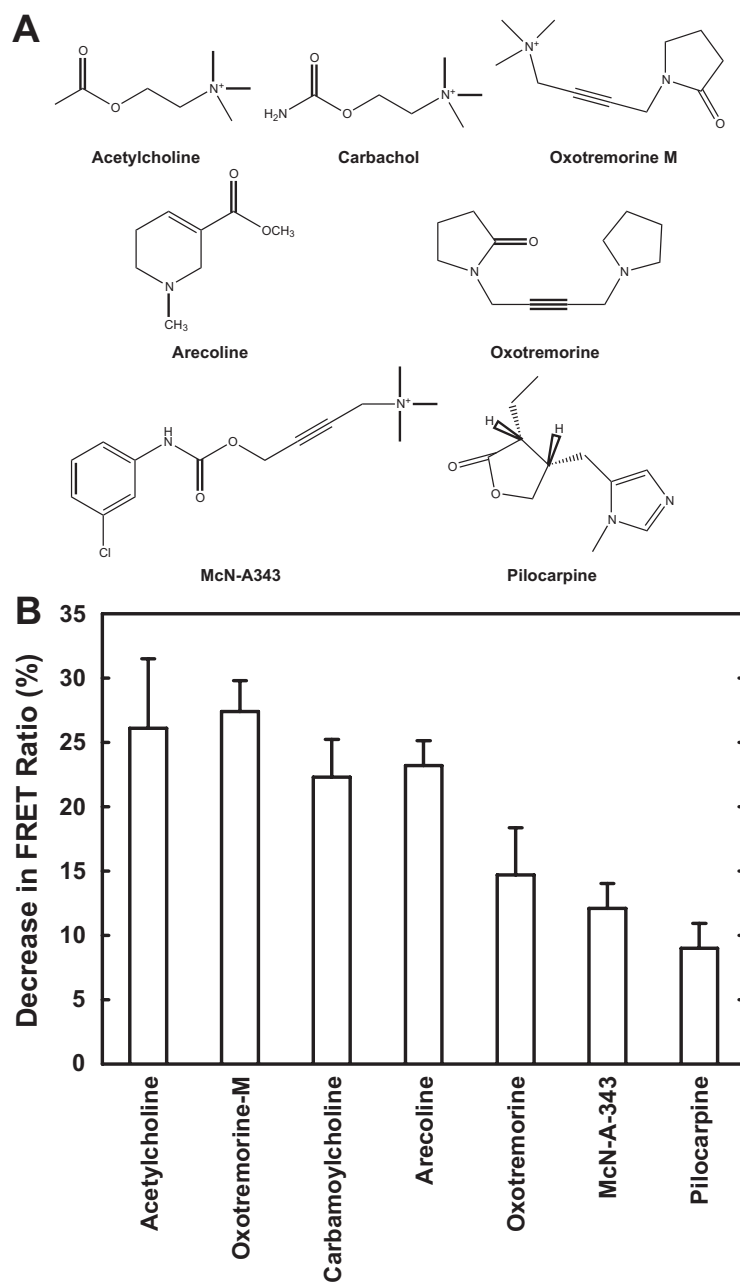


Figure 20. FRET responses of M1S-2-FIAsH to partial agonists

A. Structures of muscarinic agonists. B. Agonist-driven decreases in FRET ratio were determined at saturating concentrations of ligands, 1 mM for all ligands except oxotremorine (10 μ M). Data are means and standard deviations from triplicate measurements.

The sensor reports agonist-driven conformational changes of the M1 receptor in living cells

Because FIAsh labeling is compatible with cellular fluorescence measurement, I tested whether the sensor could detect agonist-driven conformational changes of the M1 receptor in living cells. HeLa cells that expressed M1S-2 were labeled with FIAsh and used for FRET microscopy. Cells were excited at 430 nm (excitation maximum of cp173cer cerulean FRET donor) and emissions from cp173cer cerulean FRET donor (at 475 nm) and FIAsh FRET acceptor (at 530 nm) were sequentially acquired. One cycle of acquisition took ~1.2 sec. To examine ligand-driven FRET change in cells, the sensor was first stimulated by the muscarinic agonist acetylcholine (ACh) and, once ACh-driven fluorescence change reached a plateau, the muscarinic antagonist atropine (Atr) was added to block the binding of agonist. As shown in Figures 21A and B, upon addition of ACh cerulean emission increased and FIAsh emission decreased, resulting in a decrease in the mFRET ratio (microscopic FRET ratio). Addition of atropine returned these acetylcholine-driven fluorescence changes to baseline. Change in cerulean fluorescence was accompanied by an opposing change in FIAsh fluorescence, indicating that ligand-driven change in the mFRET ratio was indeed due to the change in energy transfer efficiency associated with conformational change of the receptor (Figure 21A). Importantly, because the sensor used intramolecular FRET with a fixed acceptor to donor ratio, fluorescence changes caused by experimental variations (e.g. movement of cells) were corrected in the mFRET ratio (Figures 21A and B).

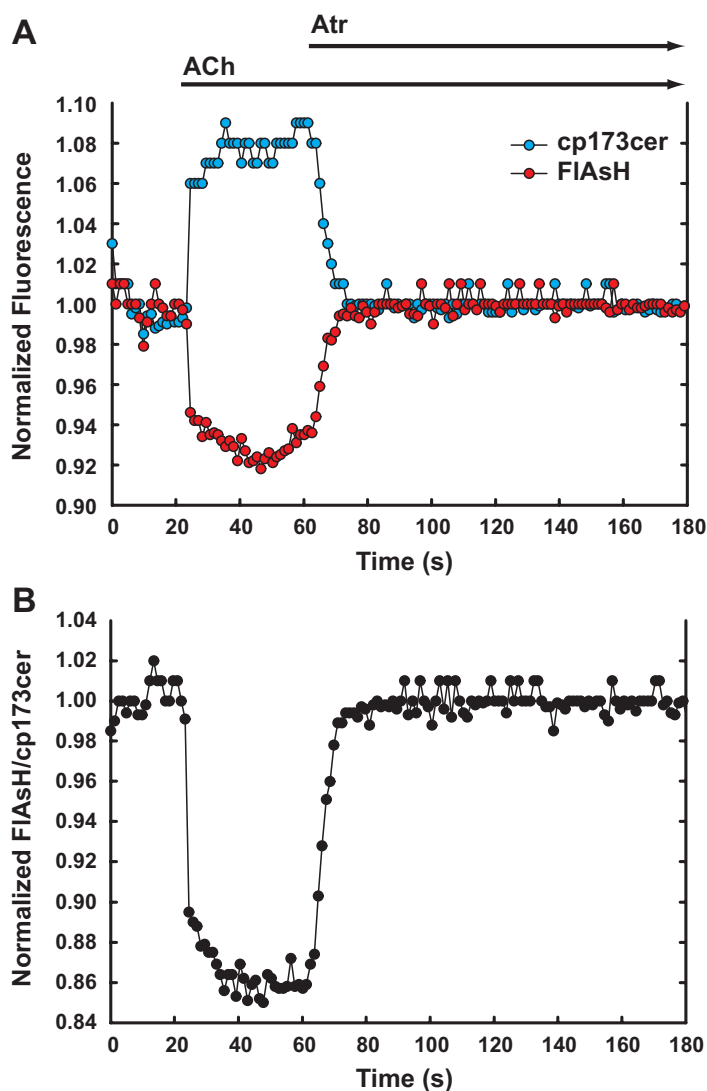


Figure 21. ACh-driven FRET changes of M1S-2-FIAsH in live HeLa cells

HeLa cells that express M1S-2 were labeled with FIAsH and visualized by two-wavelength microscopy. Cell images were bracketed manually and emission from individual cells was recorded. A. Individual time traces for emissions from cp173cer and FIAsH. Arrows indicate addition of indicated ligands. ACh was added at 2X concentration (final 1 mM) and Atr was added at 3X (final 1 mM) to minimize mixing times. Cells were excited at 433 nm (cp173cer excitation maximum) and cp173cer (475 nm, cyan) and FIAsH (530 nm, emission, red) emissions were sequentially acquired. One acquisition cycle took ~1.2 sec. Baseline-subtracted fluorescence intensity was normalized to 1 and plotted as a function of time. B. Normalized ratios of emission from FIAsH and cp173cer (FRET/cp173cer) are plotted against time.

The ACh-driven mFRET change seemed kinetically complex. As shown in Figure 21B and 22A, ~70% of the maximum ACh-driven decrease in the mFRET ratio (~0.14 of normalized FRET ratio) occurred during the addition of ACh, which was followed by a slower further decrease over ~10 sec. Because the time resolution of the FRET microscopy was ~1.2 second, it was impossible to derive reliable kinetic parameters for either process. However, because addition of ACh was slow (~1 sec) and mixing time was uncertain, the complex kinetics could be simply a mixing artifact.

The maximal ACh-driven change in mFRET ratio was ~15% (Figures 22A and B), which was lower than the corresponding change (sFRET) in membrane preparations (>20%). The difference is believed to be due to a higher fluorescence background from nonspecifically labeled FIAsH. In spectroscopic FRET measurements using membrane preparations, control membrane from labeled cells expressing wild-type M1 receptor was used to correct fluorescence for nonspecifically labeled FIAsH. This correction increased the FRET ratio and therefore the agonist-driven FRET changes. However, the corresponding correction was not made in the mFRET ratio. Indeed, if this correction was omitted, the ACh-driven percent sFRET ratio change was ~15%.

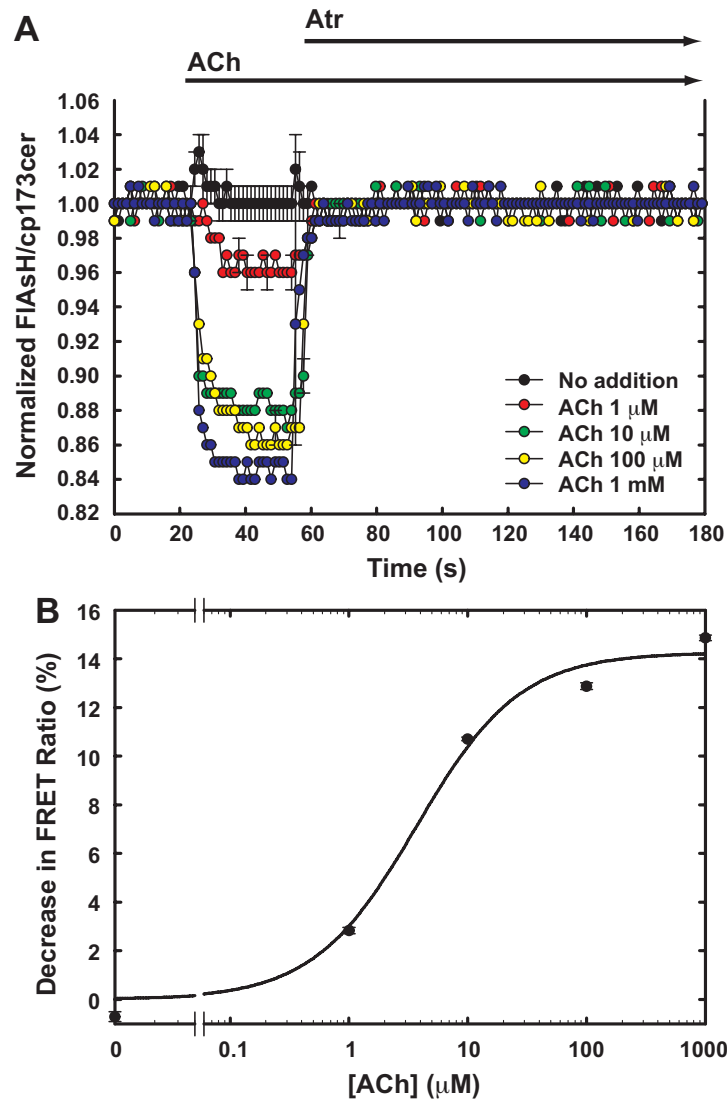


Figure 22. ACh-driven FRET changes of the M1S-2-FIAsH in cells; dose-response relationship

A. Cells that express M1S-2-FIAsH were exposed to varied concentrations of ACh and visualized as described for Figure 21A. Normalized time traces. Each trace is an average of fluorescence intensities from at least three isolated cells in the same imaging field. B. ACh-driven FRET changes at each concentration was obtained by averaging 5-10 points on the plateaus of ACh-driven FRET changes shown in panel A. Data are averages and standard deviations and fitted to the Hill equation.

Discussion

Creation of a FRET-based conformational sensor for the m1 acetylcholine receptor

A major achievement of my thesis research was the creation of a FRET-based GPCR sensor with a large response range and nearly wild-type signaling function. I believe the structure-based design strategies and molecular manipulations I employed could be applied to create FRET-based sensors for other class A GPCRs and FRET-based sensors in general.

Optimizing geometry of a FRET donor and an acceptor within a protein; distance between a donor and an acceptor

In FRET-based conformational sensors, stimulus-driven structural changes in a protein are associated with changes FRET efficiency. In many cases, including GPCRs, stimulus-driven conformational changes in a protein are much smaller than Förster radii of commonly used FRET pairs (>50 Å). For example, according to structural studies on rhodopsin and β_2 AR, agonist-driven conformational changes are less than 10 Å (Rosenbaum et al., 2011; Scheerer et al., 2008), which is less than 20% of 50 Å. Therefore, in order to detect these small conformational changes using FRET, it is critical to place a donor and an acceptor at optimal sites within a protein so that the structural changes can be maximally manifested as changes in FRET efficiency. As introduced earlier, there were two considerations in optimizing the placement of FRET donor and acceptor: (1) maximizing stimulus-driven changes in the donor-acceptor distance

and (2) optimizing the donor-acceptor distance in an unstimulated state. In the initial stage of M1 sensor development, placement of a TC motif was optimized to make the agonist-driven conformational changes in ICL3 lead to larger changes in the donor-acceptor distance. As a next step, the donor-acceptor distance was optimized such that the agonist-driven distance change could be maximally manifested as changes in the FRET efficiency. The donor-acceptor distance was varied by placing the CFP at deleted C-terminus or an extended C-terminal end with oligo-proline spacers (Pro_n). I chose relatively inflexible oligo-proline spacers against flexible linkers to systematically survey wide range of distance. Oligo-proline spacers are known to form rigid helical structures where the distance between N- and C- terminal ends is linearly proportional to the number of proline residues, up to ~15 in aqueous solutions (Best et al., 2007; Cowan et al., 1955; Stryer et al., 1967). In these helical structures, the distance between two consecutive C α is ~3 Å. Therefore, a 3 proline residue unit that I used for each increment extends the C terminus by ~10 Å, so that the maximum distance covered is 40 Å in my Pro₁₂ construct. This process improved CCh-driven FRET changes by more than two fold. Notably, the CCh-driven FRET changes reached a maximum around Pro₆, suggesting that placement of the CFP, both with deletions and oligo-proline spacers, sufficiently surveyed the distance range for the cp173cer-FIAsH FRET pair, covering a Förster radius that has not been experimentally determined.

This result clearly shows that optimizing the donor-acceptor distance in an unstimulated state is as important as optimizing stimulus-associated distance changes. Regardless of the availability of structures, I believe the deletion and

extension strategy are generally applicable to creating FRET-based sensors for any signaling proteins as well as GPCRs. One consequence of using inflexible spacers is that the expression level of the derived fusion proteins might be markedly lowered, as suggested by low expression level of all the receptor constructs with Pro_n spacers.

Optimizing geometry of a FRET donor and an acceptor within a protein; orientation

Because FRET is also a function of orientation factor (κ^2), if possible, relative orientation between the two interacting dipoles needs to be optimized. In CFP-FIAsh-based GPCR sensors, rotational freedom of both fluorophores is limited and it was possible to vary the orientation between the fluorescence dipoles. To vary the orientation factor I introduced circular permutation on CFP (Baird et al., 1999; Heinemann et al., 1995). A circularly permuted cerulean CFP markedly improved the agonist-driven FRET changes. Importantly, it should be noted that circular permutation made on a fluorescent protein also changes the distance factor and presumably quantum yield. FRET is a complex function of the distance (R) and orientation (κ^2) between two interacting fluorescence dipoles, Therefore, it would be ideal to optimize distance against orientation for the best results.

Retaining GEF activity in a FRET-based sensor; structure-guided design

In developing a FRET-based sensor for the M1 receptor, the biggest challenge was to retain GEF activity of the M1 receptor. Conserving GEF activity

(or interaction with G protein) was important to study the conformational status of a GPCR because conformational status of a GPCR is determined by complex allosteric interaction between agonist and G protein. Impaired GEF activity is a common issue in many GPCR sensors, probably because favorite sites of modification for sensors are in the presumed cytoplasmic helical extension of transmembrane helix 6 that is critical for the coupling of receptor to G protein. Size of modification in ICL3 seemed to be critical. In many of FRET-based sensor using the CFP-YFP FRET pair, GEF activity was completely lost (Hoffmann et al., 2005b; Jensen et al., 2009; Vilardaga et al., 2003). In some cases, the problem was alleviated by replacing YFP with TC-FIAsH, whose size is >10 fold smaller than YFP (Hoffmann et al., 2005b). However, as exemplified by my case, placement of any modifications in ICL3 is as critical as size of the modification for retaining GEF activity. In order to restore GEF function, which was severely impaired in the first-generation M1 sensor, placement of a TC motif in ICL3 was subsequently optimized by exploiting the presumed helical nature of the cytoplasmic end of transmembrane helix 5.

GEF activity was further improved by flexible linkers at the TC motif insertion sites. In the TC-FIAsH complex, four Cys residues in the TC motif bind to two As in the planar ring structure of FIAsH, Therefore, I postulated that upon binding to FIAsH, the TC motif would become rigid and interfere with activation-associated rotational movements of transmembrane helices 5 and 6, which were connected through the TC motif in the sensor. I intended a flexible linker to relieve the structural restraint imposed by the presumed rigidity of the TC-FIAsH

complex. A longer linker better improved the GEF function but the length had to be optimized to retain both function and FRET response.

All the molecular manipulations made to restore GEF function were chosen to solve specific problems suspected simply based on a coarse-grained homology-modeled structure of the M1 receptor. In other words, no specific residues and structural features present only in M1 receptor were needed. According to available structures, helical extension in cytoplasmic end of transmembrane helix 5 and 6 seems to be a common structural motif of many GPCRs in class A (Chien et al., 2010; Palczewski et al., 2000; Rasmussen et al., 2007; Xu et al., 2011). Therefore, the procedural and technical scheme I devised for the M1 sensor could be generically applied to developing FRET-based sensors for other GPCRs in class A.

Estimating the distance change between ICL3 and C terminus upon activation

Primary usage of the sensor is to monitor the relative fraction of activated receptor and the kinetics of receptor activation. However, in order to corroborate the structural and fluorescent rationale that I relied on to create the sensor, it is worth testing whether the movement of ICL3 estimated by FRET is in reasonable agreement with that based on the homology-modeled structures of the M1 receptor. To roughly estimate the distance (R) between two fluorophores, I used the basal and the stimulated FRET ratios shown in Figure 16. In this set of measurements, CCh-driven FRET change is ~20% with FRET ratio decreasing from ~2.5 to ~2.0. To estimate R , the FRET ratios were converted to FRET

efficiency (E). The conversion was based on the linear scaling from a minimum and maximum FRET ratio corresponding to 0 and 100% efficiency, respectively. If there is no energy transfer (0% efficiency), the FRET ratio will be ~ 0.4 , which is the ratio for cp173cer by itself. Since the FRET ratio corresponding to 100% energy transfer has not been experimentally measured, I used the FRET ratio for M1S-2/sTC/C-TC where FIAsh is directly attached to cp173cer, for the maximum FRET ratio (3.2) (Figure 16). Based on this assumption, the basal and stimulated FRET ratios, 2.5 and 2, are equivalent to FRET efficiency (E) 0.86 and 0.71, respectively. The Förster radius (R_0) of freely rotating CFP-YFP FRET pair, ~ 50 Å, was assumed for the Förster radius (R_0) for cp173cer-FIAsh FRET pair because fluorescence emission properties of cp173cer and FIAsh are similar to those of CFP and YFP. With these values, activation-associated change in the distance between ICL3 and C terminus was estimated to be ~ 7 Å. The estimated 7 Å is greater than 2-3 Å, which is the estimation based on homology-modeled structures of the M1 receptor. However, in fluorescence-based estimation, both R_0 and E are uncertain. First both cp173cer FRET donor and FIAsh FRET acceptor are not freely rotating in the sensor and thus, R_0 could be either smaller or bigger than 50 Å. Second, the maximum FRET ratio must be greater than 3.2 and thus, E should be smaller than assumed here. Considering these uncertainties, the ~ 4 Å difference between fluorescence-based and structure-based estimations, which is less than 10% of the Förster radius, is relatively small, therefore, my fluorescence-based estimation is in reasonable agreement with the structure-based estimations. This suggests that the sensor indeed

monitors the distance change between ICL3 and C terminus of the M1 receptor as anticipated based on the structures of homologous receptors.

Studying conformational dynamics of the M1 receptor in living cells

The CFP-FIAsH-based sensor is compatible with cellular FRET microscopy (Hoffmann et al., 2005), and I demonstrated that ratiometric FRET microscopy with the sensor can be used to monitor the isomerization kinetics of the M1 receptor in living cells. Unfortunately, kinetics of ligand-driven fluorescence changes could not be accurately estimated because the time resolution of the microscopy is not good enough to resolve the fast fluorescence changes, and ligand mixing is slow (~1 sec) and uncertain. For example, ~70% of ACh-driven fluorescence change takes place within ~1.2 sec, which is the maximum time resolution of the microscopy, and the addition of ligand is not much faster than 1.2 sec (Figures 21 and 22). Therefore, in the future, faster microscopy and faster ligand mixing need to be implemented for accurate estimation of agonist-driven isomerization kinetics. Technically, the time resolution of microscopy can be increased to <100 ms and ultrafast ligand mixing (<100 ms) can also be achieved with fast perfusion devices.

Once fast microscopy is established, effects of G protein on the conformational dynamics of the M1 receptor could be studied by investigating: (1) the kinetics of FRET changes resulting from the association and dissociation of agonist and (2) the absolute FRET change induced by agonist binding. As mentioned earlier, one of the big advantages of using M1 receptor is that binding affinity for agonist is enhanced more than 100 fold by the coupling of receptor to

$G\alpha_q$. Either increased association rate or decreased dissociation rate of agonist or both could result in the increased binding affinity for the receptor. Therefore, interaction of G protein with the M1 receptor might be reflected in the kinetics of FRET changes resulting from the association and dissociation of agonist. Interaction of G protein with the receptor might also affect absolute agonist-driven FRET change. There are two possibilities for this: (1) binding of G protein with the receptor drives higher fraction of receptor to activated state, or (2) binding of G protein with the receptor induces a conformational state of the receptor distinguishable from that of G-protein-unbound receptor. It will not be possible to distinguish between these possibilities simply based on changes in fluorescence intensity, and fluorescence lifetime measurement might be helpful to distinguish between them.

Probing interactive effects of $G\alpha_q$ on the conformation of the M1 receptor in cell membrane preparations

The interactive effect of G protein on GPCR is critically involved in the regulation of agonist activation of receptor. However, the effects of $G\alpha$ on the conformational dynamics of GPCRs are poorly understood. One of the primary reasons is the lack of reliable conformational sensors. Kobilka's group used a bimane-based β_2AR sensor reconstituted in lipid nano-discs to monitor the conformational changes of the receptor induced by G protein binding (Yao et al., 2009). They claimed that this sensor could probe the effect of G protein on the conformation of the receptor.

However, in the presence of G protein, the agonist binding curve of monomeric β_2 AR reconstituted in nano-discs is biphasic while it is expected to be monophasic. This suggests that nano-disc reconstitution might not be optimal for investigating, specifically, the effect of G protein on the conformation of the receptor. Moreover, the signaling function of the sensor in nano discs was not reported, and a similar sensor in micelles displayed unreasonably slow kinetics of agonist-driven receptor isomerization (several seconds to hundreds of second) (Swaminath et al., 2004). Therefore, it is not clear if G protein-induced fluorescence changes are reflective of the effect of G protein on the conformation of the wild-type receptor.

The most important feature of the M1 sensor I have developed is the retained wild-type agonist binding and GEF activity as well as reasonable isomerization kinetics in cells and membranes, suggesting the interaction with $G\alpha_q$ is minimally impaired. In order to study the effect of $G\alpha_q$ on the conformation of the M1 receptor, I initially intended to use reconstituted lipid vesicles containing *in vitro* labeled sensor because of the many obvious advantages for quantitative studies in reconstituted vesicles. Briefly, I failed to reconstitute agonist-driven FRET responses in lipid vesicles, which is the main theme of Chapter 3. As an alternative approach, I used the sensor in membrane preparations and living cells.

Guanine nucleotides do not change the FRET of the sensor in cellular membrane preparations

To test whether the effects of $G\alpha_q$ on the conformation of the M1 receptor could be detected with the sensor, I first examined the effect of various guanine nucleotides (GTP, GDP and Gpp(NH)p) on FRET of the sensor as binding of a guanine nucleotide to $G\alpha$ drives the dissociation of $G\alpha$ from agonist-bound receptor. Guanine nucleotides did not change FRET of the sensor but, under similar conditions, I could not see guanine-nucleotide-sensitive high affinity binding for agonist either, which probably indicates the agonist-bound receptor and G protein did not form a stable complex. Therefore, the result might indicate that non-optimal assay conditions (including unknown factors present in membrane preparations) were the problems rather than defects of the sensor in detecting G protein. This possibility is also supported by the fact that the sensor retained signaling function in cells, in other words, ability to interact with G proteins.

Optimizing binding assay conditions for agonist in membrane preparations

Because the high affinity site disappears in the presence of guanine nucleotides, I suspected contaminating nucleotides in crude membrane preparations as a culprit. To remove guanine nucleotides in membrane preparations, I tested two conditions: (1) including apyrase, a nonspecific nucleotide phosphatase and (2) using sub-fractionated membrane preparations in binding reactions.

The first condition used apyrase, a nonspecific nucleotide phosphatase which hydrolyzes GTP and GDP to GMP and has been shown to enhance the formation of agonist-receptor-G protein complex in the nano-disc reconstitution system (Yao et al., 2009). I examined the effect of apyrase on agonist binding of the M1 receptor in HeLa cell membrane preparations but could not detect any high-affinity agonist binding (data not shown).

Previously it was shown that sub-fractionation of crude membrane preparations could substantially remove contaminating nucleotides (Ross et al., 1977). To test whether high-affinity agonist binding could be seen in fractionated membrane preparations, crude membrane preparations were further fractionated using a discontinuous sucrose gradient. However, I could not detect high affinity agonist binding in any fractions from sucrose gradient (data not shown).

However, neither of these treatments might have substantially removed guanine nucleotides in membrane preparations. I have not quantitated the amount of guanine nucleotides in the HeLa cell membrane preparations. Recently it was shown that foscarnet, a nonhydrolyzable analogue of pyrophosphate, had the potential to act as a competitive inhibitor of guanine nucleotides for nucleotide-free $G\alpha$ subunits and thus stabilize the agonist-receptor-G protein complex in a nano-disc reconstitution system (Rasmussen et al., 2011). Therefore, it will be worth trying foscarnet in binding assays. However, as foscarnet binds to many other proteins (e.g. adenylyl cyclases)(Kudlacek et al., 2001) present in membrane preparations, indirect effects would have to be carefully considered.

Increasing the amount of $G\alpha_q$ in membrane preparations

In principle, to detect high affinity agonist binding, the ratio of $G\alpha$ to receptor should be greater than 1. Therefore, it was possible that the endogenous expression level of $G\alpha_q$ might be much lower than the expression level of the M1 receptor and the fractional high affinity binding was undetectably low. In membrane preparations, it is difficult to estimate the amount of functional $G\alpha_q$, let alone what fraction of $G\alpha_q$ can be accessed by receptors. Therefore, instead of investing time in estimating the amount of endogenous $G\alpha_q$, I directly examined whether increasing the amount of $G\alpha_q$ in the membrane would create detectable high affinity binding site.

First, $G\alpha_q$ was co-expressed with wild-type M1 receptor in HeLa cells and membrane preparations from these cells were used for binding assays. However, I could not detect high-affinity agonist binding. Second, for some receptors, it has been shown that reconstituting purified $G\alpha_q$ subunits into a crude membrane preparation helps creating high-affinity binding for the agonist (Hartman et al., 1996; Hellmich et al., 1997; Slessareva et al., 2003). I tried reconstituting purified $G\alpha_q$ into HeLa cell membrane preparations but could not create any high affinity binding. It was not clear whether reconstitution itself was achieved but I did not pursue this because of time limitations.

As described above, I have tried many things to detect high affinity agonist binding in membrane preparations but could not detect it. However, the problem could be simply that binding of $G\alpha_q$ to agonist-bound M1 receptor is

undetectably weak in HeLa cell membranes, which would be difficult to prove and fix. I believe this issue will be better addressed in reconstitution systems, which will be the theme of Chapter 3.

Chapter 3

Reconstitution of the FRET-based M1 receptor conformational sensor in phospholipid vesicles

Introduction

As described in Chapter 2, cultured mammalian cells and membrane preparations from the cells have been instrumental in developing a FRET-based sensor for the M1 receptor. The sensor reported agonist-driven conformational changes of the M1 receptor and retained nearly wild-type signaling function in living cells and cell membranes. However, cellular systems are not favorable for studying interactive effects of G protein on the conformation of the receptor because of following reasons:

- (1) difficulties in controlling the quantity of signaling components - G proteins, and guanine nucleotides
- (2) the heterogeneous nature of cellular membrane - e.g. membrane microdomains
- (3) promiscuous biochemical activities present in cellular membrane - e.g. various GTPase activities
- (4) the lack of quantitative assays for signaling molecules - e.g. receptor and G protein

All of these problems are manageable in reconstituted lipid vesicles. The M1- $G\alpha_q$ -PLC- β 1 signaling module has been reconstituted in phospholipid vesicles (Berstein et al., 1992) and reconstituted proteins retain biochemical activities that

underlie the regulatory behaviors of the signaling module observed in the native cellular context (Biddlecome et al., 1996; Turcotte et al., 2008). In order to investigate how the activity of the M1 receptor is regulated to produce the regulatory behaviors of the signaling module, I characterized the biochemical and fluorescent behaviors of the sensor in reconstituted phospholipid vesicles.

Experimental Procedures

Nomenclature

M1S-2 is a M1 receptor prototype for second-generation sensor, defined in Chapter 2. In this chapter, M1S-2-FIAsh is *in vitro* labeled M1S-2 as opposed to the M1S-2 labeled in membrane in Chapter 2.

Materials

Phospholipids are from Avanti; cholesterol hemisuccinate (CHS) from Sigma; digitonin from Sigma; Ultrogel AcA 34 from Pall Corporation; [³⁵S]GTPγS (1.2 mCi/μmol) from PerkinElmer. Wild-type M1 receptor was purified from Sf9 cells by Gloria Biddlecome (a former graduate student) (Biddlecome et al., 1996).

Expression and purification of M1S-2 and cp173cer

cDNA encoding the M1S-2 sensor described in chapter 2 was cloned into pFastBac1 vector (InVitrogen) and baculovirus for M1S-2 expression was generated using Sf9 cells (Biddlecome et al., 1996; Ciccarone, 1997; Luckow et al., 1993). Low titer baculovirus for the M1S-2 was generated by transfecting a monolayer Sf9 cells. High titer baculovirus was generated by infecting suspension culture of Sf9 cells. For large-scale expression, Sf9 cells were infected with high titer baculovirus and 40 hours after the infection cells were harvested. Atropine (0.1 μM) was included for the last 24 hours before harvesting cells. M1S-2 was solubilized from cell membranes by vigorously stirring the membrane suspended in an extraction buffer (100 mM NaHepes, pH 7.4, 100

mM NaCl, 1% digitonin and 0.3% cholate) for 1 hour at 4 °C and solubilized M1S-2 was first purified using a Ni-NTA Sepharose (Qiagen) column. Clear supernatant containing solubilized M1S-2 was applied to Ni-NTA column and the column was washed with buffers (20 mM NaHepes, pH 7.4, 0.1% digitonin) containing varying concentrations of NaCl (50 mM to 1 M). After washing, M1S-2 was eluted with a buffer (20 mM NaHepes, pH 7.4, 50 mM NaCl, 0.1% digitonin, and 125 mM imidazole) and the eluate was further purified using M1 anti-FLAG antibody column (Sigma). CaCl₂ (2 mM) was added to eluate from the Ni column and the eluate was loaded onto a M1 anti-FLAG antibody column. The column was washed with a buffer (20 mM NaHepes, pH 7.4, 150 mM NaCl, 1 mM CaCl₂, and 0.1% digitonin) and the bound M1S-2 was eluted with a buffer (20 mM NaHepes, pH 7.4, 50 mM NaCl, 2 mM EDTA, and 0.1% digitonin). Finally, to exchange the buffer, purified M1S-2 was 10 fold diluted in a loading buffer (20 mM NaHepes, pH7.4 and 0.1% digitonin) and applied to a Q Sepharose column. After washing the column with a washing buffer (20 mM NaHepes, pH 7.4, and 0.1% digitonin), M1S-2 was eluted with H₂0N₄₀₀ buffer (20 mM NaHepes, pH 7.4, 400 mM NaCl and 0.1% digitonin). This procedure produced uncleaved M1S-2 with >90% purity based on silver staining (Figure 23A). For SDS polyacrylamide gel electrophoresis, purified M1S-2 was incubated in 1% SDS plus 10 mM DTT for 30 min at 45 °C and reactive Cys were blocked with N-ethylmaleimide. M1S-2 migrated faster than the theoretical size (major lower band around 50 kDa in Figure 23A). Upon boiling at 95 °C for 5 min, the lower band was converted to an upper band (~65 kDa in Figure 23A) and cp173cer cerulean fluorescence disappeared, suggesting that the lower band was partially denatured receptor

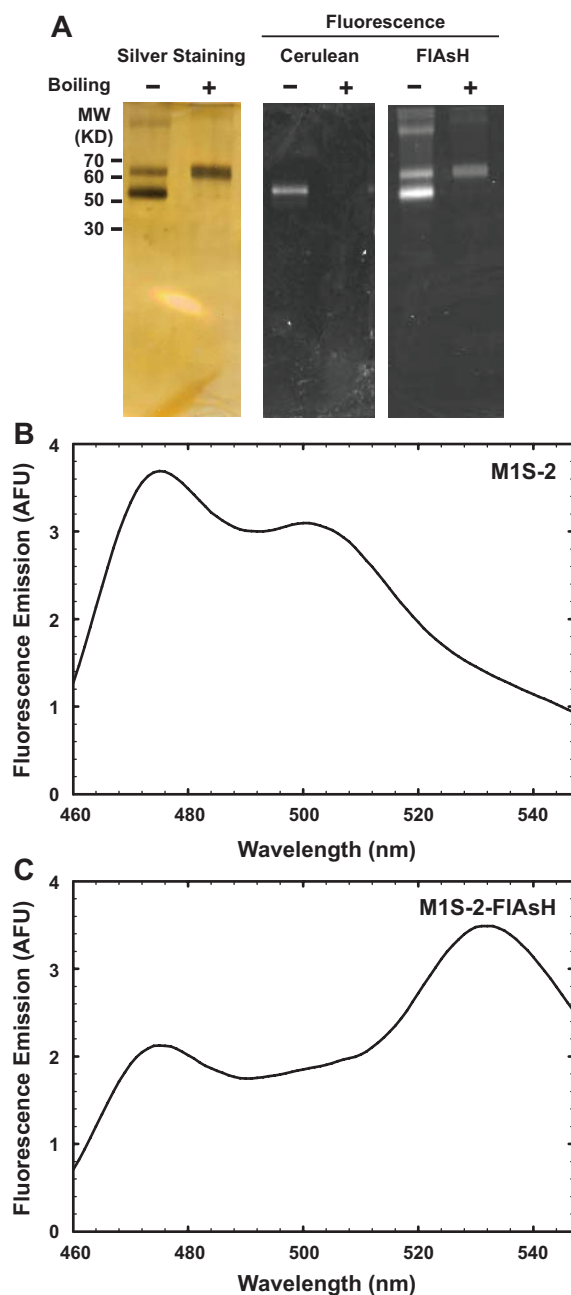


Figure 23. Fluorescent properties of purified M1S-2 with and without FIAsH labeling

A. SDS-polyacrylamide gel electrophoresis of M1S-2-FIAsH. M1S-2-FIAsH was incubated in SDS sample buffer (Experimental Procedures) either at 45 °C for 30 min (-boiling) or further incubated at 100 °C for 5 min (+boiling). Fluorescence was imaged at 473 nm (cp173cer) and 510 nm (FIAsH). The gel was then fixed and silver stained. Faint bands at high molecular weight are receptor oligomers. B, C. Emission spectra of purified M1S-2 before (B) and after (C) labeling with FIAsH. Excitation wavelength was 433 nm.

with the cerulean moiety presumably intact. Purified M1S-2 was used for *in vitro* labeling with FIAsh and reconstitution.

Circularly permuted cp173cer cerulean was purified from *E. coli* (BL21). For purification, cp173cer was modified to have 6xHis before the N terminus. cDNA encoding modified cp173cer was inserted into the pET-3d vector. cp173cer cerulean was purified through single step Ni-NTA (Qiagen) column chromatography. *E. coli* cells expressing cp173cer were lysed and the soluble fraction was applied to Ni-NTA column. The column was washed with buffers (20 mM NaHepes, pH 8, and 10 mM imidazole) containing either 1 M or 300 mM NaCl. Bound cp173cer was eluted with a buffer (20 mM NaHepes, pH 8, and 150 mM imidazole). Buffer was exchanged to a storage buffer (20 mM NaHepes, pH 7.4 and 100 mM NaCl) using an Amicon Ultra centrifugal filter (Millipore). Based on protein staining in an SDS-PAGE gel, cp173cer was more than 95% pure. Concentration of the protein was determined by the amido black method (Schaffner and Weissmann, 1973). The molar extinction coefficient of cp173cer at 433 nm was determined to be $20,000 \text{ cm}^{-1}\text{M}^{-1}$ in $\text{H}_2\text{O}/\text{N}_400$ containing 0.1% digitonin. The molar extinction coefficient might be underestimated because the fraction of cp173cer with fully matured chromophore was presumably less than 1 (Ulbrich and Isacoff, 2007). However, this underestimation did not influence conclusion presented in the Result section.

***In vitro* labeling of a purified sensor with FIAsh**

The purified M1S-2 receptor was used for *in vitro* labeling with FIAsh. First, pH was adjusted to 9 by adding an appropriate volume of NaHepes (1 M,

pH 10) and atropine was added at 0.1 μ M. To reduce the TC motif in the M1S-2, pH-adjusted M1S-2 was incubated with 1 mM TCEP on ice for 1 hour. Then, labeling was initiated by adding 1 mM β -ME and 10 fold molar excess of FIAsh and incubating at RT for 30 min to 1 hour. In order to monitor the labeling, the sFRET ratio was determined with a small aliquot of the labeling reaction taken along the reaction and was plotted against reaction time. This was possible because the fluorescence emission of FIAsh increases >10 fold upon binding to the TC motif (Adams et al., 2002; Griffin et al., 1998). Once the sFRET ratio reached a plateau, additional FIAsh was added to ensure the labeling reached completion. Then, pH was adjusted to 8 by adding an appropriate volume of NaHepes (1 M, pH 5.4). To remove unbound FIAsh and change the buffer, the labeling mixture was 10 fold diluted in a loading buffer (20 mM NaHepes, pH7.4 and 0.1% digitonin) and applied to Q Sepharose column. After washing the column with a washing buffer (20 mM NaHepes, pH 7.4, and 0.1 % digitonin), labeled receptors were eluted with an elution buffer (20 mM NaHepes, pH7.4, 400 mM NaCl and 0.1% digitonin) and ligand binding site of the eluate was estimated by measuring [3 H]QNB binding. The concentration of [3 H]QNB binding site was >1 μ M. Finally, labeled receptors were flash frozen for long-term storage at -80 $^{\circ}$ C.

Evaluation of FIAsh labeling

The amounts of total receptor protein (not the number of [3 H]QNB binding sites) and FIAsh in *in vitro* labeled M1S-2-FIAsh were determined by measuring the absorbance of cp173cer cerulean and FIAsh at 433 nm and 510 nm

respectively. The molar extinction coefficients of FIAsh (FIAsh-EDT₂ complex form) was determined to be 50,000 cm⁻¹M⁻¹ in 20 mM NaHepes (pH 7.4), 400 mM NaCl and 0.1 % digitonin. The absorbance of cp173cer at 510 nm was undetectable but the absorbance of FIAsh at 433 nm was ~7% of its absorbance at 510 nm. Therefore, the absorbance of cp173cer cerulean at 433 nm ($A_{433, cp173cer}$) in M1S-2-FIAsh was corrected for the contribution by FIAsh according to $Abs_{433, cp173cer} = Abs_{433} - 0.071 \times A_{510}$. The FIAsh to cerulean ratio of M1S-2-FIAsh was ~1.2, indicating that labeling was approximately quantitative. The sFRET ratio of M1S-2-FIAsh was ~1.6 whereas the corresponding fluorescence emission ratio of M1S-2 was ~0.4 (Figures 23B and C). Two batches of purified M1S-2 were *in vitro* labeled with FIAsh under the same conditions and the labeling stoichiometry was similar. Because of difficulties in working with reconstituted systems, I further characterized only one batch of M1S-2-FIAsh biochemically and fluorescently in reconstituted phospholipid vesicles.

The molar extinction coefficient of FIAsh was determined as FIAsh-EDT₂ complex form. There was a possibility that binding to the TC motif might change the extinction coefficient but I did not have a chance to examine this possibility. According to the literature, the molar extinction coefficient of FIAsh varies from 30,000 to 80,000 cm⁻¹M⁻¹ (Adams et al., 2002). If this range is used for the calculation, the ratio varies from 0.74 to 1.97, which also supports quantitative labeling. In the future, effects of the TC motif on the absorbance of FIAsh need to be examined.

Reconstitution

Receptors (wild-type M1 receptor or M1S-2-FIAsh) were reconstituted into phospholipid vesicles either alone or together with $G\alpha_q\beta_1\gamma_2$ complex by the size exclusion method (Berstein et al., 1992; Biddlecome et al., 1996). Briefly, a mixture of purified proteins and phospholipids was applied to 8 ml Ultrogel AcA 34 column and the column was run in buffer (20 mM NaHepes, pH 8.0, 2 mM $MgCl_2$ and 100 mM NaCl). EDTA was omitted to avoid the possible detachment of FIAsh by EDTA. The starting mixture contained 10 pmol of receptor ($[^3H]QNB$ binding site), 80-100 pmol of $G\alpha_q$ (active $G\alpha_q$ based on $GTP\gamma S$ binding)(Chidiac et al., 1999), 120-150 pmol of $G\beta_1\gamma_2$ complex and a dispersion of PE (825 μM), PS (490 μM), and CHS (90 μM). Recovery of ligand binding sites in lipid vesicles was evaluated by the $[^3H]QNB$ binding assay and was ~30%. Ligand binding sites were enriched in 3 to 4 fractions. These fractions were pooled and used for biochemical and fluorescence assays. The concentration of $[^3H]QNB$ binding sites in pooled fractions was 2-4 nM.

Assays of Reconstituted Proteins

The amount of both soluble and reconstituted receptors was estimated by $[^3H]QNB$ binding. Soluble receptors were incubated with 20 nM $[^3H]QNB$ in 10 mM Tris-Cl (pH 7.5) buffer containing 0.1% digitonin and 100 mM NaCl at 30 °C for 1 hour and bound and unbound $[^3H]QNB$ were separated by centrifugal gel filtration (Berstein et al., 1992). Vesicles were incubated with 10 nM $[^3H]QNB$ in $H_2O M_2 N_{100}$ (20 mM NaHepes, 2 mM $MgCl_2$ and 100 mM NaCl) at 30 °C for 1 hour. The binding mixture was filtered through a glass fiber filter (Whatman GF/F) that

had been pre-soaked in washing solution (20 mM Tris-Cl, pH 8.0, 10 mM MgCl₂ and 100 mM NaCl) containing 0.1 mg/ml polyethyleneimine. Filters were washed with washing solution and air-dried. Dried filters were dissolved in scintillation solution (Safety-Solve) and bound ³H was determined by liquid scintillation counting. Specific binding was defined by the difference between binding of [³H] QNB in the presence and absence of 10 μM atropine in the binding reaction. For reconstituted M1S-2 (unlabeled), total amount of receptor - active plus inactive - was estimated by fluorescence emission of the fused cp173cer. Fluorescence emission was calibrated using purified cp173cer cerulean in H₂O M₂N₁₀₀.

[³⁵S]GTPγS binding assay

The procedure for [³⁵S]GTPγS binding to reconstituted vesicles was essentially identical to one described by Brandt and Ross (Brandt et al., 1983) except that EDTA and DTT were omitted in the reactions as both have a potential to detach FIAsH from M1S-2-FIAsH. The reaction contained 20 mM NaHepes (pH 8.0), 2 mM MgCl₂, 100 mM NaHepes (pH 8.0), 100 nM [³⁵S]GTPγS, and either 1 mM carbachol or 1 μM atropine.

Extraction of M1S-2-FIAsH from HeLa cell membrane

Crude membrane preparations were made from FIAsH-labeled HeLa cells expressing M1S-2 as described in the Experimental Procedures in Chapter 2. To extract M1S-2-FIAsH, the membrane suspension (final protein concentration in extraction mixture was 1 mg/ml) was supplemented with digitonin (final

concentration of 1%) and cholate (final concentration of 0.3%) and vigorously stirred for 1 hour. A small aliquot of membrane-detergent mixture was removed for fluorescence measurements and the remainder was spun at 100 k x g and supernatant was removed for fluorescence measurements.

Results

Reconstituted biosensor retains wild-type agonist binding; formation of stable agonist-M1-G α_q complex

M1S-2-FIAsH reconstituted in lipid vesicles retained nearly wild-type agonist binding behavior as shown in Figure 24 and Table 4. To characterize the agonist binding behaviors of M1S-2-FIAsH, I examined competition binding of [³H]QNB with CCh to receptors reconstituted into lipid vesicles with and without G α_q . In the presence of G α_q , binding of CCh to wild-type M1 receptor was biphasic with IC₅₀ values of ~1 μ M (high affinity) and ~300 μ M (low affinity) (Figure 24A and Table 4). The fraction of high affinity binding was ~0.5 and high affinity binding disappeared in the presence of GTP γ S with an IC₅₀ of ~600 μ M (Figure 24A and Table 4). In the absence of G α_q , the binding was monophasic with IC₅₀ value of ~500 μ M. These binding behaviors indicated that wild-type M1 receptor in reconstituted vesicles could form an agonist-receptor-G protein (A-R-G) complex that bound the agonist with high affinity. Notably, M1S-2-FIAsH displayed all the wild-type agonist binding features with indistinguishable IC₅₀ values and fractional high affinity binding (Figure 24B and Table 4). Therefore, M1S-2-FIAsH retains wild-type ability to form a stable A-R-G complex in lipid vesicles, implying that the modifications made in the ICL3 of M1S-2-FIAsH do not impair the interaction of agonist-bound M1S-2-FIAsH with G α_q , at least under equilibrium binding conditions.

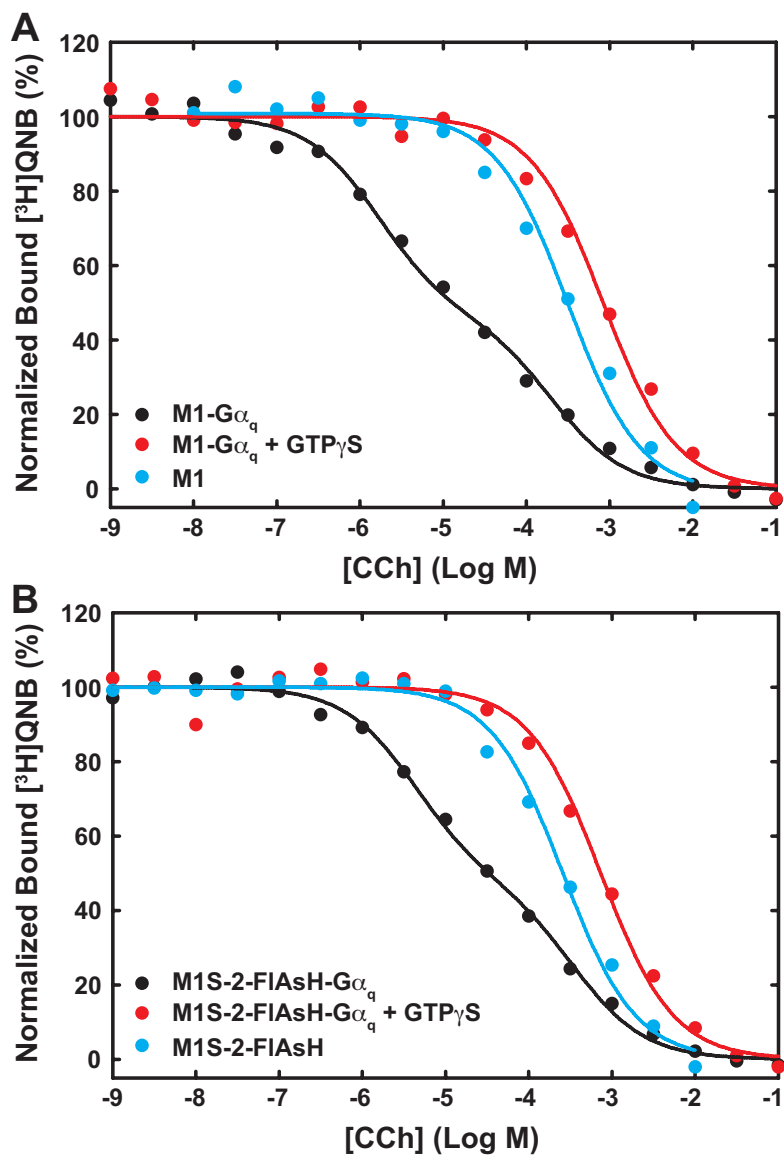


Figure 24. Agonist binding to M1S-2-FIAsH reconstituted in phospholipid vesicles CCh binding to wild-type M1 receptor (A) and *in vitro* labeled M1S-2-FIAsH (B) was measured by competition with 2 nM [³H]QNB. Receptors were reconstituted into phospholipid vesicles with (black and red) or without (cyan) G α_q . When indicated, 50 μ M GTP γ S was added in the binding reaction (red, +GTP γ S). Data are averages of duplicate determinations and are expressed as percent of maximum bound [³H]QNB. Binding in the presence of G α_q (no GTP γ S) was fitted with a two-site binding equation. Binding in the absence of G α_q or in the presence of added GTP γ S was fitted with a one-site binding equation. Results are summarized in Table 4.

Vesicles	- GTP γ S		+ GTP γ S
	IC ₅₀ (μ M) (H)	IC ₅₀ (μ M) (L)	IC ₅₀ (μ M)
M1		510 \pm 140 (n = 2)	
M1 + Gα_q	3 \pm 3 (n = 3)	290 \pm 170 (n = 3)	640 \pm 270 (n = 2)
M1S-2-FIAsh		440 \pm 140 (n = 2)	
M1S-2-FIAsh + Gα_q	5 \pm 1 (n = 2)	390 \pm 50 (n = 2)	735 (n = 1)

Table 4. Summary of CCh binding to wild-type M1 receptor and second-generation sensor (M1S-2-FIAsh) in reconstituted phospholipid vesicles

Competitive binding assays on the receptors in reconstituted phospholipid vesicles were performed using [³H]QNB as a radioligand tracer. The concentration of [³H]QNB was 2 nM. When indicated, 50 μ M GTP γ S was included in the binding reaction. Data were fitted with one- or two-site binding equation. H, high affinity binding; L, low affinity binding. Reconstituted biosensor retains GEF activity

Reconstituted sensor retains GEF activity

The wild-type agonist binding behavior of M1S-2-FIAsH in reconstituted vesicles suggests that M1S-2-FIAsH probably retains GEF (guanine nucleotide exchange factor) activity. To evaluate the GEF activity of M1S-2-FIAsH, I examined the agonist-stimulated binding of [³⁵S]GTP γ S to reconstituted lipid vesicles that contained G α_q , reconstituted as the G $\alpha\beta\gamma$ timer, and either wild-type M1 receptor or M1S-2-FIAsH. As shown in Figure 25A, the binding of [³⁵S]GTP γ S to M1-G $_q$ vesicles was markedly accelerated in the presence of CCh as compared with the binding in the presence of Atr. Binding of [³⁵S]GTP γ S to M1S-2-FIAsH-G $_q$ vesicles was also markedly promoted in the presence of CCh as compared with the binding in the presence of Atr. Because the binding of [³⁵S]GTP γ S in the presence of Atr represents spontaneous binding, receptor-mediated binding was difference between binding in the presence of CCh and Atr. The rate constants of receptor-mediated binding were $2.0 \pm 0.4 \text{ min}^{-1}$ ($n = 3$, mean \pm SD) and $0.6 \pm 0.1 \text{ min}^{-1}$ ($n = 3$, mean \pm SD) for wild-type M1 receptor and M1S-2-FIAsH, respectively. Unfortunately, the number of ligand binding sites (active receptor) was not measured and thus, binding rate per mole receptor could not be compared between wild-type M1 receptor and M1S-2-FIAsH. Assuming 2-4 nM [³H]QNB binding site that I routinely obtained in other reconstitutions, like those shown in Figure 24, the rate of receptor-mediated binding of [³⁵S]GTP γ S per mole of ligand binding site could vary from 0.4-1.2 and 0.1-0.3 $\text{min}^{-1}\text{mole}^{-1}$ for the wild-type receptor and the M1S-2-FIAsH, respectively, suggesting the GEF activity of the M1S-2-FIAsH could be 10-90% of that of the

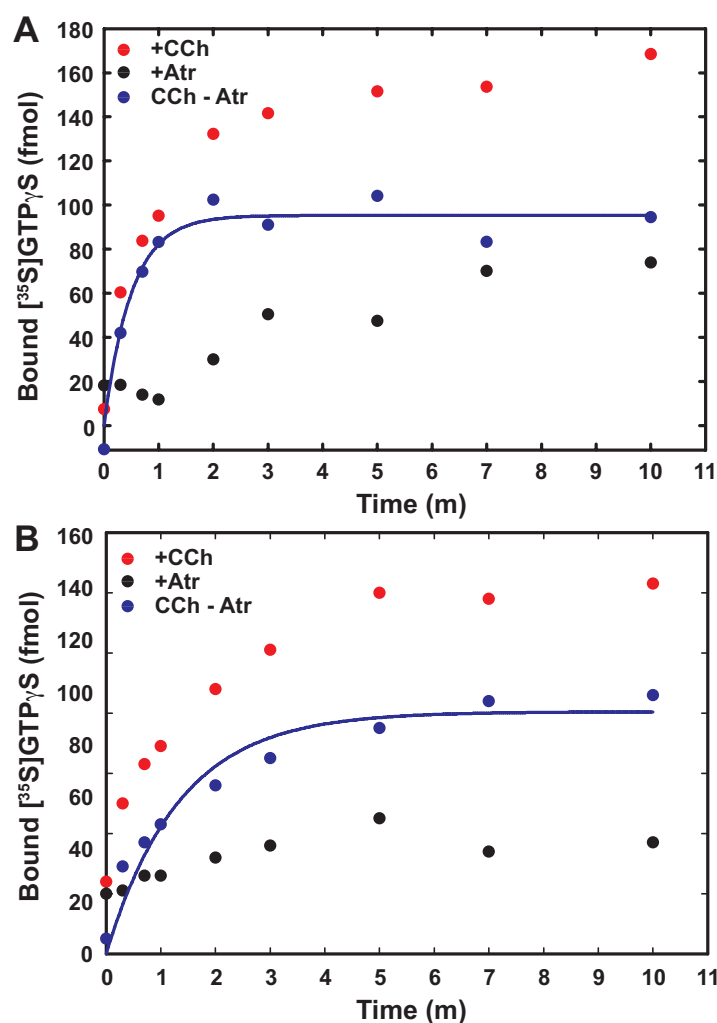


Figure 25. Carbachol-stimulated binding of GTP γ S to M1-G α_q (A) and M1S-2-FIAsH-G α_q (B) vesicles

Wild-type M1 receptor or M1S-2-FIAsH and G α_q were co-reconstituted in lipid vesicles according to the reconstitution protocol described in Experimental Procedures of Chapter 3. Reactions were initiated by adding vesicles to pre-warmed reaction buffers that contained either 1 mM carbachol (CCh) or 1 μ M atropine (Atr) and 100 nM [35 S]GTP γ S. Blue dots are the differences between binding measured in the presence of carbachol and atropine. The differences are fitted with a single first order exponential binding equation with the rate constants $2.0 \pm 0.6 \text{ min}^{-1}$ (for the wild-type M1 receptor) and $0.7 \pm 0.1 \text{ min}^{-1}$ (for M1S-2-FIAsH) (mean \pm SD). Data are from single determinations. This experiment was performed four times for the wild-type M1 receptor and three times for the M1S-2-FIAsH with similar results.

wild-type M1 receptor. Therefore, this result at least indicates that M1S-2-FIAsh in reconstituted lipid vesicles retains GEF activity.

Agonist-driven FRET change of M1S-2-FLAsH is not detected in reconstituted phospholipid vesicles

Even though M1S-2-FIAsh reconstituted in lipid vesicles retained biochemical activities of wild-type M1 receptor, the CCh-driven FRET change was not detected in reconstituted phospholipid vesicles. As shown in Figure 26, CCh did not change the cp173cer FRET donor emission or FIAsh FRET acceptor emission. This result was inconsistent with the observation in HeLa cells that CCh increased donor emission and decreased acceptor emission, resulting in ~20% decrease in FRET ratio. Notably, the basal FRET ratio, varying from 1.4 ~1.7 between reconstitutions, was lower than 2, which was the FRET ratio recorded in HeLa cell membranes. A plausible explanation for these observations is that the purified soluble receptor preparation contains a substantial amount of denatured receptor that remains fluorescent. In this case, specific ligand binding activity would be reduced and basal FRET might be low if the FIAsh is farther from the cp173cer cerulean than in the native sensor and thus, fractional change in FRET upon agonist binding would also be artifactually low.

Solubilization of the M1S-2-FIAsh in cell membranes obliterates agonist-driven FRET changes

To test the idea that receptor denaturation caused the loss of the FRET response, I monitored basal FRET and CCh-driven FRET change during

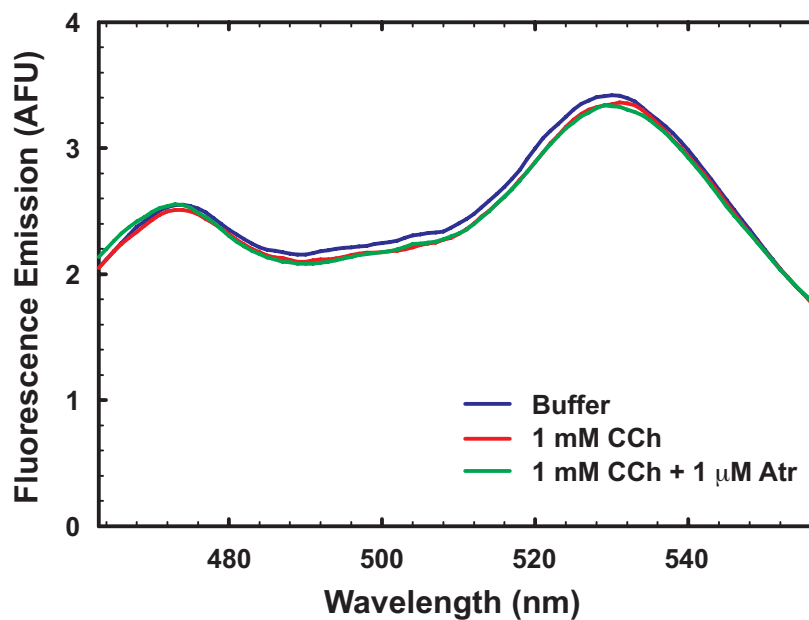


Figure 26. *In vitro* labeled sensor reconstituted in lipid vesicles loses agonist-driven FRET change

In vitro labeled sensor (M1S-2-FIAsH) was reconstituted in lipid vesicles according to the reconstitution protocol described in Experimental Procedures of Chapter 3. M1S-2-FIAsH vesicles were used for the fluorescence measurements. For fluorescence measurements, vesicles were diluted in a buffer (20 mM NaHepes, pH 7.4, 2 mM MgCl₂ and 100 mM NaCl) and the concentration of [³H]QNB binding sites was between 0.5 nM and 1 nM. Vesicles were incubated at 30°C for 5 min before the fluorescence measurements. Excitation wavelength was 433 nm and emission was scanned from 460 nm to 560 nm.

solubilization of M1S-2-FIAsH from HeLa membranes, my best source of active and responsive sensor. The M1S-2-FIAsH in membrane was solubilized in a buffer containing 1% digitonin for 1 hour and the fluorescence emission of the membrane-detergent mixture and the clear supernatant was measured. As shown in Figure 27, labeled sensor in the membrane preparation displayed basal FRET ratio of ~ 2 and $\sim 15\%$ CCh-driven FRET change. However, both the membrane-detergent mixture and the supernatant displayed a basal FRET ratio of only ~ 1.2 and no detectable CCh-driven FRET change. Therefore, denaturation of the M1S-2-FIAsH by solubilization decreased the basal FRET ratio from ~ 2 to ~ 1.2 and obliterated the CCh-driven FRET change. Because the basal FRET ratio of solubilized M1S-2-FIAsH is the weighted average of native and denatured M1S-2-FIAsH, the basal FRET ratio of denatured M1S-2-FIAsH should be lower than 1.2. If two fluorophores in denatured receptor are so far apart from each other that there is no energy transfer, basal FRET ratio of the denatured receptor would be a little higher than ~ 0.4 , the ratio for cp173cer cerulean by itself, which is the lower limit of the FRET ratio. Therefore, the 0.8 drop in FRET ratio (from 2 to 1.2) suggests at least 50% of the active fraction of the receptor in membrane was denatured during solubilization and thus, CCh-driven percent FRET change would be lower than 7%. As denatured M1S-2-FIAsH remained fluorescent and increased fluorescence background, CCh-driven FRET change might be even lower than 7%, and undetectable, which is consistent with no detectable CCh-driven FRET changes in the membrane-detergent mixture and clear supernatant.

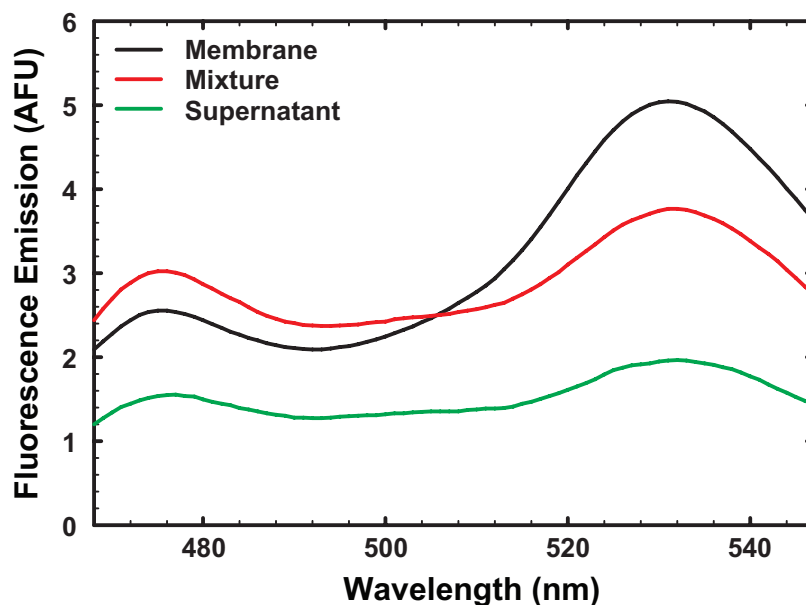


Figure 27. Effect of solubilization on the basal FRET of the sensor

HeLa cell membrane containing M1S-2-FIAsH was prepared as described under Experimental Procedures of Chapter 2. M1S-2-FIAsH was extracted from the membrane with 1% digitonin as described under Experimental Procedures of Chapter 3. The mixture of membrane and detergent was centrifuged at 100 k x g for 1 hour and clear supernatant was separated. For fluorescence measurements, membrane preparation (—) was diluted in $H_{20}M_{2}N_{100}$ buffer (20 mM NaHepes, pH 7.4, 2 mM $MgCl_2$ and 100 mM NaCl) and a membrane-detergent mixture (—) and a clear supernatant (—) were diluted in $H_{20}M_{2}N_{100}$ buffer containing 0.1% digitonin such that final digitonin concentration became 0.1%. Diluted preparations were excited at 433 nm and fluorescence emission was scanned. FRET ratio (530 nm/475 nm) was ~2, ~1.3, and ~1.3 for membrane, membrane-detergent mixture, and clear supernatant. For this experiment, membrane fluorescence background correction was omitted in calculating FRET ratio because it was not feasible to obtain corresponding backgrounds for membrane-detergent mixture and supernatant. Therefore, basal FRET ratio and CCh-driven FRET change in the membrane preparation were a little lower than those calculated from background-corrected spectra.

Fractional binding activity of M1S-2-FIAsh in solution and reconstituted vesicles is low

As suggested by the observation that solubilization denatured the receptor, ligand binding of purified M1S-2 and *in vitro* labeled M1S-2-FIAsh was lower than the 1 mole/mole calculated according to the amount of protein. Fractional binding activity was determined by measuring absorbance of cp173cer cerulean moiety (total protein; active plus inactive receptor) and [³H]QNB binding (active receptor). Fractional ligand binding activity (number of [³H]QNB binding sites/number of cp173cer moiety) of purified M1S-2 and *in vitro* labeled M1S-2-FIAsh were ~0.4 and ~0.3 respectively.

The fractional binding activity of M1S-2-FIAsh in reconstituted vesicles was also low. To test the possibility that reconstitution would remove denatured receptors and thus increase the fractional binding activity in lipid vesicles, fractional binding activity of reconstituted M1S-2-FIAsh was estimated. I used purified M1S-2 as a benchmark because cp173cer cerulean fluorescence was quenched by FIAsh in M1S-2-FIAsh and thus could not be used for fluorescence-based quantitation. Purified M1S-2 was reconstituted in lipid vesicles by the size exclusion method, as described in the Experimental Procedures. For each reconstitution fraction, the total amount of receptor and active receptor were determined by measuring cp173cer cerulean fluorescence and [³H]QNB binding. As shown in Figure 28, [³H]QNB binding site was only ~20% of total receptor (cp173cer) over all the reconstitution fractions, indicating reconstitution did not remove denatured receptors. Moreover, this result suggests that the reconstitutive behaviors of native receptors and denatured receptors are

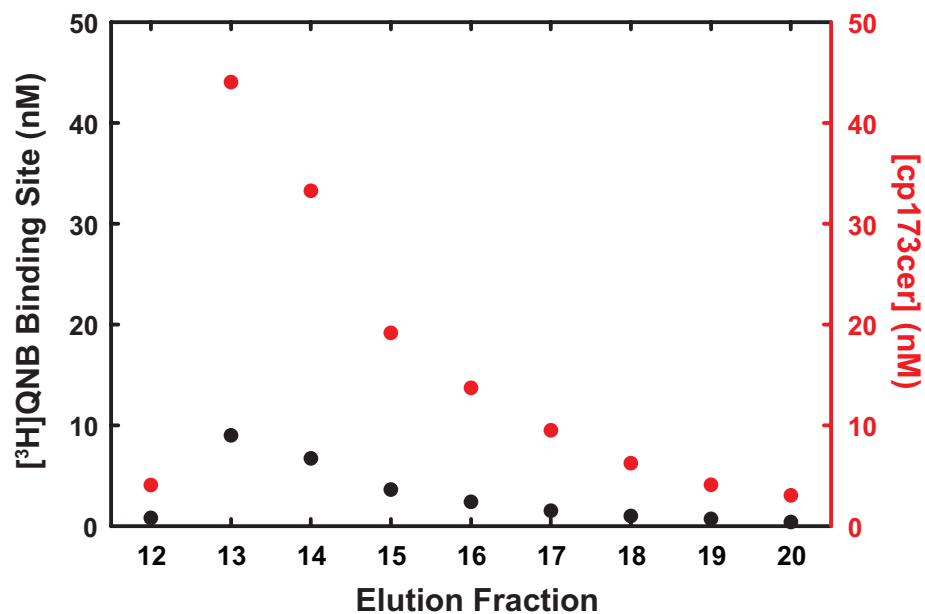


Figure 28. Fractional ligand binding activity of the M1S-2 reconstituted in lipid vesicles is low

Purified M1S-2 was reconstituted in lipid vesicles by size exclusion method as described under Experimental Procedures. Each fraction was assayed for [³H]QNB binding to indicate active receptor and for cp173cer fluorescence to indicate total receptor protein. Molar cp173cer fluorescence was calibrated using cp173cer purified from *E. coli*. Data are means of duplicate determinations. The ratio of [³H]QNB binding sites to total receptor was ~0.2 for all the fractions.

similar. Fractional binding activity of M1S-2-FIAsh in reconstituted vesicle should be also lower than 0.2 because its fractional ligand binding activity in solution (~0.3) is lower than that of M1S-2 in solution (~0.4).

The amount of total receptor was determined by measuring cp173cer cerulean fluorescence because the concentration of M1S-2 in lipid vesicles was too low to be determined by absorbance. Cerulean fluorescence of M1S-2 in lipid vesicle might have been influenced by the lipid bilayer but this possibility was not considered in calibrating cp173Cer cerulean fluorescence. However, regardless of uncertainties in fluorescence measurements, it was unlikely that fractional activity of M1S-2 in reconstituted vesicles was greater than that in solution because the reconstitutive behaviors of native receptors and denatured receptors were similar.

Discussion

In living cells and membrane preparations, agonist-driven conformational changes of the M1 receptor could be monitored with changes in the FRET of the sensor (Ch 2). The sensor retained nearly wild-type ligand binding and signaling function of the M1 receptor in membrane preparations and living cells respectively. However, interactive effects of $G\alpha_q$ on the conformation of the M1 receptor could not be investigated in cells and membrane preparations because a stable agonist-receptor-G protein (A-R-G) complex between could not be detected. In contrast, *in vitro* labeled sensor reconstituted in lipid vesicles could form stable A-R-G complex as suggested by the $G\alpha_q$ -dependent high affinity binding for agonist. However, unfortunately, the sensor reconstituted in lipid vesicles lost agonist-driven FRET change while it retained agonist binding and GEF activity. The loss of agonist-driven FRET change probably resulted from the low fractional binding activity of M1S-2-FIAsh.

Reconstituting fluorescence responses of the sensor in lipid vesicles

The major problem in reconstituting agonist-driven FRET change of the sensor in lipid vesicles was low fractional binding activity of *in vitro* labeled sensor. Solubilization, which is the first step of purification, denatured substantial fraction of receptors and thus, fractional agonist-driven FRET changes became undetectable in *in vitro* labeled sensor. This denaturation could not be prevented by the addition of high affinity antagonist atropine. Finally, reconstitution of the *in vitro* labeled sensor was not selective for the active fraction of the sensor, leading to a low fractional ligand binding activity in reconstituted vesicles. Therefore, the

key to successful reconstitution of the FRET responses will be having *in vitro* labeled sensor with high fractional binding activity.

Increasing fractional binding activity of *in vitro* labeled sensor

The low ligand binding activity of purified M1S-2 was ascribable to the purification scheme. Detergent-solubilized M1S-2 was purified through two-step affinity chromatography, a Ni-column followed by an anti-FLAG antibody column. However, these two affinity columns do not discriminate between active and inactive receptor. Therefore, fractional ligand binding activity did not increase in proportion to the increase in molar specific binding activity along the purification process. Including a ligand-based column will increase fractional ligand binding activity of *in vitro* labeled sensor as only active receptors can bind to the column. ABT-agarose (3-(2'-aminobenzhydryloxy)tropane-agarose) has been used to purify the muscarinic acetylcholine receptors in conjunction with various non-affinity chromatographic methods (Berstein et al., 1992; Biddlecome et al., 1996; Haga and Haga, 1983, 1985). ABT-based purification schemes generate muscarinic acetylcholine receptor preparations with fractional ligand binding activity close to 1. However, the low binding capacity of ABT-agarose (<30 pmol/1 ml resin) and difficulties in making quality ABT-agarose have been a problem. Nevertheless, I believe it is worth trying ABT-based purification.

The molecular status of the denatured receptors is not clear but it could be simply aggregates of denatured protein. This is suggested by the observation that passage of purified M1 receptor through a size exclusion column (SEC) could remove a substantial fraction of the receptors forming high molecular

weight complexes, presumably aggregates of denatured receptor (Kobilka B., personal communication). Assuming the receptors in aggregates do not have ligand binding activity, the fractional ligand binding activity might be increased by SEC. Therefore, it would be interesting to see whether including a SEC step could increase fractional ligand binding activity of *in vitro* labeled sensor and help in reconstituting agonist-driven FRET changes in lipid vesicles.

Reconstitution

The fractional binding activity of *in vitro* labeled sensor in reconstituted lipid vesicles was close to the fractional activity in solution. This indicates that the reconstitution did not selectively incorporate active receptor. However, as mentioned above, the inactive fraction might be a mixture of small aggregates of denatured receptors, which might have co-eluted with reconstituted vesicles because the reconstitution was based on size exclusion. This possibility might be tested in two ways. First, *in vitro* labeled sensor can be passed through a size exclusion column before reconstitution. Second, *in vitro* labeled sensor can be reconstituted in nano-discs (Banerjee et al., 2008; Whorton et al., 2007), which physically exclude the reconstitution of receptor aggregates.

Enhancing the stability of the sensor in micelles

The fractional ligand binding activity of purified M1S-2 was low and further decreased during the *in vitro* labeling procedure which involved ~1 hour incubation at RT. Moreover, the freezing and thawing of *in vitro* labeled sensor presumably denatured some fraction of the sensor. Therefore, increasing the

thermal stability of the receptor in detergent micelles would help preventing the denaturation of the sensor. Thermal stability of solubilized GPCRs varies depending on the detergent. Recently, a group of researchers introduced a new class of detergents, called maltose-neopentyl glycols (MNGs) and demonstrated that MNGs increased the thermal stability of purified muscarinic acetylcholine receptor type 3 (M3) (Chae et al., 2010). Considering the high similarity of sequence in the membrane spanning regions of M1 and M3, it would be worth testing this new class of detergents for an ability to enhance the stability of the M1 receptor.

Potential applications of the sensor

Once fluorescence responses of the sensor are reconstituted in lipid vesicles, the sensor will be instrumental in addressing the following problems.

Measuring fractional agonist-activated receptor engaged in active signaling complex

The M1-G α_q -PLC- β signaling module reconstituted in lipid vesicle retains biochemical activities that underlie regulatory behaviors of the signaling module observed in the cellular context. Activation, deactivation kinetics and signaling output at steady-state are the outcome of transient and dynamic interactions between M1, G α_q and PLC- β , which are regulated by agonist binding and hydrolysis of GTP. Quantitative biochemical assays using reconstituted vesicles and computational modeling indicate that GAP (PLC- β) accelerated turn off kinetics of the signaling module while minimally inhibiting signaling amplitude at

steady-state (Biddlecome et al., 1996; Ross, 2008; Turcotte et al., 2008). This regulatory effect of the GAP is not clearly understood because the simple G-protein monocyclus model dictates substantial inhibition of signaling amplitude by a GAP (Ross, 2008). One of the plausible explanations suggests that at steady-state, the GAP could increase the fractional agonist-activated receptor (A-R) engaged in the active signaling complex agonist-receptor-G protein (A-R-G) (Turcotte et al., 2008). However, conventional ligand binding assays cannot be used to test this possibility because they do not discriminate between A-R and A-R-G complexes. This sensor might be used for this purpose. In the A-R-G complex, the tight interaction with G protein would drive further conformational changes in the agonist-bound receptor, which might be discernable from simply agonist-driven conformational changes. In order to discriminate between A-R and A-R-G using the sensor, it would be critical to define the conformational status of the R driven by agonist alone (A-R) and agonist plus G protein (A-R-G) by measuring fluorescence intensity and fluorescence lifetime under equilibrium conditions. Then, the fluorescence information could be used in discerning A-R and A-R-G in steady-state GTPase cycles. In this respect, the M1-G α_q vesicle is ideal because G α_q enhances the binding affinity for agonist by ~100 fold, suggesting that the effect of G α_q on the the M1 receptor conformation might be relatively large and thus detection of its effect on the conformation of the M1 receptor might be relatively easy. I have already demonstrated that the sensor retains nearly wild-type ability to form the A-R-G complex and GEF activity in reconstituted vesicles. Therefore, in the future, it will be critical to examine whether the sensor can detect the binding of G protein.

Studying the mechanisms of biphasic agonist binding

The agonist binding of many GPCRs including the M1 receptor is biphasic with high-affinity and low-affinity binding. Agonist binding becomes monophasic, with only low affinity binding, in the absence of G protein or when G protein is uncoupled from the receptor by GTP (or GDP). Therefore, binding of G protein with agonist-bound receptor (A-R-G complex) enhances the binding affinity of the agonist. However, why only a fraction of receptors display high affinity binding is not clearly understood because the simple receptor model predicts that G protein monotonically shifts agonist binding with increased binding affinity. This discrepancy is a strong indication that the receptor population is conformationally heterogeneous. Whether this heterogeneity is pre-existing in the absence of G protein or induced by G protein is not clear.

The M1-G α_q vesicles provides an excellent experimental system for studying the mechanisms by which G protein creates biphasic agonist binding, because G α_q increases agonist binding affinity by several hundred fold. The sensor reconstituted in lipid vesicles retained nearly wild-type agonist binding behavior and it would be possible to use this sensor to study conformational status of the M1 receptor and how it is altered by the individual and combined effects of agonist and G protein. Using M1S-2-FIAsH-G α_q vesicles, interactive effects of G α_q on agonist binding and agonist-driven Δ FRET could be examined under equilibrium conditions by varying the concentration of GTP. However, intensity-based fluorescence measurement may not be sufficient to differentiate multiple conformational states of the receptor. This problem would be addressed

by measuring fluorescence lifetime or the kinetics of fluorescence changes. Again, the sensor's ability to detect the binding of G protein will be indispensable for this study.

BIBLIOGRAPHY

Adams, S.R., Campbell, R.E., Gross, L.A., Martin, B.R., Walkup, G.K., Yao, Y., Llopis, J., and Tsien, R.Y. (2002). New biarsenical ligands and tetracysteine motifs for protein labeling *in vitro* and *in vivo*: synthesis and biological applications. *Journal of the American Chemical Society* 124, 6063-6076.

Angers, S., Salahpour, A., and Bouvier, M. (2002). Dimerization: an emerging concept for G protein-coupled receptor ontogeny and function. *Annual Review of Pharmacology and Toxicology* 42, 409-435.

Arnold, K., Bordoli, L., Kopp, J., and Schwede, T. (2006). The SWISS-MODEL workspace: a web-based environment for protein structure homology modelling. *Bioinformatics* 22, 195-201.

Baird, G.S., Zacharias, D.A., and Tsien, R.Y. (1999). Circular permutation and receptor insertion within green fluorescent proteins. *Proceedings of the National Academy of Sciences of the United States of America* 96, 11241-11246.

Banerjee, S., Huber, T., and Sakmar, T.P. (2008). Rapid incorporation of functional rhodopsin into nanoscale apolipoprotein bound bilayer (NABB) particles. *Journal of Molecular Biology* 377, 1067-1081.

Berstein, G., Blank, J.L., Jhon, D.Y., Exton, J.H., Rhee, S.G., and Ross, E.M. (1992a). Phospholipase C- β 1 is a GTPase-activating protein for G_{q/11}, its physiologic regulator. *Cell* 70, 411-418.

Berstein, G., Blank, J.L., Smrcka, A.V., Higashijima, T., Sternweis, P.C., Exton, J.H., and Ross, E.M. (1992b). Reconstitution of agonist-stimulated phosphatidylinositol 4,5-bisphosphate hydrolysis using purified m1 muscarinic receptor, G_{q/11}, and phospholipase C- β 1. *The Journal of Biological Chemistry* 267, 8081-8088.

Best, R.B., Merchant, K.A., Gopich, I.V., Schuler B., Bax, A., and Eaton, W.A. (2007). Effect of flexibility and *cis* residues in single-molecule FRET studies of polyproline. *Proceedings of the National Academy of Sciences of the United States of America* 104, 18964-18969.

Biddlecome, G.H., Bernstein, G., and Ross, E.M. (1996). Regulation of phospholipase C- β 1 by G_q and m1 muscarinic cholinergic receptor. Steady-state balance of receptor-mediated activation and GTPase-activating protein-promoted deactivation. *The Journal of Biological Chemistry* 271, 7999-8007.

- Bradford, M.M. (1976). A rapid and sensitive method for the quantitation of microgram quantities of protein utilizing the principle of protein-dye binding. *Analytical Biochemistry* 72, 248-254.
- Brandt, D.R., Asano, T., Pedersen, S.E., and Ross, E.M. (1983). Reconstitution of catecholamine-stimulated guanosinetriphosphatase activity. *Biochemistry* 22, 4357-4362.
- Brauner-Osborne, H., Ebert, B., Brann, M.R., Falch, E., and Krosggaard-Larsen, P. (1996). Functional partial agonism at cloned human muscarinic acetylcholine receptors. *European Journal of Pharmacology* 313, 145-150.
- Chae, P.S., Rasmussen, S.G., Rana, R.R., Gotfryd, K., Chandra, R., Goren, M.A., Kruse, A.C., Nurva, S., Loland, C.J., Pierre, Y., Drew, D., Popot, J.L., Picot, D., Fox, B.G., Guan, L., Gether, U., Byrne, B., Kobilka, B., and Gellman, S.H. (2010). Maltose-neopentyl glycol (MNG) amphiphiles for solubilization, stabilization and crystallization of membrane proteins. *Nature Methods* 7, 1003-1008.
- Chen, C.K., Burns, M.E., He, W., Wensel, T.G., Baylor, D.A., and Simon, M.I. (2000). Slowed recovery of rod photoresponse in mice lacking the GTPase accelerating protein RGS9-1. *Nature* 403, 557-560.
- Cherezov, V., Rosenbaum, D.M., Hanson, M.A., Rasmussen, S.G., Thian, F.S., Kobilka, T.S., Choi, H.J., Kuhn, P., Weis, W.I., Kobilka, B.K., and Stevens, R.C. (2007). High-resolution crystal structure of an engineered human β_2 -adrenergic G protein-coupled receptor. *Science* 318, 1258-1265.
- Chidiac, P., Markin, V.S., and Ross, E.M. (1999). Kinetic control of guanine nucleotide binding to soluble $G\alpha_q$. *Biochemical pharmacology* 58, 39-48.
- Chien, E.Y., Liu, W., Zhao, Q., Katritch, V., Han, G.W., Hanson, M.A., Shi, L., Newman, A.H., Javitch, J.A., Cherezov, V., and Stevens, R.C. (2010). Structure of the human dopamine D3 receptor in complex with a D2/D3 selective antagonist. *Science* 330, 1091-1095.
- Ciccarone, V.C., Polayes, D., and Luckow, V.A., ed. (1997). Generation of Recombinant Baculovirus DNA in *E. coli* Using Baculovirus Shuttle Vector.
- Cowan, P.M., and McGavin S.(1955). Structure of poly-L-proline. *Nature* 176, 501-503.
- Damian, M., Martin, A., Mesnier, D., Pin, J.P., and Baneres, J.L. (2006). Asymmetric conformational changes in a GPCR dimer controlled by G-proteins. *The EMBO journal* 25, 5693-5702.
- Damian, M., Mary, S., Martin, A., Pin, J.P., and Baneres, J.L. (2008). G protein activation by the leukotriene B4 receptor dimer. Evidence for an absence of trans-activation. *The Journal of Biological Chemistry* 283, 21084-21092.

De Lean, A., Stadel, J.M., and Lefkowitz, R.J. (1980). A ternary complex model explains the agonist-specific binding properties of the adenylate cyclase-coupled beta-adrenergic receptor. *The Journal of Biological Chemistry* 255, 7108-7117.

Doupnik, C.A., Davidson, N., Lester, H.A., and Kofuji, P. (1997). RGS proteins reconstitute the rapid gating kinetics of G $\beta\gamma$ -activated inwardly rectifying K⁺ channels. *Proceedings of the National Academy of Sciences of the United States of America* 94, 10461-10466.

Dunham, T.D., and Farrens, D.L. (1999). Conformational changes in rhodopsin. Movement of helix f detected by site-specific chemical labeling and fluorescence spectroscopy. *The Journal of Biological Chemistry* 274, 1683-1690.

Farrens, D.L., Altenbach, C., Yang, K., Hubbell, W.L., and Khorana, H.G. (1996). Requirement of rigid-body motion of transmembrane helices for light activation of rhodopsin. *Science* 274, 768-770.

Gaietta, G., Deerinck, T.J., Adams, S.R., Bouwer, J., Tour, O., Laird, D.W., Sosinsky, G.E., Tsien, R.Y., and Ellisman, M.H. (2002). Multicolor and electron microscopic imaging of connexin trafficking. *Science* 296, 503-507.

Gether, U., Lin, S., Ghanouni, P., Ballesteros, J.A., Weinstein, H., and Kobilka, B.K. (1997). Agonists induce conformational changes in transmembrane domains III and VI of the β_2 adrenoceptor. *The EMBO Journal* 16, 6737-6747.

Gether, U., Lin, S., and Kobilka, B.K. (1995). Fluorescent labeling of purified β_2 -adrenergic receptor. Evidence for ligand-specific conformational changes. *The Journal of Biological Chemistry* 270, 28268-28275.

Ghanouni, P., Steenhuis, J.J., Farrens, D.L., and Kobilka, B.K. (2001). Agonist-induced conformational changes in the G-protein-coupling domain of the β_2 -adrenergic receptor. *Proceedings of the National Academy of Sciences of the United States of America* 98, 5997-6002.

Gilman, A.G. (1987). G proteins: transducers of receptor-generated signals. *Annual Review of Biochemistry* 56, 615-649.

Goin, J.C., and Nathanson, N.M. (2006). Quantitative analysis of muscarinic acetylcholine receptor homo- and heterodimerization in live cells: regulation of receptor down-regulation by heterodimerization. *The Journal of Biological Chemistry* 281, 5416-5425.

Griffin, B.A., Adams, S.R., and Tsien, R.Y. (1998). Specific covalent labeling of recombinant protein molecules inside live cells. *Science* 281, 269-272.

Gudermann, T., Kalkbrenner, F., and Schultz, G. (1996). Diversity and selectivity of receptor-G protein interaction. *Annual Review of Pharmacology and Toxicology* 36, 429-459.

Haga, K., and Haga, T. (1983). Affinity chromatography of the muscarinic acetylcholine receptor. *The Journal of Biological Chemistry* 258, 13575-13579.

Haga, K., and Haga, T. (1985). Purification of the muscarinic acetylcholine receptor from porcine brain. *The Journal of Biological Chemistry* 260, 7927-7935.

Haga, K., Kameyama, K., Haga, T., Kikkawa, U., Shiozaki, K., and Uchiyama, H. (1996). Phosphorylation of human m1 muscarinic acetylcholine receptors by G protein-coupled receptor kinase 2 and protein kinase C. *The Journal of Biological Chemistry* 271, 2776-2782.

Hartman, J.I., and Northup, J.K. (1996). Functional reconstitution in situ of 5-Hydroxytryptamine_{2c} (5HT_{2c}) receptors with G α_q and inverse agonism of 5HT_{2c} receptor antagonists. *The Journal of Biological Chemistry* 271, 22591-22597.

Hebert, T.E., Moffett, S., Morello, J.P., Loisel, T.P., Bichet, D.G., Barret, C., and Bouvier, M. (1996). A peptide derived from a β_2 -adrenergic receptor transmembrane domain inhibits both receptor dimerization and activation. *The Journal of Biological Chemistry* 271, 16384-16392.

Heinemann, U., and Hahn, M. (1995). Circular permutations of protein sequence: not so rare? *Trends in Biochemical Sciences* 20, 349-350.

Hellmich, M.R., Battey, J.F., and Northup, J.K. (1997). Selective reconstitution of gastrin-releasing peptide receptor with G α_q . *Proceedings of the National Academy of Sciences of the United States of America* 94, 751-756.

Hern, J.A., Baig, A.H., Mashanov, G.I., Birdsall, B., Corrie, J.E., Lazareno, S., Molloy, J.E., and Birdsall, N.J. (2010). Formation and dissociation of M1 muscarinic receptor dimers seen by total internal reflection fluorescence imaging of single molecules. *Proceedings of the National Academy of Sciences of the United States of America* 107, 2693-2698.

Hlavackova, V., Goudet, C., Kniazeff, J., Zikova, A., Maurel, D., Vol, C., Trojanova, J., Prezeau, L., Pin, J.P., and Blahos, J. (2005). Evidence for a single heptahelical domain being turned on upon activation of a dimeric GPCR. *The EMBO Journal* 24, 499-509.

Hoffman, B.B., Mullikin-Kilpatrick, D., and Lefkowitz, R.J. (1980). Heterogeneity of radioligand binding to α -adrenergic receptors. Analysis of guanine nucleotide regulation of agonist binding in relation to receptor subtypes. *The Journal of Biological Chemistry* 255, 4645-4652.

Hoffmann, C., Gaietta, G., Bunemann, M., Adams, S.R., Oberdorff-Maass, S., Behr, B., Vilardaga, J.P., Tsien, R.Y., Ellisman, M.H., and Lohse, M.J. (2005). A FIAsh-based FRET approach to determine G protein-coupled receptor activation in living cells. *Nature Methods* 2, 171-176.

Hu, J.R., and el-Fakahany, E.E. (1990). Selectivity of McN-A-343 in stimulating phosphoinositide hydrolysis mediated by M1 muscarinic receptors. *Molecular Pharmacology* 38, 895-903.

Jensen, J.B., Lyssand, J.S., Hague, C., and Hille, B. (2009). Fluorescence changes reveal kinetic steps of muscarinic receptor-mediated modulation of phosphoinositides and Kv7.2/7.3 K⁺ channels. *The Journal of General Physiology* 133, 347-359.

Jordan, B.A., and Devi, L.A. (1999). G-protein-coupled receptor heterodimerization modulates receptor function. *Nature* 399, 697-700.

Kozasa, T., Jiang, X., Hart, M.J., Sternweis, P.M., Singer, W.D., Gilman, A.G., Bollag, G., and Sternweis, P.C. (1998). p115 RhoGEF, a GTPase activating protein for G α_{12} and G α_{13} . *Science* 280, 2109-2111.

Kudlacek, O., Mitterauer, T., Nanoff, C., Hohenegger, M., Tang, W.J., Freissmuth, M., and Kleuss, C. (2001). Inhibition of adenylyl and guanylyl cyclase isoforms by the antiviral drug foscarnet. *The Journal of Biological Chemistry* 276, 3010-3016.

Kuszak, A.J., Pitchiaya, S., Anand, J.P., Mosberg, H.I., Walter, N.G., and Sunahara, R.K. (2009). Purification and functional reconstitution of monomeric mu-opioid receptors: allosteric modulation of agonist binding by G α_{i2} . *The Journal of Biological Chemistry* 284, 26732-26741.

Lakowicz, J.R. (2006). *Principles of Fluorescence Spectroscopy*, Fourth Edition.

Lameh, J., Philip, M., Sharma, Y.K., Moro, O., Ramachandran, J., and Sadee, W. (1992). Hm1 muscarinic cholinergic receptor internalization requires a domain in the third cytoplasmic loop. *The Journal of Biological Chemistry* 267, 13406-13412.

Leff, P. (1995). The two-state model of receptor activation. *Trends in Pharmacological Sciences* 16, 89-97.

Luckow, V.A., Lee, S.C., Barry, G.F., and Olins, P.O. (1993). Efficient generation of infectious recombinant baculoviruses by site-specific transposon-mediated insertion of foreign genes into a baculovirus genome propagated in *Escherichia coli*. *Journal of Virology* 67, 4566-4579.

Maeda, S., Lameh, J., Mallet, W.G., Philip, M., Ramachandran, J., and Sadee, W. (1990). Internalization of the Hm1 muscarinic cholinergic receptor involves the third cytoplasmic loop. *FEBS Letters* 269, 386-388.

Maguire, M.E., Van Arsdale, P.M., and Gilman, A.G. (1976). An agonist-specific effect of guanine nucleotides on binding to the beta adrenergic receptor. *Molecular Pharmacology* 12, 335-339.

Mansoor, S.E., McHaourab, H.S., and Farrens, D.L. (1999). Determination of protein secondary structure and solvent accessibility using site-directed fluorescence labeling. Studies of T4 lysozyme using the fluorescent probe monobromobimane. *Biochemistry* 38, 16383-16393.

Marek, K.W., and Davis, G.W. (2002). Transgenically encoded protein photoinactivation (FIAsh-FALI): acute inactivation of synaptotagmin I. *Neuron* 36, 805-813.

Mellado, M., Rodriguez-Frade, J.M., Vila-Coro, A.J., Fernandez, S., Martin de Ana, A., Jones, D.R., Toran, J.L., and Martinez, A.C. (2001). Chemokine receptor homo- or heterodimerization activates distinct signaling pathways. *The EMBO journal* 20, 2497-2507.

Mukhopadhyay, S., and Ross, E.M. (1999). Rapid GTP binding and hydrolysis by G_q promoted by receptor and GTPase-activating proteins. *Proceedings of the National Academy of Sciences of the United States of America* 96, 9539-9544.

Nathanson, N.M. (1987). Molecular properties of the muscarinic acetylcholine receptor. *Annual Review of Neuroscience* 10, 195-236.

Palczewski, K., Kumasaka, T., Hori, T., Behnke, C.A., Motoshima, H., Fox, B.A., Le Trong, I., Teller, D.C., Okada, T., Stenkamp, R.E., Yamamoto, M., and Miyano, M. (2000). Crystal structure of rhodopsin: A G protein-coupled receptor. *Science* 289, 739-745.

Parnot, C., Miserey-Lenkei, S., Bardin, S., Corvol, P., and Clauser, E. (2002). Lessons from constitutively active mutants of G protein-coupled receptors. *Trends in Endocrinology and Metabolism* 13, 336-343.

Pierce, K.L., Premont, R.T., and Lefkowitz, R.J. (2002). Seven-transmembrane receptors. *Nature Reviews Molecular Cell biology* 3, 639-650.

Rasmussen, S.G., Choi, H.J., Rosenbaum, D.M., Kobilka, T.S., Thian, F.S., Edwards, P.C., Burghammer, M., Ratnala, V.R., Sanishvili, R., Fischetti, R.F., Schertler, G.F., Weis, W.I., and Kobilka, B.K. (2007). Crystal structure of the human β_2 -adrenergic G-protein-coupled receptor. *Nature* 450, 383-387.

Rasmussen, S.G., DeVree, B.T., Zou, Y., Kruse, A.C., Chung, K.Y., Kobilka, T.S., Thian, F.S., Chae, P.S., Pardon, E., Calinski, D., Mathiesen, J.M., Shah, S.T., Lyons, J.A., Caffrey, M., Gellman, S.H., Steyaert, J., Skinioitis, G., Weis, W.I., Sunahara, R.K., and Kobilka, B.K. (2011). Crystal structure of the β_2 -adrenergic receptor-Gs protein complex. *Nature* 477, 549-555.

Rizzo, M.A., Springer, G.H., Granada, B., and Piston, D.W. (2004). An improved cyan fluorescent protein variant useful for FRET. *Nature Biotechnology* 22, 445-449.

Rodbell, M., Birnbaumer, L., Pohl, S.L., and Krans, H.M. (1971). The glucagon-sensitive adenyl cyclase system in plasma membranes of rat liver. V. An obligatory role of guanylnucleotides in glucagon action. *The Journal of Biological Chemistry* 246, 1877-1882.

Rosenbaum, D.M., Cherezov, V., Hanson, M.A., Rasmussen, S.G., Thian, F.S., Kobilka, T.S., Choi, H.J., Yao, X.J., Weis, W.I., Stevens, R.C., and Kobilka, B.K. (2007). GPCR engineering yields high-resolution structural insights into β_2 -adrenergic receptor function. *Science* 318, 1266-1273.

Rosenbaum, D.M., Zhang, C., Lyons, J.A., Holl, R., Aragao, D., Arlow, D.H., Rasmussen, S.G., Choi, H.J., Devree, B.T., Sunahara, R.K., Chae, P.S., Gellman, S.H., Dror, R.O., Shaw, D.E., Weis, W.I., Caffrey, M., Gmeiner, P., and Kobilka, B.K. (2011). Structure and function of an irreversible agonist- β_2 adrenoceptor complex. *Nature* 469, 236-240.

Ross, E.M. (2008). Coordinating speed and amplitude in G-protein signaling. *Current Biology* 18, R777-R783.

Ross, E.M., Maguire, M.E., Sturgill, T.W., Biltonen, R.L., and Gilman, A.G. (1977). Relationship between the β -adrenergic receptor and adenylate cyclase. *The Journal of Biological Chemistry* 252, 5761-5775.

Ross, E.M., and Wilkie, T.M. (2000). GTPase-activating proteins for heterotrimeric G proteins: regulators of G protein signaling (RGS) and RGS-like proteins. *Annual Review of Biochemistry* 69, 795-827.

Savitzky, A., and Golay, M.J.E. (1964). Smoothing and Differentiation of Data by Simplified Least Squares Procedures. *Analytical Chemistry* 36, 1627-1639.

Schaffner, W., and Weissmann, C. (1973). A rapid, sensitive, and specific method for the determination of protein in dilute solution. *Analytical Biochemistry* 56, 502-514.

Scheerer, P., Park, J.H., Hildebrand, P.W., Kim, Y.J., Krauss, N., Choe, H.W., Hofmann, K.P., and Ernst, O.P. (2008). Crystal structure of opsin in its G-protein-interacting conformation. *Nature* 455, 497-502.

Schimerlik, M.I. (1989). Structure and regulation of muscarinic receptors. *Annual Review of Physiology* 51, 217-227.

Schuler B., Lipman, E.A., Steinbach, P.J., Kumke, M., and Eaton W.A. (2005). Polyproline and the "spectroscopic ruler" revisited with single-molecule fluorescence. *Proceedings of the National Academy of Sciences of the United States of America* 102, 2754-2759.

Schwarz, R.D., Davis, R.E., Jaen, J.C., Spencer, C.J., Tecle, H., and Thomas, A.J. (1993). Characterization of muscarinic agonists in recombinant cell lines. *Life Sciences* 52, 465-472.

Shimamura, T., Shiroishi, M., Weyand, S., Tsujimoto, H., Winter, G., Katritch, V., Abagyan, R., Cherezov, V., Liu, W., Han, G.W., Kobayashi, T., Stevens, R.C., and Iwata, S. (2011). Structure of the human histamine H1 receptor complex with doxepin. *Nature* 475, 65-70.

Slessareva, J.E., and Graber, S.G. (2003). Reconstitution reveals additional roles for N- and C-terminal domains of G α in muscarinic receptor coupling. *Biochemistry* 42, 7552-7560.

Sternweis, P.C., and Gilman, A.G. (1979). Reconstitution of catecholamine-sensitive adenylate cyclase. Reconstitution of the uncoupled variant of the S40 lymphoma cell. *The Journal of Biological Chemistry* 254, 3333-3340.

Stroffekova, K., Proenza, C., and Beam, K.G. (2001). The protein-labeling reagent FLASH-EDT₂ binds not only to CCXXCC motifs but also non-specifically to endogenous cysteine-rich proteins. *Pflügers Archiv* 442, 859-866.

Stryer, L., and Haugland, R.P. (1967). Energy transfer: a spectroscopic ruler. *Proceedings of the National Academy of Sciences of the United States of America* 58, 719-726.

Swaminath, G., Xiang, Y., Lee, T.W., Steenhuis, J., Parnot, C., and Kobilka, B.K. (2004). Sequential binding of agonists to the β 2 adrenoceptor. Kinetic evidence for intermediate conformational states. *The Journal of Biological Chemistry* 279, 686-691.

Turcotte, M., Tang, W., and Ross, E.M. (2008). Coordinate regulation of G protein signaling via dynamic interactions of receptor and GAP. *PLoS Computational Biology* 4, e1000148.

Ulbrich, M.H., and Isacoff, E.Y. (2007). Subunit counting in membrane-bound proteins. *Nature Methods* 4, 319-321.

- Villardaga, J.P., Bunemann, M., Krasel, C., Castro, M., and Lohse, M.J. (2003). Measurement of the millisecond activation switch of G protein-coupled receptors in living cells. *Nature Biotechnology* 21, 807-812.
- Warne, T., Moukhametzianov, R., Baker, J.G., Nehme, R., Edwards, P.C., Leslie, A.G., Schertler, G.F., and Tate, C.G. (2011). The structural basis for agonist and partial agonist action on a β_1 -adrenergic receptor. *Nature* 469, 241-244.
- White, J.H., Wise, A., Main, M.J., Green, A., Fraser, N.J., Disney, G.H., Barnes, A.A., Emson, P., Foord, S.M., and Marshall, F.H. (1998). Heterodimerization is required for the formation of a functional GABA_B receptor. *Nature* 396, 679-682.
- Whorton, M.R., Bokoch, M.P., Rasmussen, S.G., Huang, B., Zare, R.N., Kobilka, B., and Sunahara, R.K. (2007). A monomeric G protein-coupled receptor isolated in a high-density lipoprotein particle efficiently activates its G protein. *Proceedings of the National Academy of Sciences of the United States of America* 104, 7682-7687.
- Whorton, M.R., Jastrzebska, B., Park, P.S., Fotiadis, D., Engel, A., Palczewski, K., and Sunahara, R.K. (2008). Efficient coupling of transducin to monomeric rhodopsin in a phospholipid bilayer. *The Journal of Biological Chemistry* 283, 4387-4394.
- Wu, B., Chien, E.Y., Mol, C.D., Fenalti, G., Liu, W., Katritch, V., Abagyan, R., Brooun, A., Wells, P., Bi, F.C., Hamel, D.J., Kuhn, P., Handel, T.M., Cherezov, V., and Stevens, R.C. (2010). Structures of the CXCR4 chemokine GPCR with small-molecule and cyclic peptide antagonists. *Science* 330, 1066-1071.
- Xu, F., Wu, H., Katritch, V., Han, G.W., Jacobson, K.A., Gao, Z.G., Cherezov, V., and Stevens, R.C. (2011). Structure of an agonist-bound human A_{2A} adenosine receptor. *Science* 332, 322-327.
- Yao, X., Parnot, C., Deupi, X., Ratnala, V.R., Swaminath, G., Farrens, D., and Kobilka, B. (2006). Coupling ligand structure to specific conformational switches in the β_2 -adrenoceptor. *Nature Chemical Biology* 2, 417-422.
- Yao, X.J., Velez Ruiz, G., Whorton, M.R., Rasmussen, S.G., DeVree, B.T., Deupi, X., Sunahara, R.K., and Kobilka, B. (2009). The effect of ligand efficacy on the formation and stability of a GPCR-G protein complex. *Proceedings of the National Academy of Sciences of the United States of America* 106, 9501-9506.
- Zacharias, D.A., Violin, J.D., Newton, A.C., and Tsien, R.Y. (2002). Partitioning of lipid-modified monomeric GFPs into membrane microdomains of live cells. *Science* 296, 913-916.
- Zhang, Q., Pacheco, M.A., and Doupnik, C.A. (2002). Gating properties of GIRK channels activated by G α_o - and G α_i -coupled muscarinic m2 receptors in

Xenopus oocytes: the role of receptor precoupling in RGS modulation. *The Journal of Physiology* 545, 355-373.